Inaugural-Dissertation

Zur Erlangung der Doktorwürde der
Naturwissenschaftlich-Mathematische Gesamtfakultät der

Ruprecht-Karls-Universität Heidelberg

vorgelegt von

M.Sc. Mohamed Eita

geboren in Ägypten (Gharbia)

Tag der mündlichen Prüfung: 31.03.2008

PhD Thesis

Department of Chemistry

University of Heidelberg

Submitted by:

M.Sc. Mohamed Eita

born in Egypt (Gharbia)

Defence on: 31.03.2008

Interaction of humic acid with clay mineral model surfaces in the presence and absence of Gd^{+3}

A study comprising QCM-D, ellipsometry and XPS

Referees:

PD. Dr. Reiner Dahint
Prof. Dr. Joachim P. Spatz

Acknowledgement:

I am very grateful to my supervisor, PD. Dr. Reiner Dahint, for his friendly and nice supervision. He taught me a lot about research and experimenting, it is owing to him that I learned a large deal about acoustic wave sensors, it is also his effort that this thesis was written in this exact form. He I hope I did not consume his patience!! I like to thank Prof. Grunze for accepting me to work at his chair and providing helpful feedback. Thanks to Prof. Joachim Spatz for accepting being the second supervisor of my thesis. Thanks to Dr. Thorsten Stumpf for his helpful cooperation and providing knowledge about humic and metal ion adsorption. I would like to thank Georg Albert for his efforts to develop a stable aluminum oxide coating, without his sincerely engagement, this work would have gone one step forward. I would like to thank to Dr. Ralf Richter for his help at the beginning of the QCM experiments, he was very friendly and tried to help whenever he could. I got most of the technical information and interpretation strategies from him. Thanks to my colleague Xinyu Cao for his help operating the XPS and for being friendly and helpful in need. Thanks to PD. Dr. Michael Zharnikov for his advices and help in interpreting the XPS spectra. Thanks to my roommate Thomas Kaltofen for being a friend and helpful colleague and for his help with ellipsometry. Thanks to all my colleagues who helped during my thesis work and in preparing the exam celebration. I would like to thank the technical and management support team for their continuous help.

A human being should thank God everywhere and all the time. My parents deserve all the thanks and gratitude for all they have done for me. Thanks to my patient wife who stood beside me in hard times. Mariam also deserves a lot of thanks for not giving her father some peace while she is awake and never slept easily. But her lovely smile is very necessary for her father.

Abstract

In this work the adsorption of humic acid on aluminum oxide surfaces is being studied in the absence (binary system) and presence (ternary system) of gadolinium. The study is related to the evaluation of environmental risks associated with the long-term operation of repositories for nuclear waste. For this purpose, the various interactions between radionuclides and their environment, i.e. the surrounding rock or soil, have to be studied in detail. The groundwater in such repositories is usually enriched with organic matter from biological decomposition reactions, so-called humic material. As they exhibit pronounced complexation and redox capabilities, they are assumed to be of high relevance for the retention and the transport of radionuclides. In the present study, aluminium oxide serves a model surface for clay, one of the most important geological barriers discussed for waste repositories. Gadolinium serves as an analogue for trivalent actinides.

The main technique employed in this study is gravimetric using a quartz crystal microbalance system with dissipation monitoring (QCM-D). Ellipsometry and X-ray photoelectron spectroscopy (XPS) supplement the studies. The most challenging task of this work was the development of stable aluminum oxide coatings for QCM sensors. Various coating methods such as sputtering and thermal evaporation were tested and optimized to finally obtain a reasonably stable coating.

Using QCM-D, we focused on studying the adsorption processes as a function of pH and humic concentration. Varying pH was found to play an interesting role in the adsorption of the multifunctional humic acid. Adsorption at pH 5, 6.8 and 9 only resulted in a humic monolayer. However at pH 3 a two-step process was observed where monolayer adsorption is followed by physically aggregated molecules. Varying concentration revealed that most of the monolayer forms at a dilute concentration about 1-5 mg/l, followed by saturation at a concentration of 10-20 mg/l. Although the measured isotherms are well fitted by a Langmuir process, the fact that the humic films are irreversible attached to the surface contradicts this way of data interpretation. The adsorption characteristics are more consistently explained by an unfolding of adsorbed humic acid, which yields thinner films if formed from lower concentrated solutions.

The adsorption phenomenon in the ternary system show similar trends with respect to pH and concentration effects as the binary system. The structure of the adsorbed species in the ternary system is assumed to consist of a humic monolayer linked vertically to another humic overlayer via a gadolinium bridge. This may also explain why adsorption kinetics is delayed in the ternary system.

Zusammenfassung

In Rahmen dieser Arbeit wurde die Adsorption von Huminsäure auf Aluminiumoxidoberflächen in Abwesenheit (binäres System) und Gegenwart (ternäres System) von Gadolinium studiert. Die Untersuchungen stehen im Zusammenhang mit der Bewertung von Umweltrisiken, die mit dem Langzeitbetrieb eines Endlagers für radioaktive Abfälle verbunden sind. Zu diesem Zweck müssen die verschiedenen Wechselwirkungsprozesse zwischen Radionukliden und ihrer Umgebung, d.h. dem umgebenden Gestein oder Boden, im Detail untersucht werden. Das Grundwasser in solchen Endlagern ist üblicherweise mit organischen Stoffen aus biologischen Abbauprozessen angereichert, den sogenannten Huminstoffen. Da diese ausgeprägte Komplexierungs- und Redoxeigenschaften aufweisen, wird ihnen eine große Bedeutung für die Rückhaltung und den Transport von Radionukliden zugeschrieben. In der vorliegenden Untersuchung dient Aluminiumoxid als eine Modelloberfläche für Ton, eine der wichtigsten geologischen Barrieren, die für Endlagerstätten diskutiert werden. Gadolinium wird als Analogon für dreiwertige Aktinide verwendet.

Die Haupttechnik, die in dieser Studie eingesetzt wurde, ist Gravimetrie mittels Schwingquarztechnologie (QCM-D, Quartz Crystal Microbalance with Dissipation Monitoring). Ellipsometrie und Röntgenphotoelektronenspektroskopie (XPS) ergänzen die Untersuchungen. Eine der größten Herausforderungen der Arbeit war die Herstellung stabiler Aluminiumoxidbeschichtungen für QCM-Sensoren. Hierzu wurden verschiedene Beschichtungsmethoden, wie Sputtern und thermische Bedampfung, getestet und optimiert, um schließlich vergleichsweise stabile Schichten zu erhalten.

Unter Verwendung der QCM-D-Technologie konzentrierten wir uns auf das Studium der Adsorptionsprozesse als Funktion des pH-Wertes und der Huminstoff-konzentration. Die Variation des pH-Wertes ergab dabei einen interessanten Einfluss auf das Adsorptionsverhalten der multifunktionalen Huminstoffe. Adsorption bei pH 5, 6.8 und 9 führte nur zur Ausbildung einer Huminstoff-Monolage. Bei pH 3 wurde hingegen ein Zwei-Stufen-Prozess beobachtet, bei dem auf die Monolagen-adsorption die Physisorption von Molekülaggregaten folgt. Eine Variation der

Huminstoffkonzentration ergab, dass der größte Teil der Monolage bereits bei niedrigen Konzentrationen von 1-5 mg/l gebildet wird und bei einer Konzentration von 10-20 mg/l Sättigung auftritt. Obwohl sich die gemessenen Isothermen gut mit einem Langmuir-Mechanismus fitten lassen, widerspricht die Tatsache, dass die Huminstofffilme irreversibel adsorbiert sind, einer derartigen Dateninterpretation. Das Adsorptionsverhalten lässt sich besser durch die Entfaltung adsorbierter Huminstoffmoleküle erklären. Auf diese Weise bilden sich dünnere Schichten aus, wenn die Filme aus höher verdünnten Lösungen abgeschieden werden.

Die Adsorptionsphänomene im ternären System zeigen ähnliche Tendenzen hinsichtlich pH- und Konzentrationseffekten, wie sie auch für das binäre System beobachtet werden. Die Struktur der Adsorbatschicht im ternären System besteht vermutlich aus einer Huminstoff-Monolage, an die über Gadoliniumbrücken eine zweite Huminstoffschicht gebunden ist. Dies kann auch die verlangsamte Adsorptionskinetik im ternären System erklären.

Table of content

Introduction

Underground disposal of nuclear waste represents a considerable environmental issue. To assure the safety of these repositories a detailed understanding of the interaction of the content of that waste, e.g. radionuclides and other metals, with the surrounding environment is needed. The interaction of radionuclides with the geochemical environment underground may be described by interfacial reactions such like adsorption, ion exchange and complexation of these metals by natural ligands. In order to facilitate a predictive modelling, a complete characterization of such a process would involve both quantitative thermodynamics and kinetics approaches. A thermodynamic approach could define the tendency of radionuclides to undergo adsorption and/or complexation, the kinetic approach would then describe the rates or time dependency of these processes, which is an essential factor in terms of the long term storage of radionuclides having long time decay.

The geochemical environment underground is complex in composition; however let us consider its basic constituents as clay minerals, organic matter or natural products and water. The minerals are mostly coated with the organic matter. The mobility of radionuclides in this environment will be affected and may be retarded by these surroundings. The basic constituents of organic matter in soil are humic materials, which are known to have a high affinity toward metal ions [1]. Thus, humic materials are believed to play an essential role in retention and mobilization of metal ions in aquatic environments, especially upon further adsorption on clay minerals.

In recent years a great attention has been directed toward studying the system of clay, humic materials and actinides. Lanthanides have been employed as an analogue for actinides in some cases. The actinides used in these studies present a wide range of decay time intervals and valences, too. Techniques applied in these studies varied from different spectroscopic methods to colloidal and surface science approaches, and other analytical chemistry methods. The main outcome of this research confirms the adsorption of humic acid on clay minerals such as alumina, aluminum oxide Al_2O_3, and silica, i.e. silicon oxide SiO_2. On the other hand complexation of radionuclides by humic materials was assured. However most of these studies, except for time resolved laser fluorescence spectroscopy (TRLFS), are

batch experiments and hence do not allow in-situ real time kinetics. On the other hand these studies applied labelling techniques and hence direct detection of the concerned species is not possible. Furthermore we are going to consider the adsorption of humic acid monolayer and the accompanied conditions from a surface science point of view.

In this thesis, we shall focus on the interactions in the system humic acid (as the natural organic matter), aluminum oxide (as a model surface for a clay mineral) and gadolinium chloride (as analogue for trivalent actinides). These components will be classified into two systems: a binary system consisting of humic acid and an aluminum oxide surface, and a ternary system, which additionally contains gadolinium chloride. Mainly, an in-situ label free detection of the adsorbate is considered which would result in real time kinetic studies of the adsorption process. Thermodynamics of adsorption is also in focus, aiming at drawing the adsorption isotherms and calculating the free energy and equilibrium constants of adsorption in the binary as well as in the ternary system.

The main technique applied in this study is QCM-D, which belongs to the acoustic wave sensors family. QCM-D offers the possibility to detect adsorbed masses with sensitivity down to the nanogram scale. Moreover, it monitors in real time the kinetics of the ongoing process. Measuring the dissipation factor in a QCM-D measurement provides additional information about energy losses occurring at the vibrating sensor surface upon contact with the adsorbate. In parallel, ellipsometry will provide evidence for adsorption kinetics and the adsorbed amounts of material. Spectroscopic information on the adsorbed species is going to be obtained by XPS, which will be applied as a third technique for quantifying the amount of material involved in adsorption and desorption processes.

2. Theory: Adsorption, humic material and metal oxides

2.1 Adsorption

2.1.1. Adsorption isotherms

Considering adsorption of gases, adsorption isotherms describe the amount of the adsorbed gas (adsorbate) as a function of the applied gas pressure at constant temperature [2]. Different types of adsorption isotherms have been developed depending on the adsorption characteristics.

The simplest isotherm is the Langmuir isotherm which assumes that every adsorption site is equivalent and that adsorbate-adsorbate interactions are not allowed. Hence it is limited to a monolayer and characterized by rapid progress rate at the first stage which is followed by fully surface coverage (fig. 2.1).

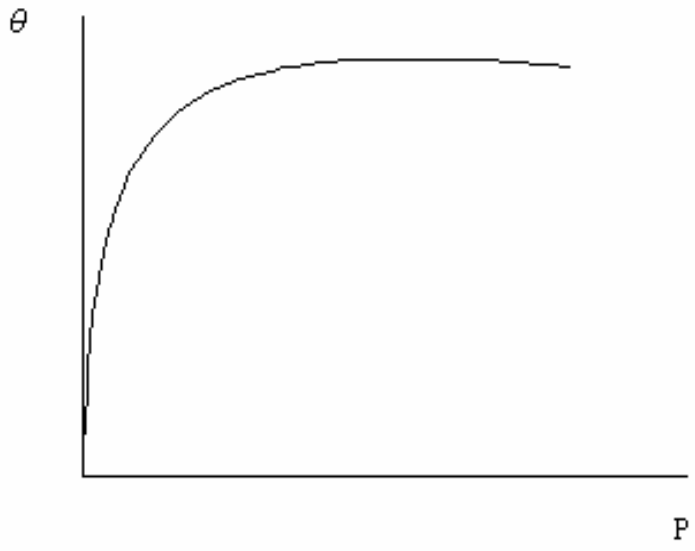

Fig. 2.1: Schematic diagram of a Langmuir isotherm showing the first stage of a monolayer coverage followed by levelling-off due to saturation

To derive an expression for the Langmuir isotherm let us consider the adsorption of a gas (A) on a substrate (M), with k_a as the rate of adsorption and k_d as the rate of desorption, θ is the surface coverage and N the total number of sites. The change of surface coverage, $d\theta/dt$, due to adsorption is proportional to the gas pressure p and the total number of vacant sites $N(1-\theta)$:

$$d\theta/dt = k_a\, pN(1-\theta)$$

The change of surface coverage due to desorption is proportional to the total number of adsorbed species N θ:

$$d\theta/dt = k_d\, N\, \theta$$

At equilibrium, the two rates are equal, so that we come up with the following expression for the Langmuir isotherm:

$$\theta = \frac{kp}{1+kp} \qquad , \; k = \frac{k_a}{k_d} \qquad 2.1$$

where θ is the surface coverage, p is the gas pressure, k_a is the rate of adsorption and k_d is the rate of desorption.

A different adsorption isotherm is the BET isotherm named after its founders Stephen Brunauer, Paul Emmit and Edward Teller. The BET isotherm is concerned with the special case that the adsorbed monolayer after full coverage acts itself as a substrate for further multilayer adsorption. An example of that is the adsorption of gases into porous materials which can be then followed by gas condensation into the pores giving rise to indefinite adsorption. There is also the Freundlich isotherm which corresponds to logarithmic changes of the surface coverage with respect to the applied adsorbate pressure.

We are going to consider only the simplest case which is Langmuir isotherm, paying special attention to the adsorption at the solid/liquid interface. Despite of being first derived for gas adsorption, the Langmuir isotherm was formalised to match adsorption from solutions [3]. The Langmuir model assumes, similar to the case of gas adsorption, the surface to consist of adsorption sites with the area per site being σ^o. All adsorbed species interact only with one site not with each other, and adsorption is thus limited to a monolayer. However, in case of solutions this monolayer would be considered as an ideal (no solute/solute, solute/solvent and solvent/solvent interactions) two dimensional solution of equal size solvent and solute molecules of area σ^o.

In comparison of the first case, adsorption of gases, and the second case, adsorption from solutions, one finds some differences. The lateral interactions, which are absent

in the first case, cancel out in the ideal solution layer because of being independent of composition. σ^o is a property of the solid lattice in the first case, while in the second it is a property of the adsorbed species. Fortunately, both versions lead to the same algebraic formula. Considering the surface concentrations as mole fractions, this adsorption can be written as:

A (solute in solution, N_2) + B (adsorbed solvent, N_1^s) = A (adsorbed solute, N_2^s) + B (solvent in solution, N_1)

The equilibrium constant of this reaction is

$$K = \frac{N_2^s a_1}{N_1^s a_2} \qquad 2.2$$

where a_1 and a_2 are the solute and solvent activities in solution. Based on the model, the activities in the adsorbed layer are given by the mole fractions N_1^s and N_2^s. In dilute solutions a_1 is constant and $N_2^s + N_1^s = 1$. Assuming $b = K / a_1$ equation 2.2 can be written as:

$$N_2^s = \frac{ba_2}{(1+ba_2)} \qquad 2.3$$

Moles of solute adsorbed per gram adsorbent can be expressed as $n_2^s = N_2^s\, n^s$, where n^s is the number of moles of adsorption sites per gram adsorbent, thus equation 2.3 can be written as:

$$n_2^s = \frac{n^s ba_2}{(1+ba_2)} \qquad 2.4$$

Substituting a_2 by C_2

$$\frac{C_2}{n_2^s} = \frac{1}{n^s b} + \frac{C_2}{n^s} \qquad 2.5$$

A plot of C_2/n_2^s against C_2 should give a straight line of a slope $1/n^s$ and Y- intercept of $1/n^s b$. n^s is a measure of the capacity of the adsorbent and the equilibrium

constant k is involved in the expression of b. k can then be further applied in the calculation of the free energy of adsorption as described in the next sub-chapters.

2.1.2. Thermodynamics of adsorption

Let us consider the basic thermodynamics functions that can describe the probability of a chemical reaction to happen as well as its heat inputs or outputs. In case of adsorption reactions these are the free energy of adsorption, the enthalpy of adsorption and entropy of adsorption. The free energy of adsorption or Gibbs function can be calculated directly from the value of the equilibrium constant K [2]:

$$\Delta G = -RT\ln K \qquad 2.6$$

The free energy is an expression of the tendency of a reaction to take place. Here, we can differentiate among three cases:

1. Negative value of the change in free energy, ΔG < 0: the reaction in this case is spontaneous.
2. Positive value of the change in free energy, ΔG > 0: the reaction is not spontaneous and, therefore, requires activation energy to pass the energy barrier.
3. ΔG = 0: the reaction reached equilibrium.

Thus adsorption needs a negative free energy difference to take place.

To determine the enthalpy of adsorption, the same set of experiments should be performed at different temperatures. The value of K is measured at each temperature and ln K is to be plotted versus 1/T as in equation 2.7, known as Van't Hoff equation to obtain ΔH_{ads}:

$$\frac{d\ln K}{d\left(\frac{1}{T}\right)} = -\frac{\Delta H_{ads}}{R} \qquad 2.7$$

The enthalpy of reaction is an expression of energy inputs or outputs. A negative enthalpy value indicates an exothermic reaction, a positive enthalpy value indicates an endothermic reaction.

Entropy of adsorption can then be calculated as well by:

$$\Delta G = \Delta H - T\Delta S \qquad 2.8$$

The basic definition of entropy is that it is a measure of the order of the system. A negative value of entropy change indicates that the translational or conformational freedom of the reactants has been reduced, and vice versa. Therefore, adsorption is always accompanied by negative entropy unless the adsorbate does not dissociate upon adsorption. Since spontaneous adsorption requires a negative free energy change and is always accompanied by negative entropy changes, it follows from equation 2.8 that ΔH must be negative, too.

2.1.3. Physisorption and chemisorption

Physisorption (an abbreviation of physical adsorption) involves the attachment of molecules to the surface by means of physical forces, in many cases through Van der Waal's interactions [2]. Energy released from a physisorption reaction is at the same order of magnitude as the enthalpy of condensation. Table 2.1 shows enthalpy values of some physiorbed molecules. In addition, physisorption does not involve any change of the chemical state of either the adsorbate or the adsorbent.

Table 2.1:

Enthalpy of physisorption [2]

adsorbate	enthalpy ($kJmol^{-1}$)
CH_4	-21
H_2	-84
H_2O	-59
N_2	-21

Chemisorption (an abbreviation of chemical adsorption) involves an adsorption process in which the adsorbate-adsorbent bond reaches the strength of an ordinary chemical bond and is accompanied by a change of the chemical nature of the adsorbate. Enthalpy of chemisorption can be distinctively differentiated from the enthalpies of physisorption as it is mostly higher by one order of magnitude (table 2.2).

adsorbate	adsorbent		
	Cr	Fe	Ni
C_2H_4	-427	-285	-209
CO		-192	
H_2	-188	-134	
NH_3		-188	-155

Table 2.2: Enthalpies of chemisorption ($kJmol^{-1}$) for different adsorbates on different adsorbents [2].

Thus the most distinguishable difference between physisorption and chemisorption is the enthalpy. Spectroscopic analysis of the adsorbed species can provide evidence that chemisorption is accompanied by a change of the chemical state of the adsorbate.

Infrared spectroscopy plays an important role in identifying the adsorbed species [3]. An example of that is the adsorption $^{15}N_2$ on a silica supported nickel substrate giving rise to a band at 2128 cm^{-1} which shifts to 2160 cm^{-1} if ^{14}N-^{15}N was adsorbed [4]. In a different experiment the adsorption of a mixture of CO and NO on various metal surfaces led to a band at 2260 cm^{-1} characteristic of chemisorbed isocyanate species M-NCO [5]. In that sense IR spectroscopy can also be used in reflection mode rather than in transmission through powder [6].

Other techniques like X-ray photoelectron spectroscopy (XPS), ultraviolet photoelectron spectroscopy (UPS) and electron stimulated desorption (ESD) can also be useful for identifying the adsorbed species [7].

The Langmuir isotherm has been considered as a fundamental isotherm for chemisorption, although it does not apply in some cases of chemisorption [3]. Some difficulties are confronted in special cases of lateral interaction or if dissociation occurs on adsorption. Other isotherms like Freundlich or Temkin isotherms can also be applied to chemisorption, however they have the problem that they might fit only quite well in the middle range of the adsorption isotherm. An example for that is the adsorption of nitrogen on iron powder which fits in the middle region of the adsorption isotherm to either the Langmuir, the Freundlich or to the Temkin equation [8].

2.2. Components of the system

2.2.1. Aluminum oxide

Aluminum belongs to the group III elements which are characterized by a semi vacant p-orbital. Aluminum has an atomic number of 13 and an electronic structure of Al^{13}: [Ne] $3s^2$, $3p^1$ [9]. Elemental aluminum is metallic; however it is still on the borderline between ionic and covalent character in its compounds.

Aluminum is widely found in nature as hydroxo oxide (bauxite) and as cryolite (Na_3AlF_6). Aluminum is hard and white in colour, highly electropositive, however resistant to corrosion because of a hard oxide film forming on the surface. If the protecting oxide film is overcome, for example by scratching or by amalgamation, rapid attack even by water can occur [9]. Under normal conditions, the metal is attacked by hot alkali hydroxides, halogens and various non-metals.

Aluminum usually undergoes chemical reactions in the trivalent state. Stoichiometrically, there is only one type of aluminum oxide, alumina Al_2O_3; however various polymorphs and hydrated species exist. There are two kinds of anhydrous Al_2O_3: α-Al_2O_3 and γ-Al_2O_3, distinguishable by differences in the lattice geometry. Oxide ions in α-Al_2O_3 form a hexagonally closely packed array in which the aluminum ions are symmetrically distributed. In contrast, γ-Al_2O_3 is characterized by a defect spinal structure. α-Al_2O_3 is very hard and resistant to hydration attacks by acids; γ-Al_2O_3 however takes up water readily and dissolves in acids. In chapter

2.2.3, which is related to humic acid, a brief review of the application of aluminum oxide as adsorbent in humic acid adsorption will be given.

2.2.2. Lanthanides, Gadolinium

Lanthanides are the fourteen elements in which the 4f level is being filled after the Lanthanum configuration. Therefore, they form a group of elements with similar chemistry. Lanthanum is the prototype element and hence came the name [9]. Lanthanides exist as oxide mixtures and are not really rare earth elements as they were called in old usage. In fact, they exist in quite large deposits in some places around the world. The most important mineral containing lanthanides is monazite, which is heavy dark sand of variable composition. All lanthanides form stable M^{+3} species; the oxidation states +2 and +4 are much less stable and, thus, are less in occurrence. Gadolinium is an element in the lanthanide group, its electronic structure can be written as Gd: [Xe]; $4f^7$, $5d^1$, $6s^2$, and its trivalent cation has the configuration $4f^7$ after Xenon.

The lanthanides in general have fewer tendencies to form complexes in comparison to the d-block transition elements, lanthanides complexes are especially build up with oxygen compounds. This is attributed to the unavailability of f orbitals to make up hybrid orbitals to form covalent bonds. Moreover, the radii of lanthanides are larger than those of transitions metals like Cr^{+3} and Fe^{+3}, which in turn decreases attraction by electrostatic forces. The most important complexes in case of lanthanides are the chelate ligand complexes. Chelate ligands forming water soluble complexes are hydroxo acids such as tartaric or citric acids and other amino acids as well.

Complexation of actinides, lanthanides and transition metals by humic materials is going to be discussed in the next chapter.

2.3.3. Humic acid

Humic substances are natural organic materials existing in soils and natural waters and are products of the long range degradation of living organisms and life matter in general [1,10]. An exact definition of humic substances in the last century was nearly

a scientific mystery and has, therefore, been the subject of a tremendous number of studies. Being of various chemical compositions, molecular structure and largely varying molecular weight and molecular weight distribution, attempts to exactly define humic substances were useless. Berzelius introduced this question in his publications about 200 years ago [10], and one of his students published a formula in 1840, $C_{40}H_{30}O_{15}$, proposing it to be the molecular formula of humic acid [11]. However, this was followed by several attempts of researchers everywhere coming up with the fact that a search for a universal molecular structure of humic acid is meaningless. A similar formula to what was published in 1840 appeared again as a general formula for humic acids [12], and has been accompanied by spectroscopic and analytical evidence (fig. 2.2) [12,13]. Moreover, different humic acid samples have been analyzed by MALDI-TOF MS (Matrix Assisted Laser Desorption/Ionization Time of Flight Mass Spectroscopy). The spectra show masses in the range of 100-200 kDa and a wide molecular weight distribution [12,14]. MALDI-TOF MS is a reliable technique for measuring molecular weights and giving a picture how the molecular weight distribution looks like.

However, due to the complexity of humic substances it is hard to define their structural parameters, a problem which is significantly easier to solve in case of regular synthetic or natural polymers.

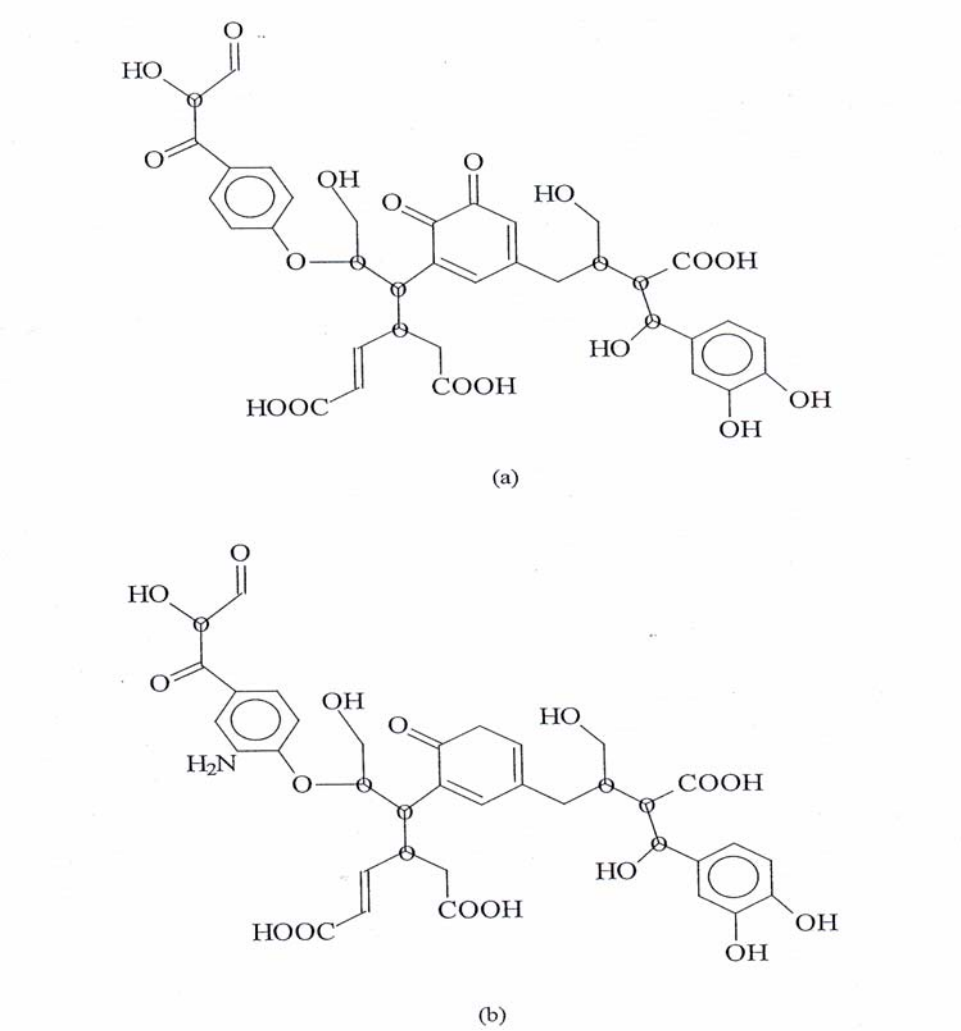

Fig. 2.2: Proposed molecular structures of (a) steelink and (b) TNB humic acid monomers showing chiral centres as open circles [12, 13].

2.3. Adsorption and complexation of humic acid by metal oxides

2.3.1. Binary system

Humic substances such as humic acid and fulvic acid are natural weak polyelectrolytes known for their activity toward metal ions [15-17]. This determines their great importance for the mobility and transport of ions, nutrients and contaminants in soils and aquifers [18-19]. Humic substances have strong affinity toward clay minerals and various metal oxides as well [20-21]. Adsorption of humic

acid and fulvic acid on metal oxides has been studied by various analytical methods and as a function of different variables such as pH, electrolyte concentration and the type of humic acid [22-27].

In the same way humic substances are believed to play an important role in the speciation and migration of radiotoxic cations, such as actinides, which is considered an essential aspect in the assessment of radioactive waste disposal [28-29]. In order to adequately understand the underlying processes, the reactions involved have to be characterized thermodynamically and kinetically with respect to interactions occurring between the three components: soil or clay minerals, humic substances and metal ions [30-32].

We are first going to consider the binary system, humic acid/clay minerals, focusing on selected physicochemical parameters and what are their effects on the adsorption process. Then, we move to the ternary system which involves humic acid, clay minerals and metal ions. The major factors that have been considered in humic adsorption are: humic concentration, pH and ionic strength. It has been proven that humic acid adsorbs on different minerals like alumina, silica, iron oxide and also on mixtures of these minerals [22-28].

The effect of humic concentration has been extensively studied. Typically, adsorption increases with increasing humic concentration, regardless of the metal oxide used [33-42]. Regarding pH, it has been reported that humic adsorption is maximum at low pH values starting from 3 and decreasing as the pH goes upwards until it vanishes at alkaline pH like 10 [38-42]. The effect of salinity or ionic strength has been studied as well. It suggests a mild ionic strength of about 0.1-0.5 M to enhance adsorption. Lower ionic strengths decrease adsorption tendencies, while higher ionic strengths lead to aggregation [43, 44].

The higher adsorption at acidic pH values was explained by the assumption that the adsorption is taking place mainly in the first step by electrostatic interaction as the deriving force [33,38,45]. In the theory of electrostatic interaction, the positively charged metal oxide is being attacked by the negatively charged organic acid. This condition is fulfilled in case of humic acid which, according to zeta potential

measurements, is negatively charged over the pH range 3-10, and clay minerals like alumina, which are positively charged in acidic medium. Thus, adsorption of humic acid on alumina is the strongest when alumina is at its maximum positive charge (lower pH), decreases as alumina is approaching its point of zero charge, at a pH about 8.7, and then tends to vanish as alumina starts to have partially negative charge.

The mechanism involved is believed to be, according to spectroscopic evidence [46], ligand exchange between the hydroxyl groups of the oxide surface and the oxygen of carboxylate group of humic acid. On the nature of binding of humic acid with minerals, FTIR analysis of the adsorbed species was done on natural organic materials (NOM) on hematite [47]. The results indicate that both carboxylic and hydroxyl groups are involved in binding. Similar results were shown in case of organic matter binding to goethite [48]. In another study on the adsorption of organic acids containing carboxylic or phenolic groups [47,49], it was found that compounds having carboxylic groups preferably adsorb at lower pH whereas those having phenolic groups adsorb in larger amount at alkaline pH. This actually is attributed to the nature of alkyl and the phenyl groups as the former is an electron withdrawing group while the later is electron giving group. Similar results were presented on the adsorption of catechol (carboxyl containing compound) and benzoic acid (phenol containing compound) on aluminum oxide [50]. Here the fact emerges that all metal oxides, that are actually positively charged compounds, act in the same way at low pH. However, it is the attacking organic functional group that is going to play the decisive role. Consequently, the role of the metal oxide on adsorption is only important at alkaline pH since it is no longer an electropositive entity.

In a study on the adsorption of compost leachate, which is supposed to contain humic acid [42], the spectra of the carboxylate groups were measured by means of infrared linear dichroism, which indicated that the carboxylate groups are not free to rotate. This rotation prohibition was interpreted by the author to be due to the bidentate of the carboxyl groups formed with a single adsorption site. In the same study, the enthalpy of adsorption was calculated by means of calorimetry to be 100 $kJmol^{-1}$. This high enthalpy value was also attributed to the fact that two or more carboxyl groups are coordinating to a single adsorption site.

Different studies to determine the adsorption isotherm and to define the adsorbed species in case of humic adsorption were carried out [51-54]. On a model surface consisting of amino-terminated polypyrole, XPS shows a chemical shift of the nitrogen peak, which can be fitted to yield - in addition to the sub peaks of NH and N - a new peak corresponding to N^+. Another shift was noticed for the NH_2 peak from the amino-coated surface, yielding a new sub peak corresponding to NH_3^+. From the adsorbed humic acid, the peak corresponding to COO^- was easily fitted in all of these studies. Therefore, the authors assumed a chemical binding via these species. In the same studies, humic adsorption on different model surfaces was found to fit well to a Langmuir isotherm as well as to a Freundlich isotherm.

2.3.2. Ternary system

In the following paragraphs, we shall consider the behaviour of the ternary system. The ternary system including clay minerals, humic acid and metal ions has been studied by different researchers all over the world. Experiments were done on lanthanides as well as on actinides. The valence of the metal ion varied among monovalent, divalent, trivalent and tetravalent. In different studies [55-59], the adsorption of metal ions on mineral oxides in presence of humic acid was reported to be enhanced at low pH and reduced at higher pH, which is in contrary to the case of metal ions alone in contact with minerals [58]. The latter behaviour is due to the variation of charging by variation of pH. At low pH, both the mineral surface and the metal ions are positively charged. While at alkaline pH, especially above the point of zero charge of the mineral (about pH 8.7 for alumina [60]), the charge of the mineral is inversed to be negative, the metal ions stay positive. Therefore, their sorption increases.

As an example of ternary systems, fig. 2.3 shows the sorption of a trivalent lanthanide, europium, and a trivalent actinide, americium, as a function of pH and ionic strength in presence and in absence of humic acid [28]. Some studies on the ternary system using Cu^{+2} [61] and Co^{+2} [62] concluded that the mechanism of sorption in the ternary system follows the additive approach, which means in short that the metal ions are to be added to humic acid and vice versa, hence the adsorbed product is additive. In the current example (fig. 2.3), the adsorption isotherm of the

ternary system (presented by triangles, circles and squares) and that of only the metal ion on hematite (represented by dashed lines), i.e. without humic acid, is plotted as a function of pH. In case of the ternary system and due to the existence of humic acid, the adsorption is maximum at lower pH (about 3) and decreases by increasing the pH, especially noticed in case of lower ionic strengths. This behaviour indicates that the existence of humic acid plays an important role in adsorption, since adsorption was enhanced at lower pH which is in favour of humic acid as discussed above. The opposite case is the adsorption of metal ions alone on hematite (both figures indicated by dashed lines). Here, adsorption is minimum at lower pH due to the absence of electrostatic attraction as a deriving force. It follows that the ion exchange mechanism between two positively charge entities is not possible. By raising up the pH, adsorption of metal ions increases since the surface is accumulating partial negative charges, and thus the electrostatic attraction is effective.

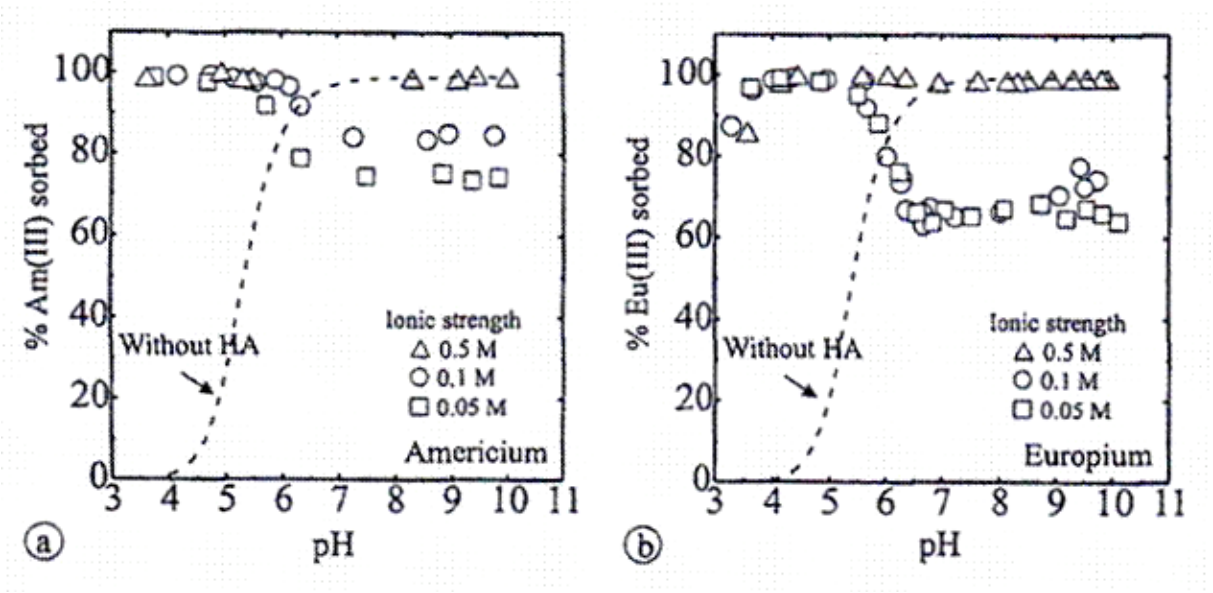

Fig. 2.3: Adsorption of Am^{+3} and Eu^{+3} on hematite as a function of pH and ionic strength. The dashed line represents the absence of humic acid, the triangles, circles and squares indicate ionic strengths of 0.5, 0.1 and 0.05 respectively.

Other studies on Am^{+3} and Cm^{+3} came up with the same result [59]. In general, the concentration and pH effects studied in ternary systems lead to the same conclusions regardless of the metals used and also for various minerals [56, 57, 63-66].

Recently, modern spectroscopic techniques have been applied to identify the adsorbed species and the interaction mechanisms involved. In a study on the adsorption of Cm^{+3} onto γ-Al_2O_3 using time resolved laser fluorescence spectroscopy (TRLFS) [67], it was proven that at lower pH the metal ion keeps its complete hydration sphere indicating outer sphere complexation. However, by increasing pH an inner sphere complex was detected. Also microscopy was applied to define the structure of adsorbed species. In a study of the ternary system Eu^{+3}/Humic acid/silica it was proven by AFM that binding of humic is stronger in the presence of Eu^{+3} by about one order of magnitude [68]. This effect favoured the hypothesis of polyvalent metal ion bridges which couple humic molecules to the surface of silica.

An essential difference between the adsorption on alumina and silica is that the former is electropositive at lower pH and its point of zero charge is observed at relatively alkaline pH, while the latter is more or less negatively charged even at low pH [69]. This leads to completely different adsorption phenomena, since both adsorption and binding of humic acid on alumina is obviously stronger. Therefore, researchers went to interpret the underlying mechanism in both cases to a chemical binding or coordination between the positive aluminum oxide and the negative humic acid, while in case of silica they favoured the Van der Waal's interaction and the diffuse double layer repulsion [28, 69-70].

Characterization techniques

2.4. Quartz Crystal Microbalance (QCM)

2.4.1. Acoustic wave sensors, TSM, QCM

Acoustic wave sensors are devices based on the piezoelectric properties of a crystal which allow the conversion of electric into acoustic signals and vice versa [71]. Acoustic wave sensors have different designs and constructions according to the sensor application. Among these designs are the thickness shear mode (TSM), the surface acoustic wave (SAW), the acoustic plate mode (APM) and the flexural plate wave (FPW) devices. The thickness shear mode (TSM) sensors are widely known as Quartz Crystal Microbalance (QCM). The sensor itself consists typically of an AT-cut quartz disc fig. 2.4. [72], in which the surface normal lies within the crystalline YZ plane and forms an angle of 37° 15` with the y axis. The quartz disc is sandwiched by two electrodes from the upper and lower side; the electrodes are connected to each other by contacts located at the side of the sensor.

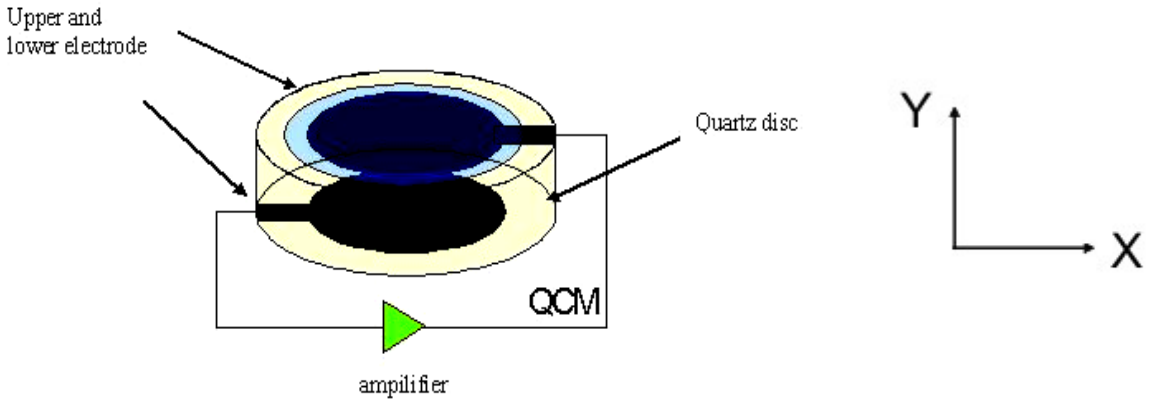

Fig. 2.4: Schematic drawing of the QCM sensor disc, indicating the quartz disc sandwiched between the upper and lower electrode. The whole sensor is connected to an electrical circuit. Shear waves are excited via the piezoelectric effect and propagate along the sensor thickness.

2.4.2. Working principle

Piezoelectricity plays the main role in the wave excitation and sensing mechanism of the QCM apparatus. Due to piezoelectricity; the application of an alternating voltage between the electrodes stimulates the excitation of shear waves at specific frequencies which propagate along the sensor thickness. The shear waves generate deformations in the sensor material with a displacement maximum at both electrodes, making the sensor sensitive to surface perturbations. Among these surface perturbations are the formation of an add layer, the contact with Newtonian fluids, and the formation of viscoelastic films [71].

The shear waves formed at each electrode are of opposite polarities. The displacement occurring, u_x, is then a superposition of these two waves:

$$u_x(y,t) = (Ae^{jky} + Be^{-jky})e^{j\omega t} \qquad 2.8$$

where A and B are constants, ω is the angular excitation frequency ($\omega=2\pi f$), k is the wave number ($k=2\pi/\lambda$), t denotes time, and j is $(-1)^{1/2}$. Once a wave hits the opposite surface, it will be reflected gaining a phase shift of π due to reflection. It then propagates in the other direction until it is reflected again with another phase shift of π. Resonance occurs if constructive interference of these shear waves takes place and a standing wave is formed. Thus,

$$h_q = N\left(\frac{\lambda_N}{2}\right) \qquad 2.9$$

$$\text{or} \quad f_N = \frac{N\,\nu_s}{2\,h_q} \qquad 2.10$$

where h_q is the thickness of the quartz disc, λ_N is the wavelength of the shear wave, f_N is the resonance frequency, N =1, 3, 5… the order of the mode, and ν_s the shear wave velocity, which is also defined as:

$$v_s = \left(\frac{\mu_q}{\rho_q} \right)^{1/2} \qquad 2.11$$

Here, μ_q is the shear stiffness and ρ_q is the mass density of quartz. Equation 2.9 defines the thickness of quartz to be a multiple integer of half the wavelength for resonance to occur, fig. 2.5 [71]. According to equation 2.10, the quartz resonator can be excited at a number of resonance frequencies corresponding to the value of N. The resonance frequency can be calculated from equation 2.9 and 2.10. E.g. an AT-cut quartz having ρ_q = 2.65 g/cm^3, μ_q = 2.95 x 10^{11} dyne/cm^2 and h_q = 0.033 cm would have a fundamental frequency f_1 of 5.06 MHz.

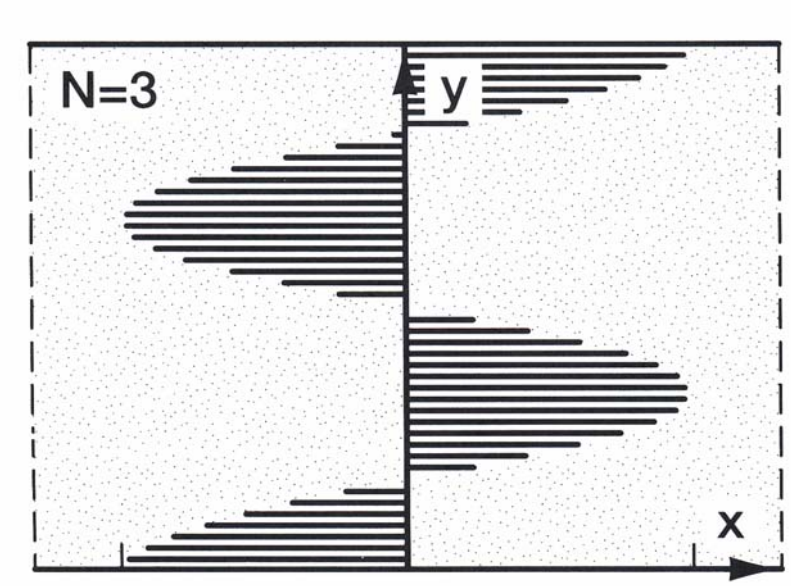

Fig. 2.5: Shear displacement profile along the quartz resonator of the third overtone number [71].

2.4.3. Mass sensitivity (Sauerbrey equation)

In 1959 G. Sauerbrey published a paper in the physics journal 'Zeitschrift für Physik', which is the basis of mass and thickness determination by TSM sensors until now [73]. The work of Sauerbrey resulted in establishing a relationship between the adsorbed mass and the frequency shift of the QCM sensor. According to Sauerbrey, adsorption of a film of thickness h_f is going to increase the thickness and the mass per unit area of the quartz crystal by Δh and Δm, respectively. Consequently, the new

thickness and mass would in turn affect the resonance frequency, and shift its value by Δ*f*:

$$\frac{\Delta f_N}{f_N} = -\frac{\Delta h}{h_q} = -\frac{\Delta m}{\rho_q h_q} \qquad 2.12$$

Substituting the value of h_q from equation 2.10, and the term f_N/N by the fundamental frequency f_1 yields:

$$\Delta f_N = -N \frac{2 f_1^2}{\nu_s \rho_q} \Delta m \qquad 2.13$$

This can also be written as $\Delta m = -C\Delta f_N / N$, where C is a constant. Considering an AT-cut quartz crystal with a fundamental frequency of 5 MHz, ρ_q = 2.65 g.cm^{-3}, and ν_s = 3340 m.s^{-1}, we obtain C = 17.7 ng.cm^{-2}.Hz^{-1}. Practically, the adsorbed mass in [ng.cm^{-2}] can be calculated directly by multiplying the frequency shift in its normalized form, $\Delta f_N/N$ in [Hz], N = 1, 3, 5..., occurring upon adsorption by the constant C, which is 17.7 ng.cm^{-2}.Hz^{-1}.

Prerequisites for applying Sauerbrey equation are the no-slip conditions [73], i.e. the adsorbed mass is rigidly attached to the resonating crystal. Since Sauerbrey´s studies, TSM sensors have been a widely used tool in identifying surface processes. In the beginning, TSM sensors were only applicable in vacuum, e.g. to the adsorption of gases. However, later on they have been developed to study a large number of surfaces and interface processes in liquids [74-76], such as lipid adsorption [77, 78] and protein adsorption [79].

2.4.4. Dissipation

Dissipation is a term related to the decrease of the amplitude of the propagating wave due to energy losses caused by the propagation medium [71]. Dissipation is the inverse of the quality factor Q [80], which is defined as the ratio of the total energy stored in the crystal and the energy dissipated upon oscillation [71]. Equation 2.14 presents the mathematical relation between Q and D [71, 80]:

$$D = \frac{1}{Q} = \frac{E_{dissipated}}{2\pi E_{stored}} \qquad 2.14$$

The amplitude of a sinusoidal wave decays exponentially with time upon propagation through a specific medium (fig. 2.6). The amplitude at time *t*, *A(t)*, can be written as:

$$A(t) = A_0 e^{-t/\tau} \sin(2\pi f t + \varphi) \qquad 2.15$$

where A_0 is the amplitude at time t=0, τ the decay time, and φ the phase angle.

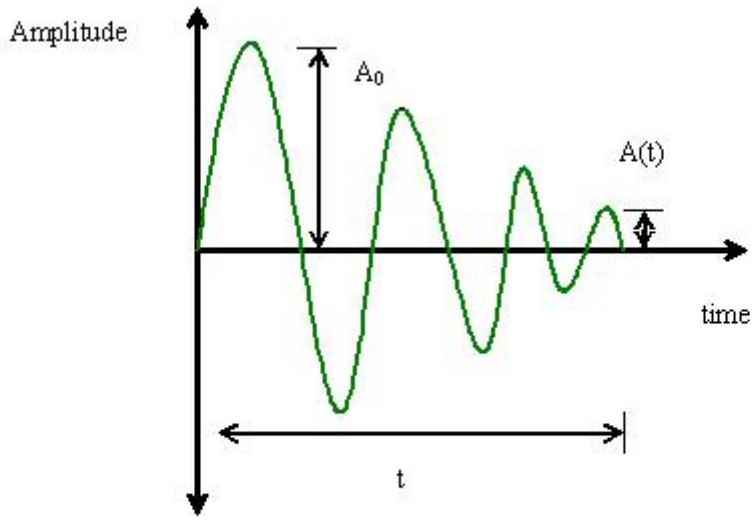

Fig. 2.6: schematic drawing of the exponential decay of a sinusoidal wave as a function of time.

Since dissipation is strongly dependent on the energy losses experienced in a certain medium, the decay time varies drastically with the physical properties of the medium of propagation. A practical example of that is the oscillation of the quartz crystal in air, where it oscillates freely. It takes a relatively long time until it loses its energy. In contrast, the oscillation decays much faster if the crystal is in contact with water. The same principle holds for other liquids of higher viscosity and density. Following the same argument, attachment of molecules to the surface may enhance the decay of the amplitude of oscillation, until theses molecules are once again removed from the

surface. In addition, viscoelastic effects can also change the oscillation frequency. Dissipation is inversely proportional to frequency [80], a relationship, which can also be derived from equation 2.14.

$$D = \frac{1}{\pi f \tau} \qquad 2.16$$

In practice, the quartz crystal is excited by application of an alternating voltage (sequence of on- and off-pulses) which induces the acoustic wave. The crystal starts oscillating and experiences some bulk or surface effect which in turn affects the frequency and the amplitude of oscillation. By recording the output signal and fitting it numerically to equation 2.15, we are able to monitor frequency and dissipation simultaneously.

Knowledge of the value of dissipation is essential for calculating the adsorbed mass by the Sauerbrey equation, since Sauerbrey requires no slip conditions, i.e. dissipation should be approaching zero. This condition is actually only fulfilled, as seen in the results and discussion section, in case of rigidly attached monolayers without internal viscoelasticity. Therefore monitoring dissipation provides additional fruitful information about the nature of the adsorbed film. A soft film containing high ratio of the solvent would show behaviour similar to that of the bulk of the solution. A rigidly adsorbed film, however, would follow the oscillation without phase lag or slip, since it is strongly bound to the surface. Thus it will cause very little dissipation.

2.4.5. In contact with liquid

Upon contact with liquid the oscillation of the quartz crystal is going to be affected by the new conditions, mainly the viscosity and density of the fluid. Figure 2.7 presents a sketch of the oscillation of a quartz sensor with one side in contact with liquid [71].

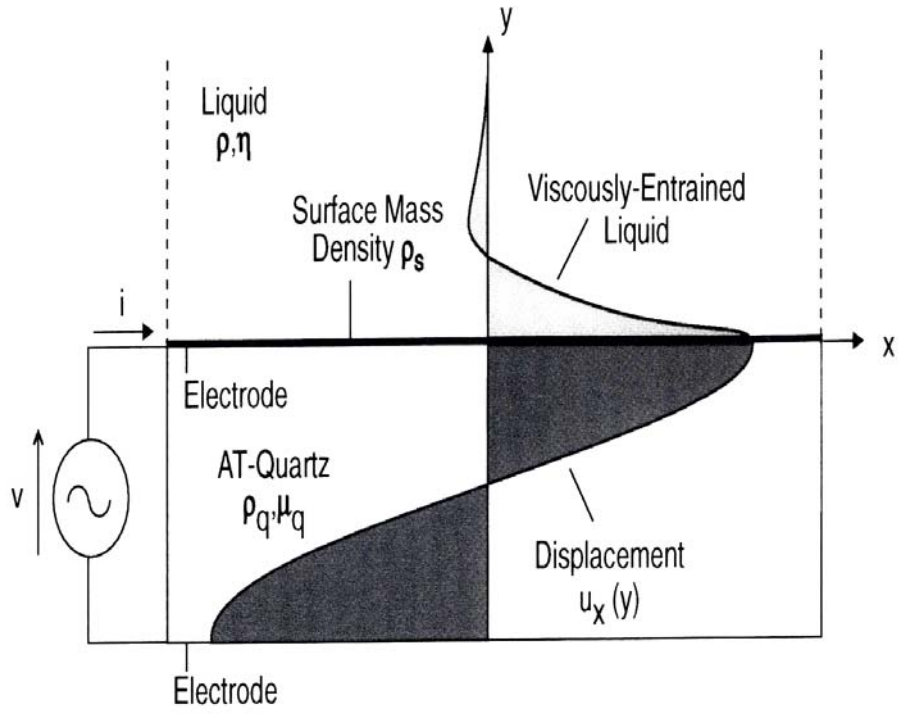

Fig. 2.7: Cross-sectional view of a TSM resonator. The application of alternating voltage excites the quartz sensor causing displacement U_x. The shear wave propagates along the sensor in y-direction passing through the adsorbed film of a certain mass density ρ_s. A decaying acoustic wave field extends into the liquid in contact with the sensor [71].

Both frequency and dissipation are going to vary according to the new conditions. Evidently they will show a dependency of the density and viscosity of the contacting liquid, ρ_l and η_l, respectively. The frequency dependence, equation 2.17, was introduced for the first time by Kanasawa et al [81], the dissipation dependence, equation 2.18, was obtained from another source [82,83].

$$\Delta f = \sqrt{\frac{f_0^3}{\pi \mu_q \rho_q}} \sqrt{\eta_l \rho_l} \qquad 2.17$$

$$\Delta D = \frac{1}{\sqrt{\pi f_0} h_q \rho_q} \sqrt{\rho_l \eta_l} \qquad 2.18$$

Yang and Thomson [84] reported on the contribution of fringing electric fields to the frequency response, in a so-called acoustoelectric coupling, of a TSM sensor in

contact with one side to liquid. Acoustoelectric effects are proposed to occur at the quartz crystal surface in contact with a conducting liquid. The mechanism of acoustoelectric effects is assumed to be as follows [84]: the propagating acoustic wave in quartz generates charges on the surface because of the induced electrical polarization. Thus, an external electric field associated with the acoustic wave is formed at the crystal surface. If the quartz crystal gets in contact with a conducting liquid, the external field will interact with the ions of the solution resulting in changes in the storage and dissipation of electrical energy which in turn affects the frequency response of the quartz sensor. Equation 2.19 gives the value of frequency shift due to acoustoelectric coupling. The frequency shift depends on the conductivity and dielectric constant of the solution in contact with the sensor.

$$\frac{\Delta f}{f_0} = \frac{K^2}{\pi^2} \frac{\varepsilon_s}{\varepsilon_s + \varepsilon_1} \frac{\sigma^2}{\sigma^2 + \omega^2 (\varepsilon_s + \varepsilon_1)^2} \qquad 2.19$$

where K^2 is the electromechanical factor with a value of 3.4×10^{-3} [84] for AT-cut quartz, σ is the conductivity of the liquid, ε_s is the dielectric constant of quartz, ε_s = $4.55\,\varepsilon_0$, where ε_0 is the dielectric constant of air with a value of 8.854×10^{-12} F.m^{-1} [85], ε_1 is the dielectric constant of the liquid in contact with the quartz crystal.

2.4.6. Viscoelastic films

Viscoelastic films are films having their own viscosity and elasticity, these two physical properties can be expressed in the combined term of viscoelasticity. Due to viscoelasticity, these films, when adsorbed on the quartz sensor, cannot follow the oscillation of the sensor, in comparison to a rigidly attached film, and thus the sensor will experience a higher dissipation. Consequently the adsorption of these viscoelastic films on the quartz sensor is going to impose its own viscoelastic effect on the frequency and dissipation of the oscillating sensor in a way that the simple dependence in equations 2.17 and 2.18 is not valid anymore. In that case, other terms such as the shear viscosity coefficient η and the shear elasticity modulus μ of

the adsorbed film have to be considered in order to calculate the corresponding frequency and dissipation shifts.

Vionova et al [86] constructed a model (fig. 2.8) to describe the adsorption of viscoelastic films on the TSM quartz sensor and succeeded in finding the corresponding frequency and dissipation shifts by applying the Voigt model of viscoelasticity to that system. The Voigt model considers a viscoelastic system consisting of a spring and dashpot in parallel. The response of that system to a shear stress is a combination of elastic and viscous responses of the spring and the dashpot, respectively. Further analysis follows by deriving a general solution of the wave equation of a bulk shear wave propagating in a viscoelastic medium assuming the no slip conditions. In the current case, the model consists of two viscoelastic films adsorbed on the surface of the quartz crystal. The upper film is in direct contact to the bulk liquid.

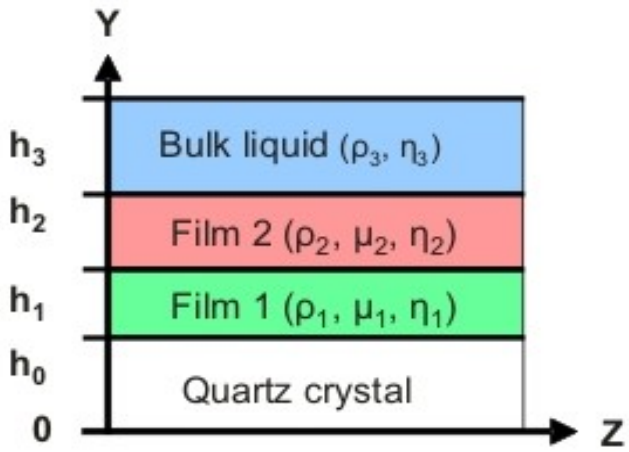

Fig. 2.8: The viscoelastic model as assumed by Vionova, consisting of two adsorbed viscoelastic films on the quartz sensor and in contact with the bulk liquid. Each film has its own density, shear viscosity and shear elasticity.

Equations 2.20-2.22 are the mathematical expressions for the frequency and dissipation shifts according to Vionova.

$$\Delta f \approx \frac{1}{2\pi\rho_0 h_0}\left\{\frac{\eta_3}{\delta_3} + \sum_{j=1,2}\left[h_j\rho_j\omega - 2h_j\left(\frac{\eta_3}{\delta_3}\right)^2 \frac{\eta_j\omega^2}{\mu_j^2+\omega^2\eta_j^2}\right]\right\} \qquad 2.20$$

$$\delta_j = \sqrt{\frac{2\eta_j}{\rho_j \omega}} \qquad 2.21$$

$$\Delta D \approx \frac{1}{2\pi f \rho_0 h_0}\left\{\frac{\eta_3}{\delta_3} + \sum_{j=1,2}\left[2h_j\left(\frac{\eta_3}{\delta_3}\right)^2 \frac{\mu_j \omega}{\mu_j^2 + \omega^2 \eta_j^2}\right]\right\} \qquad 2.22$$

ρ_0 and h_0 are density and viscosity of quartz, indices 0,1, 2 and 3 are for quartz, viscoelastic film 1, viscoelastic film 2 and bulk liquid, respectively. η is the shear viscosity coefficient, μ the shear elasticity modulus, δ the viscous penetration depth defined in equation 2.21, and ω the angular velocity.

Practically, the model developed by Vionova is integrated in the Q-tool software obtained from the company q-sense. It will be described in the results and discussion section that the viscoelastic model must only be applied in case of viscoelastic films of high dissipation values. In case of thin rigidly adsorbed films with little dissipation, application of the model yields the same results as the Sauerbrey equation. To test the validity of equations 2.20 and 2.22 we assume two different cases; the first case considers a rigidly adsorbed film which is not affected by the bulk properties, the second case considers the sensor in contact with a viscous liquid without adsorbed films in between. In the first case every term concerning the second film or the bulk liquid will equal zero and hence we come up with these mathematical expressions for Δf and ΔD:

$$\Delta f \approx \frac{\rho_1 h_1 f_0}{\rho_0 h_0} \quad \text{or} \quad \Delta f \approx \frac{f_0}{\rho_0 h_0}\Delta m \qquad 2.20`$$

$$\Delta D \approx 0 \qquad 2.22`$$

Equation 2.20` is actually Sauerbrey equation, see equation 2.12, and equation 2.22` means that dissipation should be zero as a prerequisite of applying Sauerbrey in calculating adsorbed masses.

In the second case every term concerning the first and second adsorbed films cancel which results in these expressions of Δf and ΔD:

$$\Delta f \approx \frac{1}{2\rho_0 h_0}\sqrt{\frac{\rho_3 \eta_3 f_0}{\pi}} \qquad 2.20``$$

$$\Delta D \approx \frac{1}{\rho_0 h_0}\sqrt{\frac{\rho_3 \eta_3}{\pi f_0}} \qquad 2.22``$$

Equations 2.20`` and 2.22`` are the mathematical expressions for frequency and dissipation shifts for a QCM quartz sensor in contact with a viscous liquid. Equation 2.20`` has a quite different form than equation 2.17 however they yield the same numerical values.

2.5. X-ray Photoelectron Spectroscopy (XPS)

2.5.1. Principle

Since the discovery of the photoelectric process at the beginning of the twentieth century, its application in surface analysis has been the subject of intensive developing and optimization processes [87]. It was first recorded in the year 1954 that the Swedish group of Siegbahn has operated a high resolution electron spectrometer for low energy electrons generated by X-ray excitation [88]. In 1958 the same group reported the appearance of photoelectron peaks which are attributed to specific electronic structures and which made it possible to use X-rays for chemical analysis. Shortly later it was discovered that distinguishable peaks appear for metals and their oxides, which was known as chemical shifts, and established the use of XPS in surface characterization

The basic principle of XPS originates from the ionization of the target atom by a high energy photon, X-ray photon, which results in the excitation and ejection of one core level electron (fig. 2.9). The ejected electron, called also photoelectron, reaches the detector; where its kinetic energy, *KE*, can be measured. As the energy of the incident photon, $h\nu$, is known, the binding energy, *BE*, of the ejected photoelectron can be calculated as:

$$KE = h\nu - BE \qquad 2.23$$

Determination of the binding energy of the photoelectron has its significance. Considering the electronic structure outward of the nucleus we realize that the binding energy increases in the direction of the nucleus and hence each electron in a specific orbital is characterized by a certain binding energy. Accordingly, on the atomic scale, the core level electrons of a specific atom have individual binding energies, depending on the charge of the nucleus. However in multi-electron systems, the individual energy levels do not only depend on the charge of the nucleus but on many parameters, e.g. electron spin, orbital angular momentum and others which differs significantly according to the atom. Thus, it becomes possible to identify these atoms.

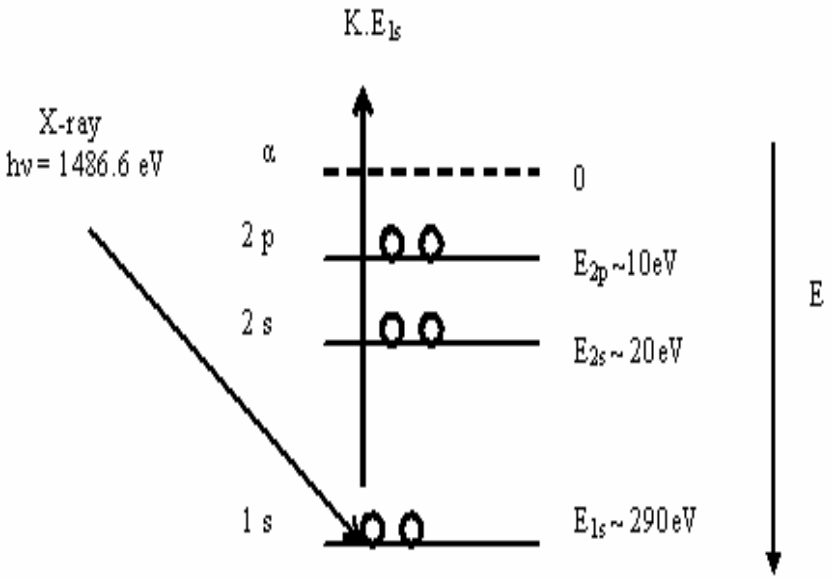

Fig. 2.9: An incident photon of sufficiently high energy can eject a photoelectron from the core level electrons outside the atom. The binding energy of each orbital is different and increases in the direction of the nucleus.

Typical photon energies used in commercial X-ray spectrometers are 1486.6 eV (Al K_α) and 1254 eV (Mg K_α). Noticeable is the variation of the peak intensities of certain atomic spectra, since the probability of photoelectron ejection differs according to the orbital. This is known as the photoionization cross section. Taking carbon as an example, the cross section for the 1s level is larger than that of the 2s and 2p levels. Thus, the peak intensity of the 1s level is the largest.

2.5.2. The chemical shift

The photoelectron peaks appearing in XPS spectra take sometimes different positions than usual, or in other words, their binding energy can be shifted. The reason of that shift is attributed to the change of the electronic environment around the core electrons by varying the atoms or functional groups around the atom to be excited. Therefore, this effect is called “chemical shift”. Figure 2.10 shows an interesting case of chemical shift, taken from the spectra of polyethylene terephthalate which is a common polymer for industrial applications [88]. The spectrum on the right is the carbon 1s spectrum. However, it does not appear as a single peak but shows different subpeaks due to the chemical shift.

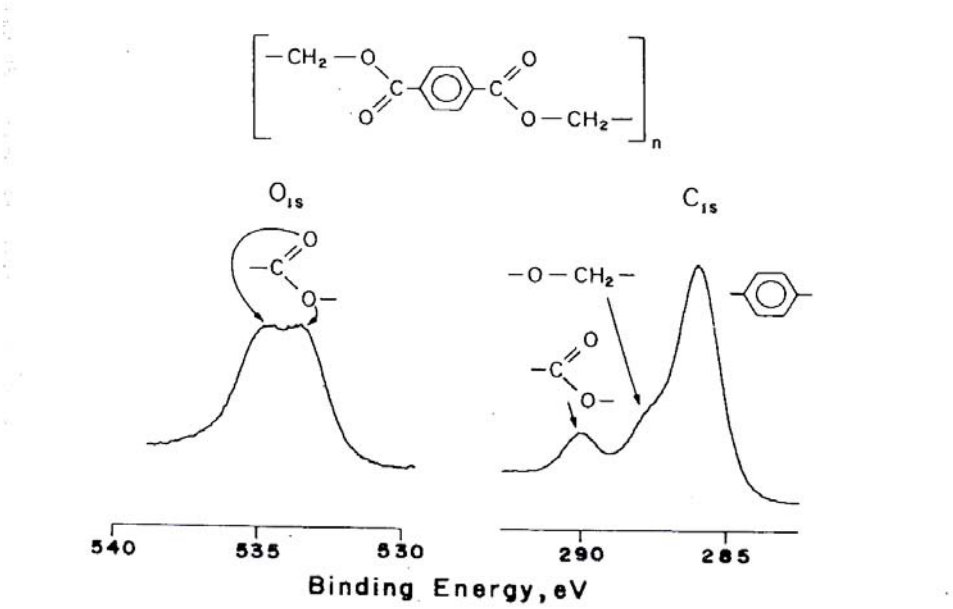

Fig. 2.10: Spectra of carbon (right) and oxygen (left) of polyethylene terephthalate. The spectra appear as multipeaks due to the chemical shift. One can distinguish between the carbon of benzene ring, methelene carbon and ester carbon, and also between the single and double bond oxygen atoms of the ester group [88].

The chemical shift is due to the different electronic environment around the atom, as there are different types of carbon atoms. Each of them appears at a different position in the spectrum. Electronegativity is the reason of this chemical shift. The more electronegative the group attached to the carbon atom, the more withdrawn are the carbon electrons by that group, thus, enhancing the binding of the core level electrons by the positively charged nucleus. Consequently, we find that the C1s peak of the ester carbon atom appears at the highest binding energy in fig. 2.10, since it is

bound to the most electronegative group, while the ester methylene group appears at lower binding energy, and an even lower binding energy is observed for the benzene carbon. The same argument holds for the oxygen atoms of the ester group (fig. 2.10 left). The double bond oxygen atom is experiencing high electronegativity attributed to the double bond and, thus, it appears at higher binding energy than the single bond oxygen of the same ester group. Chemical shift is an important feature of XPS spectra as it helps us to differentiate between the different functional groups and, thus, plays a key role in surface characterization by XPS.

A different case of chemical shifts is the shift to higher binding energy in inorganic elements upon oxidation. The shift is often about 1 eV for one oxidation unit [88]. The reason of that chemical shift is the decrease of the negative charge around the atom due to oxidation and loss of electrons, which in turn increases the nucleus effect on binding the core electrons giving them higher binding energy. An example for that kind of chemical shift is aluminum oxide. Since aluminum is always covered by its oxide layer, Al_2O_3, it appears always as a doublet, where the peak of higher energy is for the oxide and that of lower energy is for neutral aluminum underneath (fig. 2.11). The sharpness and intensity of the peaks depend on the thickness of the oxide layer.

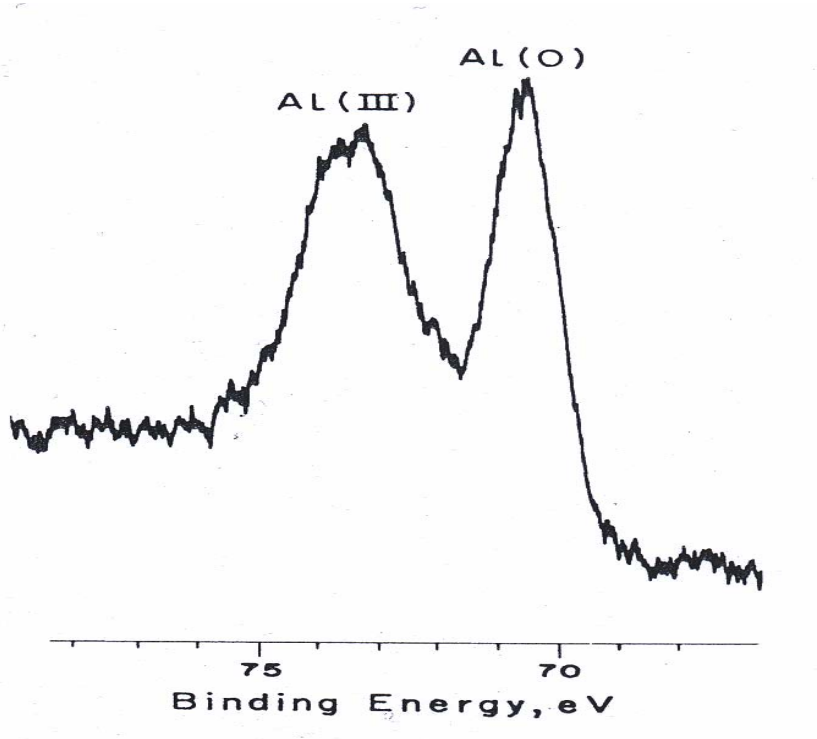

Fig. 2.11: Spectrum of aluminum oxide appearing as a doublet because of oxidation. The peak at higher binding energy represents the top layer of aluminum oxide, Al^{+3}, and that at lower energy the neutral aluminum, Al^{0}, underneath.

2.5.2. Spin-orbital splitting

Another phenomenon of XPS spectra is the appearance of doublets or split peaks in elements, what is known as spin-orbital splitting. After ejection of the photoelectron, leaving an unpaired electron in the core level, this unpaired electron tends to couple with the angular momentum (*l*) of the orbital. Since the electron has the spin number either (+1/2) or (-1/2) there are two possible quantum states as a result of this coupling: (*l* + [1/2]) and (*l* - [1/2]). E.g. the 2p orbital (*l* = 1) is split into $2p_{1/2}$ and $2p_{3/2}$, the 3d orbital (*l*=2) into $3d_{3/2}$ and $3d_{5/2}$. Figure 2.12 shows the spectra of palladium and its oxide. In this special case, there is a doublet of doublet: a first doublet because of the spin-orbital splitting to $3d_{3/2}$ and $3d_{5/2}$, and a second because of a chemical shift due to oxidation [88].

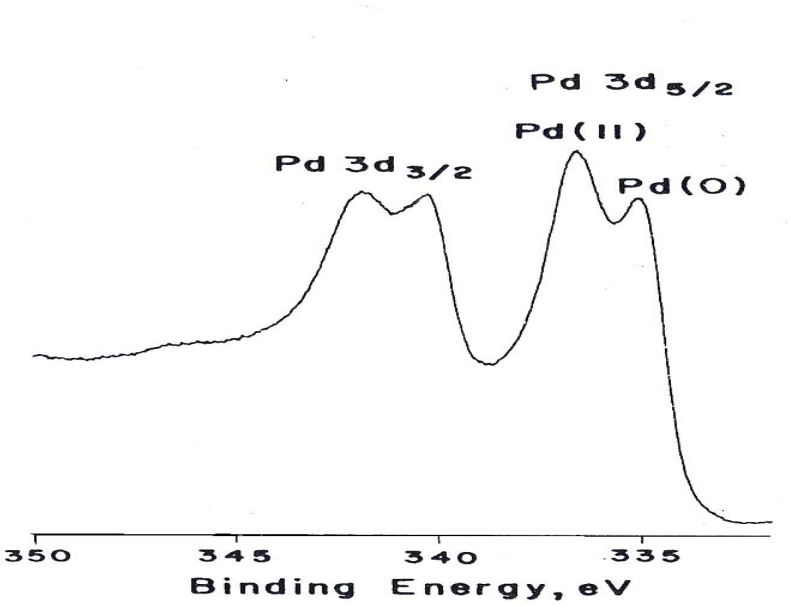

Fig. 2.12: Spectra of palladium and its oxide showing a special case of a doublet of doublet. The first doublet is due to spin-orbital splitting while the other is due to a chemical shift upon oxidation.

2.5.4. Thickness determination

Let us consider Lambert-Beer´s law, which describes the absorption of light passing through a liquid sample of width d [2]:

$$I = I_0 \, e^{-\varepsilon c d} \qquad 2.24$$

where I is the refracted intensity, I_0 is the incident intensity, c is the solution concentration, ε is the absorption coefficient, and d is the pathway length in the solution. The same concept can be applied in case of X-ray photoemission (fig. 2.13) [89], by substituting the inverse product of concentration and absorption coefficient with the inelastic mean free path (λ) of the photoelectrons emitted from the sample: [90-91]:

$$I = I_0 e^{-d/\lambda\cos\theta} \qquad 2.25$$

or

$$d = \lambda\cos\theta \ln\frac{I_0}{I} \qquad 2.25`$$

Here, I is the peak intensity of the substrate with an adsorbed film of thickness d, I_0 is the peak intensity of the bare substrate, i.e. without adsorbed film, λ is the inelastic mean free path, λ=31 Å for aromatic adsorbates [90], and θ is the angle between direction of the emitted electrons and the surface normal, fixed in this study at 0°.

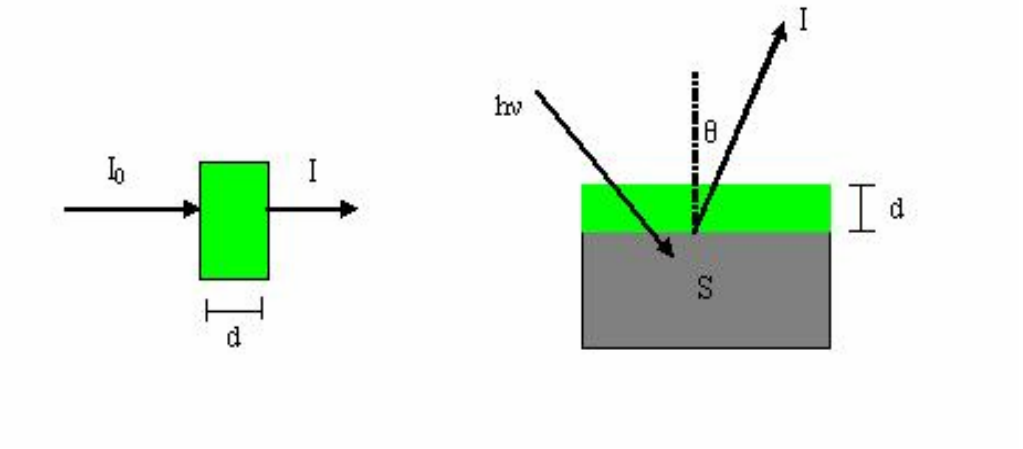

Fig. 2.13: The application of Beer's-Lambert law for the transmitted light from a sample of width d, left, can be used to calculate the thickness of an adsorbed film in XPS measurements, right, by introducing the mean free path term (λ).

2.6. Ellipsometry

2.6.1. Principle

Ellipsometry is an optical technique known since the sixties of the twentieth century, it has been developed in the last five decades to include various setups and to serve in a variety of applications. We are going here to introduce briefly the basic principles of ellipsometry, the quantities measured and how they can be correlated to the thickness of a thin film.

Ellipsometry measures the change in the polarization state of a polarized light beam after being reflected at a planar surface. In figure 2.14, a linearly polarized light beam is incident on a planar surface at a certain angle of incidence φ, and then being reflected leaving the surface with a change in the polarization state from linear to elliptical polarization [92]. Light is a transverse electromagnetic wave, a linearly polarized light consists of two components lying in two planes which are perpendicular to each other and perpendicular to the direction of propagation. These components are defined as the p-plane (parallel) and the s-plane (perpendicular). Both components are going to be reflected differently giving rise to a change in the polarization state of the reflected beam.

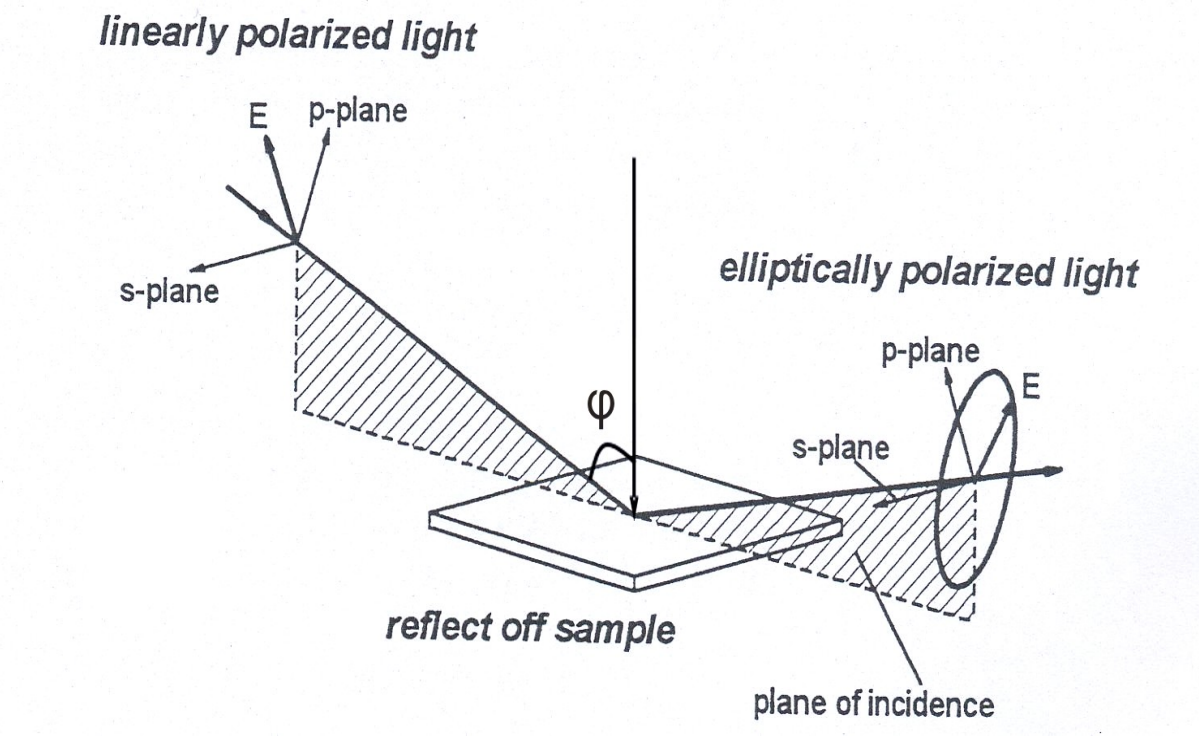

Fig. 2.14: A linearly polarized light beam with its two components, the s-component and the p-component, lying in the s-plane and p-plane. The two components are perpendicular to each other and to the propagation direction. The beam is incident at angle of incidence φ and then reflected experiencing a change in its polarization state.

2.6.2. Measured parameters

To define the parameters measured by ellipsometry we should first consider the case of an incident beam reflected by a thin film. In figure 2.15, a film of thickness d and refractive index N_2 is on top of a substrate of refractive index N_3 and in contact with air (refractive index N_1). A polarized beam is incident at an angle ϕ_1 with respect to the surface normal. The incident light beam is reflected or transmitted at the different interfaces. Angles of refraction are ϕ_2 for the air/film and ϕ_3 for the film/substrate interface. The various reflected waves add up to yield the total reflected beam, which is analyzed.

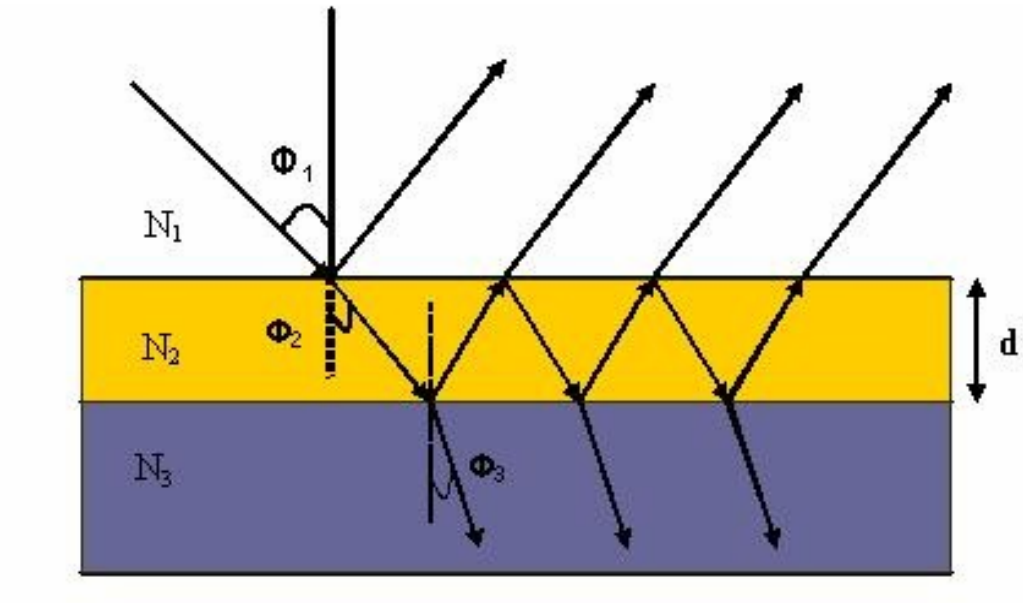

Fig. 2.15: Reflection of a polarized light beam by a thin film on top of a substrate. There are two interfaces at each of which the beam experiences reflection and refraction (transmission). A family of reflected and transmitted beams is generated as illustrated.

The reflectivity coefficients R^p and R^s for the p- and s-polarized light are given by the Airy formula [92]:

$$R^p = \frac{E_r^p}{E_0^p} = \frac{r_{12}^p + r_{23}^p e^{(-2ib)}}{1 + r_{12}^p r_{23}^p e^{(-2ib)}} \qquad R^s = \frac{E_r^s}{E_0^s} = \frac{r_{12}^s + r_{23}^s e^{(-2ib)}}{1 + r_{12}^s r_{23}^s e^{(-2ib)}} \qquad 2.26$$

$$b = \frac{2\pi d}{\lambda} N_2 \cos\phi_2 \qquad 2.27$$

where E_r and E_0 are the amplitudes of the incident and reflected waves, and r_{12} and r_{23} are the Fresnel coefficients for interfaces 1 and 2, respectively.
The Fresnel coefficients are given by:

$$r_{12}^p = \frac{N_2 \cos\phi_1 - N_1 \cos\phi_2}{N_2 \cos\phi_1 + N_1 \cos\phi_2} \qquad r_{12}^s = \frac{N_1 \cos\phi_1 - N_2 \cos\phi_2}{N_1 \cos\phi_1 + N_2 \cos\phi_2} \qquad 2.28$$

Ellipsometry measures the relative reflection, $\tan\psi$, and phase shift, Δ, of the s- and p-polarized light.

$$\tan\psi = \frac{\left|R^p\right|}{\left|R^s\right|} \qquad 2.29$$

$$\Delta = \delta_p - \delta_s \qquad 2.30$$

δ_p and δ_s are expressions for the absolute phases of the p- and s-components, respectively. ψ and Δ are also called the ellipsometry angles. They are combined to a complex number in the fundamental equation of ellipsometry

$$\rho = \frac{R^p}{R^s} = \tan\psi e^{i\Delta} \qquad 2.31$$

which is practically the outcome of every ellipsometry measurement.

2.6.3. Cauchy model

To measure the film thickness d we still need to determine the refractive index of the thin film and the angle of incidence. In a typical ellipsometry measurement performed at different wavelengths (spectral ellipsometry), a substrate of known optical constants is used in a first calibration step, in which the measured data of that substrate can be fitted to a previously given optical constants of that substrate to obtain the angle of incidence. The angle of incidence should then be kept constant for measuring the thickness of the thin film of interest. The Cauchy model defines the relation between the wavelength of an incident beam and the refractive index of the medium, in which the beam propagates [92]:

$$n = n_0 + \frac{A}{\lambda^2} + \frac{B}{\lambda^4} \qquad 2.32$$

Here, *n* is the refractive index of the medium of transmission (here the thin film), n_0 the refractive index for high wavelengths, λ the wavelength of the incident light beam, and *A* and *B* are constants known as Cauchy coefficients.

3. Experiments

3.1. Materials

- Humic acid: Gohy-573 obtained from the German “Gorleben” underwater.
- Sodium hydroxide: NaOH, 1 mol/l volumetric solution, VWR.
- Perchloric acid: $HClO_4$, solution, concentration of 70-72%, J.T. Baker.
- Sodium perchlorate monohydrate: $NaClO_4.H_2O$, solid, pro analysis, Merck.
- Gadolinium chloride hexahydrate: $GdCl_3.6H_2O$, solid, purity 99.9%, Alfa Aesar.
- Aluminum chloride hexahydrate: $AlCl_3.6H_2O$, solid, Molekula.
- Tridecanoic acid: $CH_3\ (CH_2)_{11}COOH$, solid, purity ≥ 98%, Aldrich.
- Ethyl alcohol: C_2H_5, absolute, Riedel de Haen.
- Water: Millipore water, electrical resistance of about 18 MΩ/cm, MilliQ-plus.
- Hydrogen peroxide: H_2O_2, 30%, J. T. Baker.
- Ammonium hydroxide: NH_4OH, solution, 25%, J. T. Baker
- Buffer pH 6.8 and pH 9.1, WTW.
- Sodium dodecyl sulphate: solid, J. T. Baker.
- Iodine solution: self-prepared, 5% KI/I_2 solution.
- Hellmanex: alkaline solution of pH 11.7 at a concentration of 1%, Fluka.
- Aluminum target: pure aluminum bought from Oerlikin Balzers, Lichtenstein.
- Tungsten boats: bought from Leybold Optics GmbH.

Laboratory Equipment

- Magnetic stirrer
- pH meter: pH 540 GLP, WTW.
- Ultrasonic bath with temperature control
- pH stripes: different pH ranges, Merck
- UV lamp: inside a hood in air, power 150 Watt.
- Plasma irradiation: in oxygen atmosphere at a pressure 0.4 mbar, and a power of 150 watt, TePla100E plasma system
- Immersion glasses: transparent, diameter 25 mm, height 50 mm.
- Glass cutter

- Tweezers of different shapes
- Para film
- Gloves

3.2. Optimization of the aluminum oxide sensor

As illustrated in chapter 4.2.2, the commercially available aluminum oxide-coated quartz sensors did not show sufficient stability if exposed to salt containing or acidic liquids. Improved techniques for the fabrication of aluminum oxide coated quartz sensors and aluminum coated wafers were developed at our institute thanks to the efforts of Dipl.-Phys. Georg Albert. Aluminum oxide coatings were fabricated following two pathways, sputtering and thermal evaporation, in order to obtain optimum stability. In the next subchapters we are going to describe in short the methodology by which the coating process was carried out, Specific physical and technical description are found in reference [93].

3.2.1. Sputtering

The sputtering setup consists of the metal substrate to be coated, the aluminum target of pure aluminum bought from Oerlikin Balzers, Lichtenstein. The vicinity in between is filled by argon. The aluminum target is to be connected to the cathode and the substrate to the earth (voltage 0 V), a high voltage of 1000 V is applied at the aluminum target which generates a current of 500 mA (fig. 3.1). Under this high voltage and at an argon gas pressure of about 3-6 x 10^{-4} mbar, plasma will be created. The argon ions are going to bombard the aluminum cathode resulting in releasing aluminum atoms from the target. The flying aluminum atoms are carried by the argon ions and directed to the earth connected substrate, where they will be condensed and thus the aluminum coating is obtained.

Sputtering of aluminum is followed by flushing oxygen in the sputtering unit in order to oxidize the aluminum coated substrate to generate the aluminum oxide upper layer. Prior to aluminium sputtering, a titanium layer is deposited which acts as an adhesion promoter. During this process, the pressure in the chamber is about 10^{-6} mbar.

Various thicknesses can be achieved by sputtering. The first attempt was to obtain a thickness of 150 nm aluminum which was then reduced to 50 nm to reduce the surface roughness. This was the typical thickness chosen to coat quartz sensors as well as the silicon wafers. The silicon wafers had the dimensions of about 100 mm diameter and 1000 µm thickness. Worth to mention is that the quartz sensors have an upper electrode which is typically gold. However, sensors with silicon oxide electrodes were also used in the studies for optimization purposes.

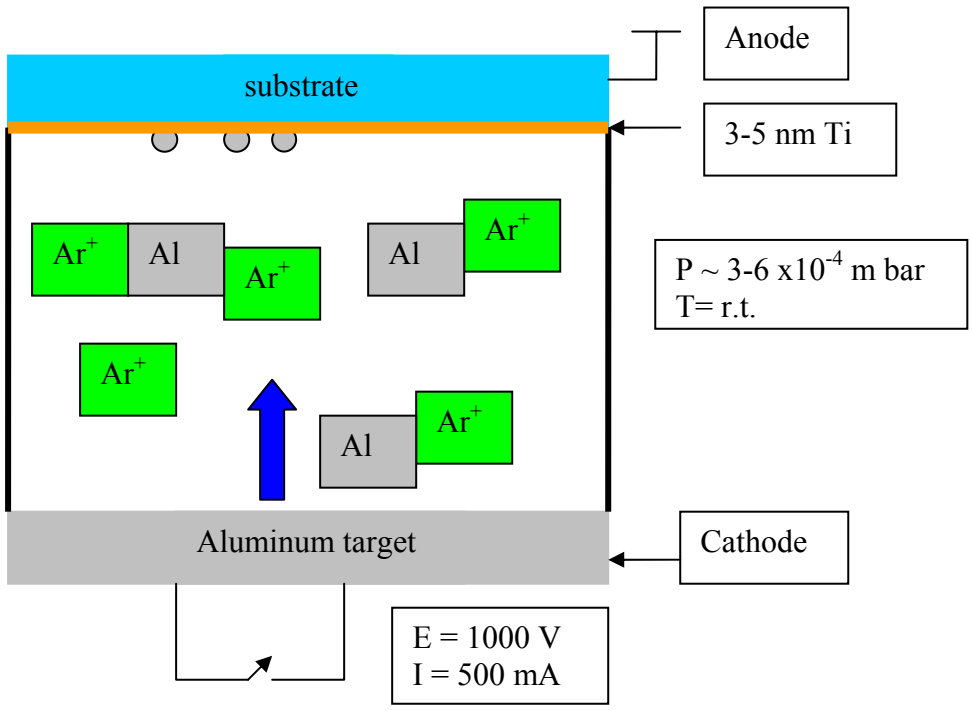

Fig. 3.1: Schematic drawing of the sputtering process of aluminum. By application of a high voltage, plasma is created. The argon ions will bombard the target releasing aluminum atoms, which will be carried by the argon ions and then deposited on the substrate (anode).

3.2.2. Thermal evaporation

The thermal evaporation setup involves the substrate to be coated in addition to the so-called tungsten boat in which the coating raw material is placed (fig. 3.2). Tungsten boats were bought from Leybold Optics GmbH, Germany. Tungsten is a metal whose physical properties allow it to be illuminated upon passage of electrical current without being burnt. Therefore, it has been used for a long time in lighting industry. The driving force in thermal evaporation is the passage of electric current through the tungsten boat which in turn heats and evaporates the raw aluminum. Aluminum travels through the vacuum and deposits on the substrate as soon as it

arrives there. The process is performed at room temperature, the pressure inside the evaporation unit is adjusted at 10^{-7} mbar. The substrate needs to be preheated at 300°C for three hours to obtain an optimum reactivity. Similar to sputtering, a thin film of titanium of about 3-5 nm thickness is deposited first as an adhesion promoter. The maximum thickness that can be reached by thermal evaporation according to our facilities is about 50 nm.

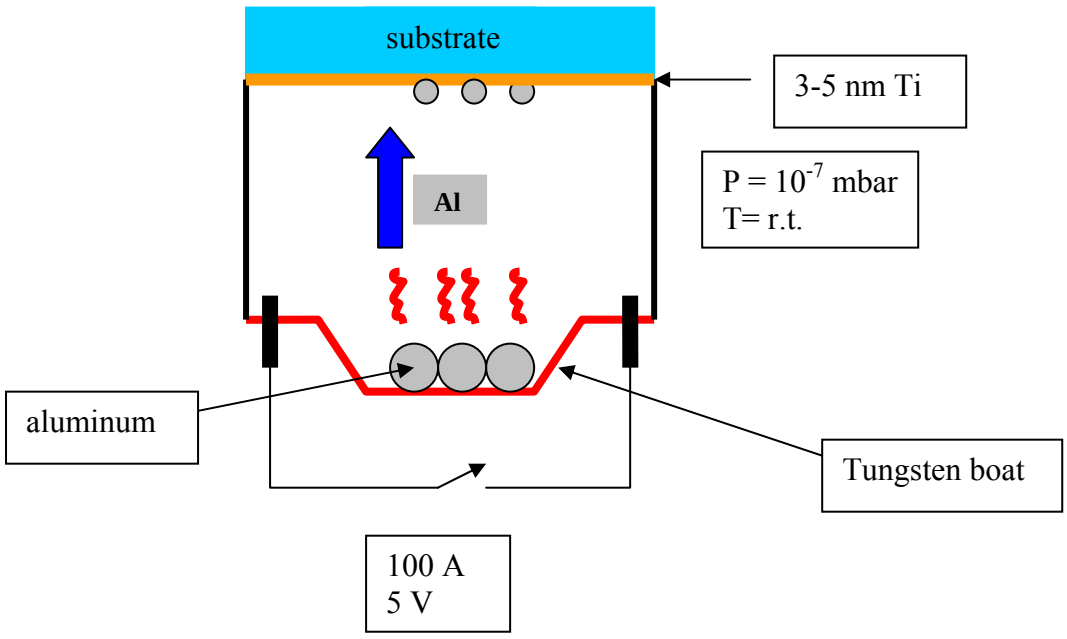

Fig. 3.2: Schematic drawing of the thermal evaporation of aluminum. The tungsten boat is heated by the electric current which fuses the aluminum raw material without being fused itself.

The thickness can be simultaneously determined during the coating by means of an internal quartz microbalance system. As it is going to be shown in chapter 4.2.2; thermal deposition yielded better stability of the aluminum oxide coating than sputtering. Beside, also the roughness of the aluminum oxide surface has been reduced. It has been recorded by means of atomic force microscopy (AFM) that the roughness of the aluminum oxide coating produced by sputtering is in the range of 10-15 nm, however, that produced by evaporation is only about 3 nm. The reduction of roughness was aimed at intentionally to help perform successful ellipsometry measurements since the thickness of the humic monolayer is in the range of 1-2 nm.

A variety of thicknesses and coatings tricks were tested, such like sputtering at high temperature. But due to the complication of the setup it resulted in unfavourable coatings like coating the round gold electrode (see figs. 2.4 and 3.3 for the sensor geometry) at the bridging connection to the contact electrode at the lower side of the sensor. Thus, electrical contact of the upper and lower electrodes is forbidden. In another case the lower electrode side was coated also. That electrode should be in contact with the gold-coated tips in the base of the QCM chamber. Through these tips the lower electrode receives the electrical signal necessary for exciting the vibration. Both effects cause the sensor not to vibrate at all. Another attempt was to remove the gold coating from the quartz sensor by iodine solution and then to coat aluminum directly on quartz. Some sensors that have been coated this way did not vibrate at all. We realized that iodine dissolved not only the gold coating but also the round gold electrode which passes the electrical signal to the quartz to vibrate. To deal with this problem, a special cell made of Teflon was built for gold dissolution. It has a circular opening, which can be filled with the iodine solution, and is sealed such that the round electrode is protected from the etching solution as it lies outside the liquid cell. However this coating method did not yield reasonable stabilities, since we did not succeed in getting the original quartz surface clean and active as it was before dissolution of the gold film.

In addition, attempts were made to recover the sensors by removing already deposited aluminum films from the sensor surface. This was achieved by immersing the sensors in a mixture of NH_4OH:H_2O_2:H_2O at a ratio of 1:1:5 at 70°C for about 30 minutes. This mixture is strongly corrosive and effervescent, and thus removed aluminum successfully from the surface. However, further aluminum coating on that surface did not deliver reasonable stabilities.

The best coating stability was obtained by thermal evaporation of aluminum on gold as well as on silicon oxide coated sensors (note: there is a little preference for silicon oxide than gold). In that procedure, the surface is to be preheated and to be bombarded by argon atoms (without aluminum target) as a cleaning step. This was the final attempt which resulted in the best stability of aluminum oxide-coated sensors. Sensors coated this way tended to keep stable until the end of the experiment which lasted about two to three hours. Some of them were even

regenerated by UV light and reused once again but without reasonable stability in the second set of experiments. The question of absolutely stable aluminum oxide coated-sensors is still open despite the better stabilities obtained, also in comparison with commercial products.

3.3. Preparation of humic and humic/Gd^{+3} solutions

Firstly; a stock of 0.1 M sodium perchlorate, hereafter indicated as salt, was prepared in which a concentration of 100 mg/l humic acid was dissolved. Since humic acid dissolves only in alkaline solutions, about 150 µl of 0.1 M sodium hydroxide has to be added to 100 ml humic solution, which is then stirred on the magnetic stirrer until complete dissolution. If particles are still visible, more sodium hydroxide should be added gently. After complete dissolution, the pH should higher than 11, and can be then adjusted to the preferred range. From this stock, various diluted concentrations of humic acid down to 1 mg/l can be prepared. Note that dilution has to be done with 0.1 M sodium perchlorate to keep the ionic strength constant. Humic solutions should not be kept at room temperature for long time as the solution coagulates and precipitates can be clearly seen. Thus, after performing a measurement, solutions should be directly kept in the fridge.

Gadolinium solution was first prepared in a stock at a concentration of 10^{-4} M, also in 0.1 M salt. From this stock, consistent amounts were added to humic solutions to obtain a concentration of 10^{-6} M, which was kept constant in all experiments. Humic/Gd solutions should be kept in a fridge, too. However, special attention has to be paid to the time period between mixing gadolinium to humic since a complexation reaction is going to happen. Complexing gadolinium by humic happens fast and takes few hours to be completed. However, long time aging of the solutions results in the formation of oligomers, and, hence, adsorption measurements will show variations. The standard time used in this study did not exceed half a day. Solutions were mixed in the morning to measure in the evening or in the evening to measure the next day.

3.4. Preparation of thin films for ellipsometry and XPS measurements

Preparation of humic acid and humic/Gd thin films on aluminum oxide were carried out by simple immersion of the aluminum oxide substrates in the solutions. First adsorption substrates were cut off, at a size of approximately 1 x 2 cm, from the wafer by the glass cutter. To prepare the surface for adsorption it has to be cleaned from any contamination. Refreshment of the surface was done by irradiation with UV light for 10 -15 minutes under a UV lamp of 150 watt power, which is placed in a hood to avoid health risks by ozone. Note to store the substrates in a Petri dish filled with nitrogen gas and sealed with parafilm after UV irradiation. They should not be exposed to air again until immersion.

Immersion glasses have to be acutely cleaned. A cleaning scheme was developed as follows: The glasses should be fully immersed in 1% Hellmanex solution in a suitable beaker. The whole beaker is placed in the ultrasonic bath, and sonicated at a temperature of about 30-40°C for about 20 minutes. The whole beaker is flushed by tap water for some minutes. Then each glass is flushed by Millipore water individually (gloves and tweezers should be used) and then dried in the oven at 50°C for a few minutes.

Solutions are poured in the glasses at volumes of about 10 ml, substrates are immersed in the solutions, and glasses are covered by parafilm until the immersion time is over. For concentration effect studies by ellipsometry and XPS a constant immersion time was selected which was 30 minutes for humic acid alone (binary system) and 120 minutes for humic/Gd (ternary system). The immersion time was estimated according to previous information from QCM measurements, which was later confirmed by ellipsometry kinetic experiments.

In case of the binary system, humic solution was decanted from the glass after adsorption, simultaneously water was flushed in, and the glass was then sonicated at room temperature for about 5 minutes. The substrate was then withdrawn from the glass by a pair of tweezers, dried with nitrogen and stored in a Petri dish sealed with parafilm. In case of the ternary system, the same procedure holds except that the sonication step was skipped, because we were not sure what could be the effect of

sonication on the humic/Gd complex. Instead, an equivalent and milder approach was applied: The whole glass was placed in a larger beaker, then the humic/Gd was decanted from the glass gently, and Millipore water was filled in gently until sufficient amounts of water overflow.

3.5 QCM measurements

3.5.1. Experimental setup

The QCM experiment starts by irradiating the quartz sensor for 10 min with UV light to get rid of contaminants. The sensor is then placed in its holder in the liquid chamber. By means of the software Qsoft401 from q-sense, Sweden, the measurement can be started by looking for the 4 overtone frequencies at 5, 15, 25 and 35 MHz. Next, a baseline should be measured first in air, and then in water or the solvent used. Stability of the base line in addition to the correct starting values of dissipation is prerequisite to start the measurement [94]. The solution of interest is supplied to the sensor by a peristaltic pump, which speed was kept constant at 90 µl/min in all measurements throughout this work.

The working temperature was kept constant at 24°C in all measurements. The temperature of solutions must not be lower, it is rather advisable to be one or two degrees higher than the working temperature. Contamination is among the most serious problems in QCM measurements. Therefore one should take care that the sensor surface is free of any contaminants and the applied solutions too. The problem of air bubble formation is a fatal problem while working with QCM. Its origin can be some air dissolved in the solutions, the high temperatures that generate bubbles, or that the solution temperature is lower than the working temperature, which stimulates bubble formation inside the chamber. To overcome the problem of air bubbles during a measurement, one should follow the instructions written in the QCM user manual [94], which advises connecting the inlet to a hanged pipette, and pumping the same liquid from the sensor out tube through the QCM chamber by a syringe or a pipette until one sees the bubbles going up in the hanged pipette.

Figure 3.3 shows the quartz sensor with its two sides [94]: the active side, usually coated with gold, which will be in contact with the liquid, and the contact side which transfers the oscillation signal to the electrodes in the chamber. The active electrode and the contact electrode are connected to an external circuit at the periphery of the quartz disc, and thus the signal can be transferred through this bridge. The quartz disc is in between, and it is the active side that was coated with aluminum oxide in our setup. It is worth to mention that a part of this work was dedicated to work with silicon oxide coated sensors as an alternative of aluminum oxide coated sensors. The corresponding results are presented in chapter 4.9. Actually, silicon oxide sensors are of high stability; however, they showed the problem of irregular responses or irreproducibility.

Figure 3.4 shows the whole QCM set up: the applied solution, the peristaltic pump, and the QCM chamber. The chamber is equipped with a valve to control the solution pathway inside. The valve allows directing the solutions to the sensor or to the T-loop out tubing, which is used to dispose waste solutions or air bubbles.

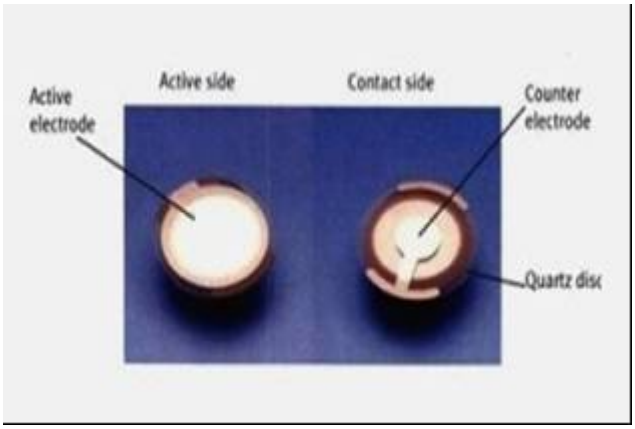

Fig. 3.3: The quartz sensor with its two sides: The active side which will be in contact with the liquid and the contact side which transfers the oscillation signal to the electrodes in the chamber [94].

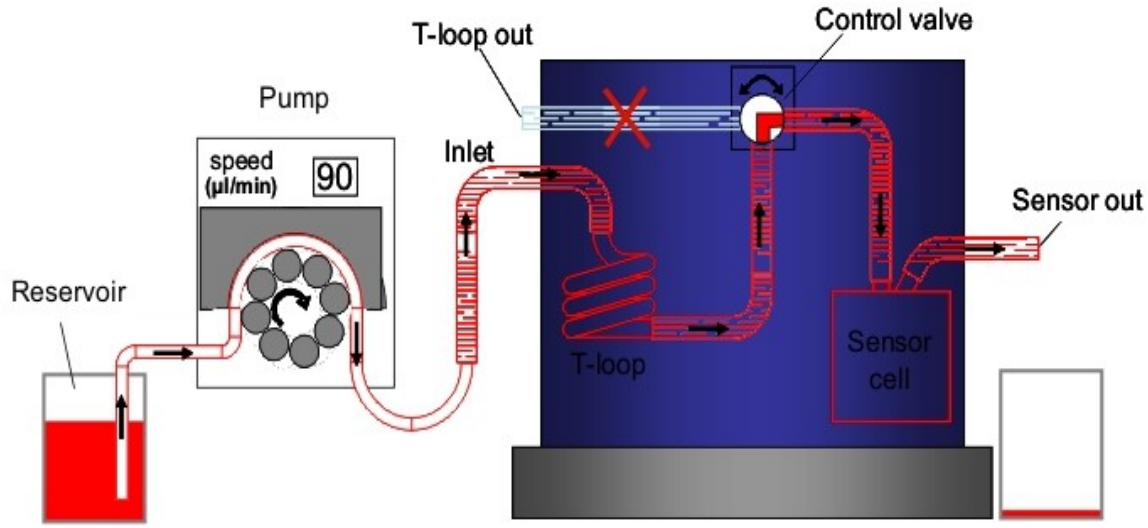

Fig. 3.4: The QCM setup: the axial flow chamber QAFC 302, and a peristaltic pump to deliver the liquid at a fixed speed of 90 µl/min [95].

3.5.2. Regenerating the sensor

Regenerating the sensor means to bring the surface in its state prior to adsorption, i.e. cleaning and reactivating the surface. Regenerating silicon oxide sensors was attempted using different methods: (i) plasma irradiation, UV for 10 min / SDS bath for 30 min at 28°C / UV for 10 min and (ii) exposure to a NH_4OH:H_2O_2:H_2O mixture at a ratio of 1:1:5 and temperature of 70°C for 5 min. The latter chemical mixture was used for a while and showed considerable cleaning efficiency. However, it is too corrosive so that it dissolves the silicon surface after being applied twice. The results of these regenerating methods are discussed in chapter 4.9.

Regenerating aluminum oxide sensors was considered with special care. The same methods used with silicon were repeated in case of aluminum oxide in addition to immersion in the organic solvent dimethylsulphoxide, DMF, and a sulphuric acid-hydrogen peroxide mixture (1:1). The latter was too corrosive so that the film dissolved immediately, and the other methods did not show any effect. Therefore, a dry cleaning method such as UV irradiation for long periods was tested. The results of these attempts are shown in chapter 4.4.2.

3.5.3. Modelling

In order to determine the thicknesses of the adsorbed film a model calculation was applied. The model is included in the software Q-tools supplied for data analysis from q-sense, Sweden. Actually two models can be applied: the viscoelastic model for f and D, and the extended viscoelastic model for f and D. Both models calculate the thickness of the adsorbed film based on the measured frequency shift and dissipation. The difference of the two models, however, is that the former assumes a rigid film and, thus, the film does not have significant viscoelastic properties that would induce additional frequency shifts and dissipation. Hence, its contribution to frequency change is limited to its mass so that the corresponding thickness calculation always yields values typical of the Sauerbrey equation. The extended model, in contrast, is adapted to viscoelastic films that cause additional frequency shifts and dissipation effects due to their viscoelasticity. The theoretical background of both the Sauerbrey equation and the model calculations for viscoelastic films are introduced in chapters 2.4.3 and 2.4.6. The results of modelling and comparison of the two approaches are presented in chapter 4.3.2.

Practically, it can be generalized that the extended model only has to be applied in case of films with high dissipation values. This is a special case since the Sauerbrey equation is not valid at all. Running the model follows a standard procedure: the viscoelastic model applied is that of Voigt, and standard shear and viscosity values are previously given as starting values. Actually, they are very broadly ranged so that they will cover various types of adsorbates.

Figure 3.5 shows an example of fitting, where the three frequency overtones and their dissipation curves are plotted. The water level is taken as the zero level and the fit should only be run in the marked area between the two red lines. In that fit, the extended viscoelasticity model was applied which takes into account frequency dependence on the viscosity and shear of the adsorbed layer.

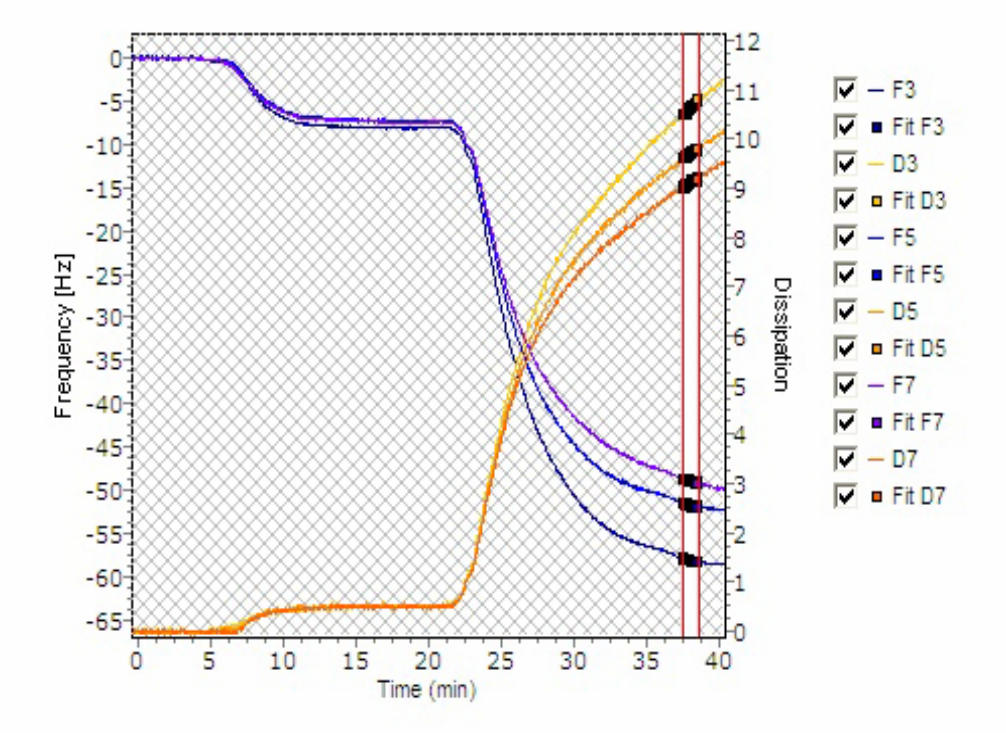

Fig. 3.5: Fit using the viscoelastic model. Back points represent the calculated frequency and dissipation according to the model. This fitting was done on data of humic acid adsorption at pH 3, chapter 4.3.1.1. Thickness calculated is 1.5 nm for the first and 17.2 nm for the second adsorption step.

3.6. Ellipsometry measurements

Ellipsometry measurements were performed on the spectral ellipsometer M 44, J. A. Wollam Co. at a fixed angle of incidence of 75°. A xenon lamp which provides a wide range of wavelengths was used as a light source. A measurement starts with a calibration step, using a silicon substrate of known thickness and optical constants. In the ellipsometry measurement of that known substrate, ψ and Δ values could be measured and then fitted to the given values of the same substrate. Note that the optical constants and thickness are already known. According to that fit the incidence angle can be exactly calculated (see equations 2.26 and 2.27). Then a model of the substrate to be studied is created. Once a new wafer was used a new model was created and was applied only for this wafer since there might be slight changes in metal film thickness from one wafer to the other which makes the fit not appropriate. The model consists of a silicon substrate of 500 µm thickness and an aluminum layer on top. The thickness of aluminum was about 50 nm, however, other thicknesses

were also used. A measurement of the reference surface is followed by a single scan, in that ψ and Δ values of this reference can be calculated. Since the thickness of aluminum is given and its optical constants are already saved in the software, a fitting of point by point results in calculating the optical constants of our own reference. Noticeably, the top layer of the model should be fitted to the optical constants of aluminum and not aluminum oxide, since an oxide film would exist anyway on top of aluminium.

After creating a sequence of layers which is consistent with our substrate, one can measure the humic film thickness by a single scan. To calculate the thickness, a Cauchy model was assumed for the humic layer on top of the reference. The Cauchy model assumes constant values of n_0, A and B to calculate the refractive index of the adsorbed thin film. Then the thickness can be calculated by fitting the measured ψ and Δ.

3.7. XPS measurements

XPS measurements were performed on a MAX-200 spectrometer, Leybold Heraeus, using the X-ray radiation of aluminum K_α (14.86.6 eV) at a pressure of about 10^{-10} mbar in the measuring chamber. Spectra were normalized to the aluminum reference, Al 2p, at 71.7 eV. Peak intensities were calculated by the software origin using the Gauss model. Fitting multipeaks was mostly done by origin, except for the carbon peak of humic acid in chapter 4.8. As this peak could not be fitted by origin to yield the four subpeaks, XPSPEAK41 software was used. Fitting these peaks was performed using fixed values of FWHM (full width at half maximum) of 1.4 eV, a Lorentzian to Gaussian ratio of 80%, and Shirley background subtraction.

4. Results and discussion

4.1. Sensor response to bulk effects

4.1.1. Responses to variation of ionic strength

To evaluate the frequency response, a basic measurement was performed which aims at changing the bulk properties, e.g. density and conductivity, of the liquid in contact with the sensor, and monitoring the corresponding frequency shift. Humic solutions used in this work were all kept at a constant ionic strength of 0.1 M sodium perchlorate. Changing the bulk properties was achieved by applying sodium perchlorate solutions of varying concentrations. The expression salt, hereafter, always denotes sodium perchlorate solution. The sensor used for this experiment was a silicon oxide sensor. As the salt concentration increases, frequency shifts to more negative values proportionally to concentration (figure 4.1) and so does the dissipation too. However its response is in the opposite direction.

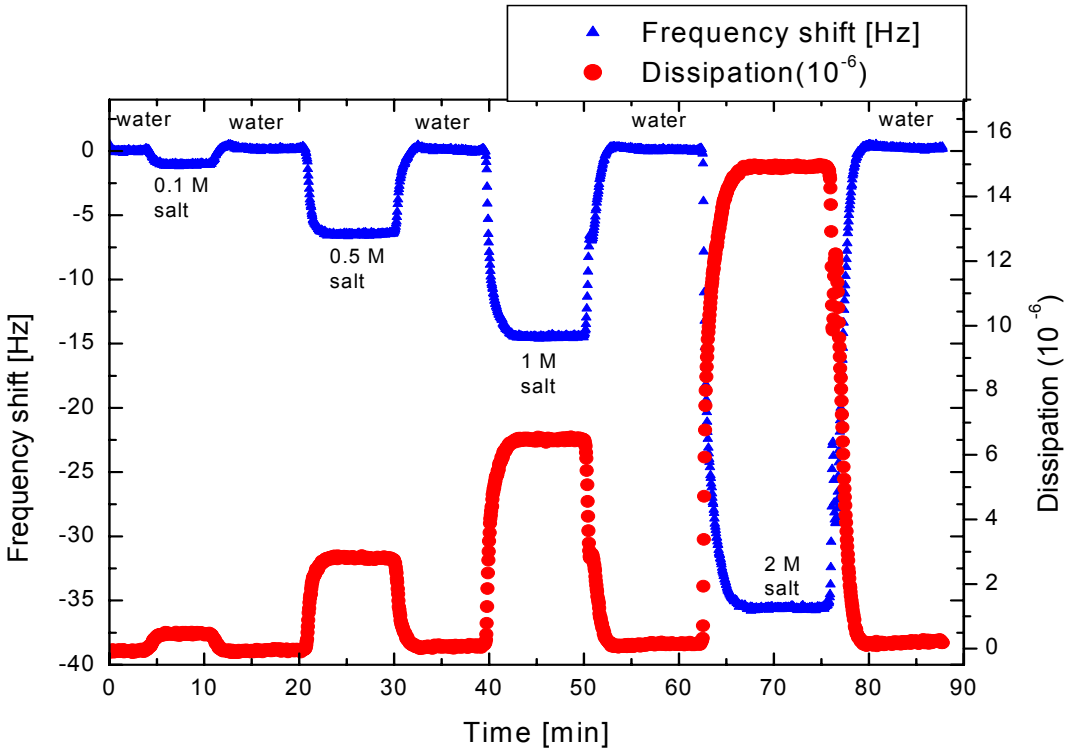

Fig. 4.1: Frequency and dissipation responses of a silicon oxide sensor upon changing the salt concentration. These shifts have been measured for the fifth overtone, f = 25 MHz, and normalized by dividing by 5.

The basic parameters that are responsible for a frequency shift in case of bulk effects, i.e. no adsorption is taking place, are viscosity, density and conductivity, all of which are proportional to variations of concentration in case of dilute solutions. The response appears reversible and stable as it goes back to the base line of water smoothly, which is the first prerequisite for a successful QCM measurement.

In order to interpret such frequency and dissipation responses, a comparison between the theoretically predicted and experimentally determined frequency response was performed. Theoretical values were calculated applying equations 2.17 and 2.18 [81]. For the values of viscosity and density used in the equations, data for sodium chloride were taken as the corresponding values for perchlorate do not exist in the reference [85]. Figure 4.2 (a) and (b) present plotted frequency and dissipation responses obtained by calculation and experimentally.

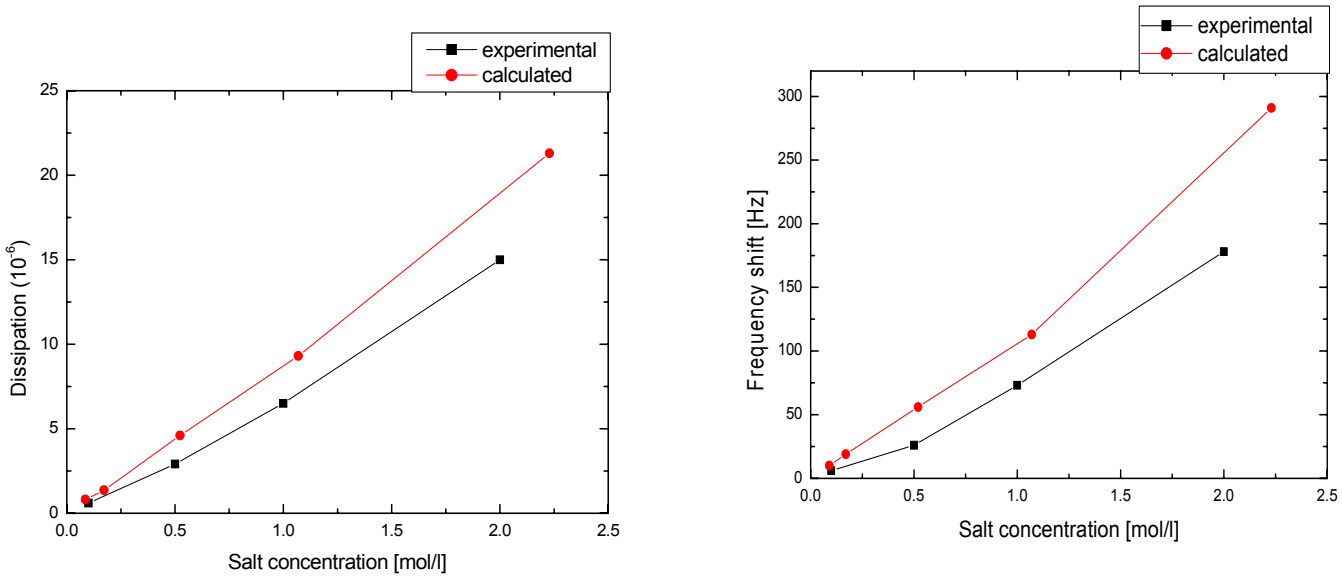

(a) **(b)**

Fig.4.2: Calculated and experimental dissipation (a) and frequency responses (b) plotted against salt concentration. Experimental and calculated values of frequency shift, figure b, are shown for the fifth overtone without normalization. The calculated values were obtained directly from equation 2.17 by substituting 25 MHz for f_0.

Both curves in figure 4.2 show at the first sight a linear relationship between frequency or dissipation and the salt concentration. Moreover, the curves show almost coincidence of the calculated and experimental values which indicates that

the observed response may be explained by density changes in the bulk solution. On the other hand to fully exclude the contribution of acoustoelectric effects to the frequency response, another calculation was performed applying the equation 2.19 [84]. The frequency response for 0.1 M salt should be 8738 Hz in case of acoustoelectric effects, which excludes the importance of acoustoelectric effects in our setup totally.

4.1.2. Response to pH variation

Humic acid is very rich in functional groups. Thus, most of its reactions are significantly affected by the pH value. Therefore, one of the specific aims of this work was to study the effect of pH on the adsorption of humic acid. In order to determine the neat frequency response due to adsorption, bulk effects should be subtracted. Hence, an experiment was designed in which the pH value of a 0.1 M salt solution was varied (fig. 4.3). In some measurements, perchlorate at different pH values caused some instabilities of the sensor, the reason of which is unknown. Thus, the salt used here is sodium chloride.

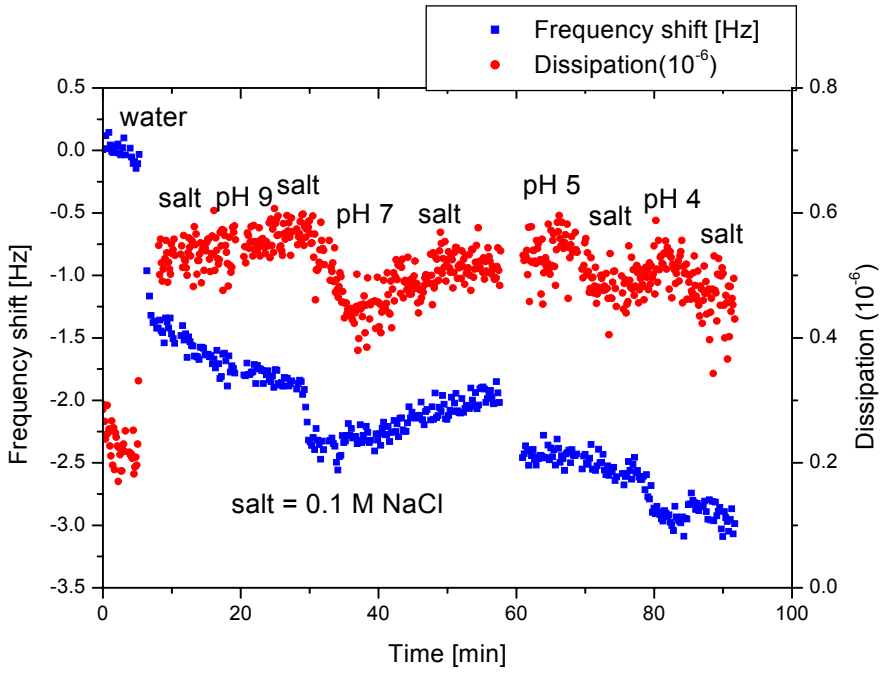

Fig. 4.3: Frequency response to variation of pH from alkaline to acidic medium. Exchanging solutions from water to salt (pH about 6.5) yielded the usual frequency shift of about 2 Hz. However variation of pH over a wide range yielded hardly about 1 Hz frequency shift.

Figure 4.3 presents the frequency response to variation of pH of a 0.1 M sodium chloride solution. The experiment involved exchange from water to neutral salt solutions, having pH of 6.5, and then to salt solutions of varying pH. Thus, the shift represents both ionic strength and pH effects. Interestingly, the exchange of water to neutral salt solution yields its well known frequency shift value. However, the variation of solution pH over a wide range gave hardly more than one Hertz frequency shift. Although variation of pH implies orders of magnitude of $[H^+]$ concentration changes, the amounts of either acid or base added hardly change the ionic strength of the solution due to the high salt concentration (0.1 M) in water. To subtract even these tiny effects occurring due to pH variation in an adsorption experiment, we shall keep in mind to change either to neutral water or neutral salt solutions at the end of an experiment and then calculate the difference from this level and the baseline.

4.2. Aluminum oxide-coated sensors

4.2.1. Stability of aluminum oxide-coated sensors

Working for the first time with aluminum oxide sensors provided by q-sense, Sweden, we noticed that these sensors did not show any stability toward acidified water or salt solutions (figs. 4.4 and 4.5). Once the sensor was mounted in the chamber and a stable baseline in water was reached, the application of slightly acidic water at pH 5 increased frequency by a huge value of about 800 Hz, then it stabilized again. Actually, the frequency rise is attributed to dissolution of the aluminium oxide coating, which vanished totally during this measurement. In another measurement, a PBS solution was applied to a new sensor to examine the effect of salt. Here, the same phenomenon happened again (fig. 4.4). Thus, it was clear that working with these sensors is impossible and the real challenge was to obtain a stable aluminium oxide coating.

Therefore, the first adsorption measurement was carried out on aluminum coated sensors from q-sense. The coating consists of 100 nm aluminum deposited on a gold-coated sensor surface. The aluminum film will have an oxide layer on top anyway. These sensors showed very limited stability so that they did not survive a

single experiment, which would take about one hour on average. However, the first adsorption curve for humic acid at pH 3 was recorded with these sensors (fig. 4.8).

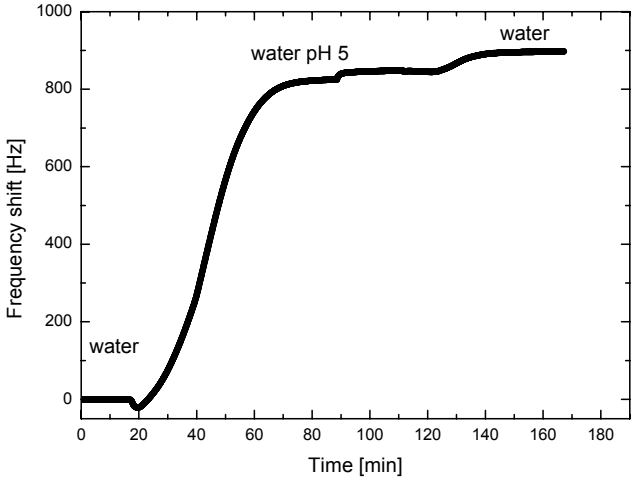

Fig. 4.4: Effect of water at pH 5 on the aluminum oxide coated sensors. The huge frequency shift in the opposite direction is attributed to dissolution of the aluminum oxide coating.

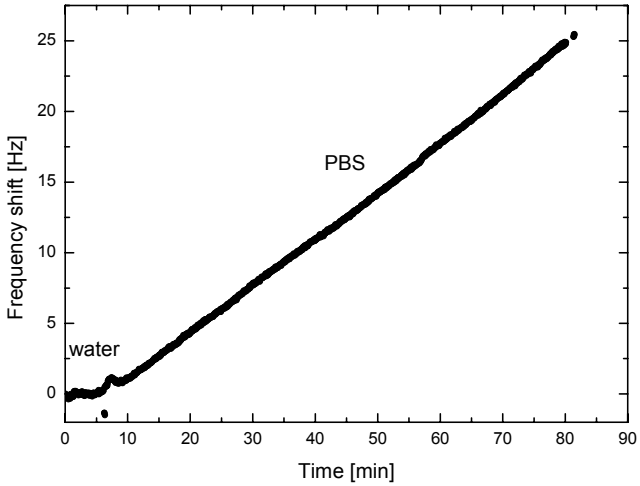

Fig. 4.5: Effect of a salt (phosphate buffer saline) on the stability of aluminum oxide coated sensor. Again, frequency rises up because of dissolution of the coating.

4.2.2. Optimization of the aluminum oxide coatings

Aluminum oxide coatings for the sensors were further developed by our coating specialist, Dipl.-Phys. Georg Albert, at our institute. His first attempt was to coat aluminum on gold sensors by sputtering at a thickness of 150 nm using titanium as adhesion promoter at a thickness of 3-5 nm. The aluminum coating was then oxidized in an oxygen atmosphere for several hours or overnight in order to obtain a fully oxidized upper layer. Since the problem of aluminum pealing-off was noticed at pH 3, an adsorption measurement was performed at a higher pH of 5, in which one of our in-house coated sensors was used (fig 4.6). This time, a silicon dioxide coated

sensor was used as a substrate for aluminum deposition instead of the gold-coated ones, as it yielded slightly better stability. However, the problem of pealing-off happened with these sensors, too. It was a problem that happened irregularly without obvious reasons. Different stabilities were even observed for sensors coated in parallel, i.e. which came from the same batch and were coated in the same way, and had all a uniformly shining surface.

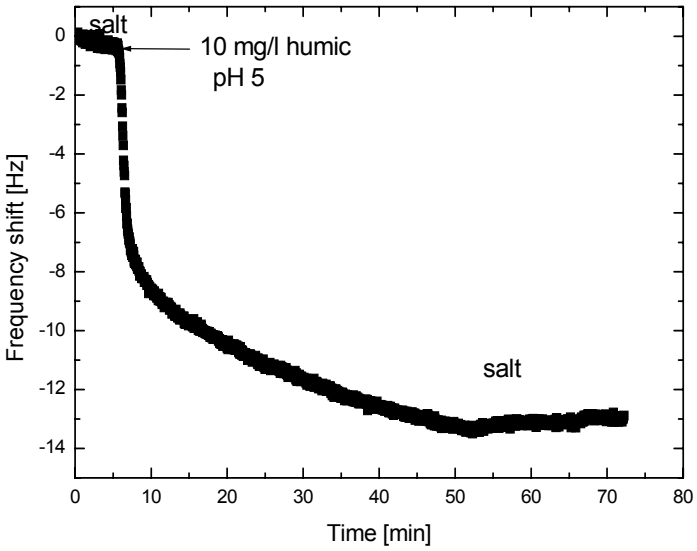

Fig. 4.6: Adsorption of humic acid on aluminum oxide coated sensors prepared by our own technology. Aluminum was coated onto a silicon dioxide film by sputtering yielding a thickness of 150 nm. The coating shows better stability than the earlier sensors used in figures 4.4 and 4.5.

Since it was still urgent to further improve the coating, a new approach was chosen which was coating by thermal evaporation instead of sputtering. Evaporation is a technique that is characterized by applying high temperatures and provides better sticking properties. The thickness that can be reached by evaporation in our facilities is only 50 nm. However, this does not negatively influence either the vibrational frequency of the sensor or the adsorption process in question.

Actually, evaporation yielded considerably better stabilities than sputtering. Fig. 4.7 presents the adsorption curve of humic acid at pH 6.8 as concentration increases. Frequency shifts upon concentration variation will be further investigated in the next subchapters. However, the fact that a sensor could persist until the end of a measurement is itself a great success. Nevertheless, pealing-off was noticed in few cases, which might be because of some bad sites or unseen dirt on the original substrate, or because of the low thickness of the coating.

To deal with the low thickness, an approach was undertaken to combine sputtering and evaporation in order to combine the advantage of high film thickness and better sticking. This combined approach was actually a sputtering process at a temperature of about 300°C. Note, that sputtering normally takes place at room temperature (see chapter 3.2.1). This approach also delivers reasonable stabilities (fig. 4.13) but came up with the problem that due to the complication of sputtering and vaporization at the same time, see chapter 3.2.2, part of the gold electrode that transfers the electrical excitation signal to the sensor surface (see figs. 2.4 and 3.3 for the geometry of the quartz sensor) can be also coated and, hence, the contact is shorted-out which in turn prohibits vibration. In a different case, the lower surface of the sensor, which consists of the gold electrode that is contacted by the golden tips in the base of the QCM chamber, can be also coated, which also prohibits vibration.

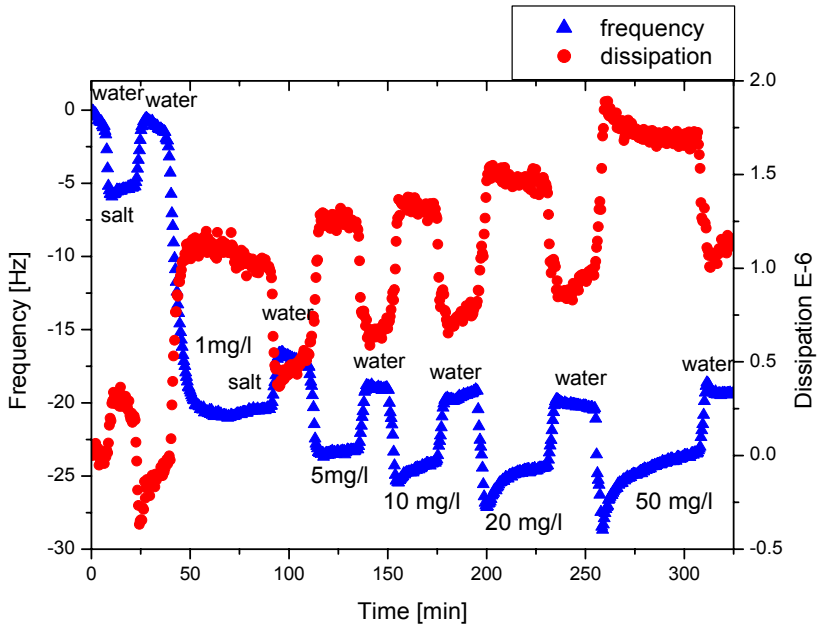

Fig. 4.7: A successful measurement of humic adsorption at pH 6.8 while raising the humic concentration. The sensor was coated by evaporation of aluminum onto a gold substrate.

To overcome that problem, a special mask was designed which shields all critical areas and allows only the sensor surface to be coated. However, we were left with the problem of bad sites or surface contamination of the original substrate. We then decided to remove the gold electrode and to coat aluminum directly onto the quartz with titanium as an adhesion promoter in between. Removal of gold was carried out by iodide solution, I_2/KI/water at a ratio of 1:4:80, which could also attack and

dissolve the gold electrode, thus, preventing vibration. To avoid that, a special liquid cell was designed for gold removal which is sealed such that it allows exposure of the gold surface to the iodide solution while the gold electrode is located outside the liquid chamber and, thus, protected.

The last optimization attempt involved a surface pre-treatment of the original gold substrate by preheating followed by plasma cleaning. This is followed by thermal evaporation of aluminum to obtain a final thickness of 50 nm. Because of some technical inconvenience which made the aluminum raw material evaporate completely before reaching the desirable thickness, the coating was done in two runs, 25 nm each, and, thus, without titanium as an adhesion promoter. Titanium was not additionally inserted in the vacuum chamber in this two-step process to avoid uncontrolled evaporation of titanium which may result in a mixed layer of aluminum and titanium. In that attempt we should have got rid of surface contamination on the original surface and made use of thermal evaporation which provides better stabilities. However, the absence of titanium could also decrease the sticking quality. Sensors coated by this approach were used in chapter 4.4, and all survived the whole measurement except those at pH 3, which will be discussed later. pH 3 is on one hand quite aggressive to the coating and on the other hand it leads to much higher loading of the surface with humic that increases the stress occurring on the coating.

At that point the optimization attempts, which were the real challenge and the most time consuming experiments in this work, were ended. Because of these complications, the use of silicon oxide coated sensors was always considered as an alternative (see chapter 4.9). However, a large deal of technical information about aluminum coatings was gained, and hopefully we have reached a reasonable coating scheme which could be helpful for other researchers in the future.

4.3. Adsorption of humic acid on aluminum oxide (binary system)

4.3.1. Effect of pH

4.3.1.1. pH 3, a special case

Adsorption of humic acid was detected by QCM at a concentration of 10 mg/l and pH 3. A typical adsorption curve obtained from several measurements is presented in figure 3.1. After a stable baseline for water had been obtained, humic solution was applied to the sensor. The frequency started to shift to negative values, and dissipation went to positive values in parallel. Both frequency and dissipation tended to level out after few minutes giving the impression that the adsorption process has been completed. However, after stabilizing for a couple of minutes, both frequency and dissipation continued to drop and rise, respectively, until significantly higher values were reached compared to the first adsorption step.

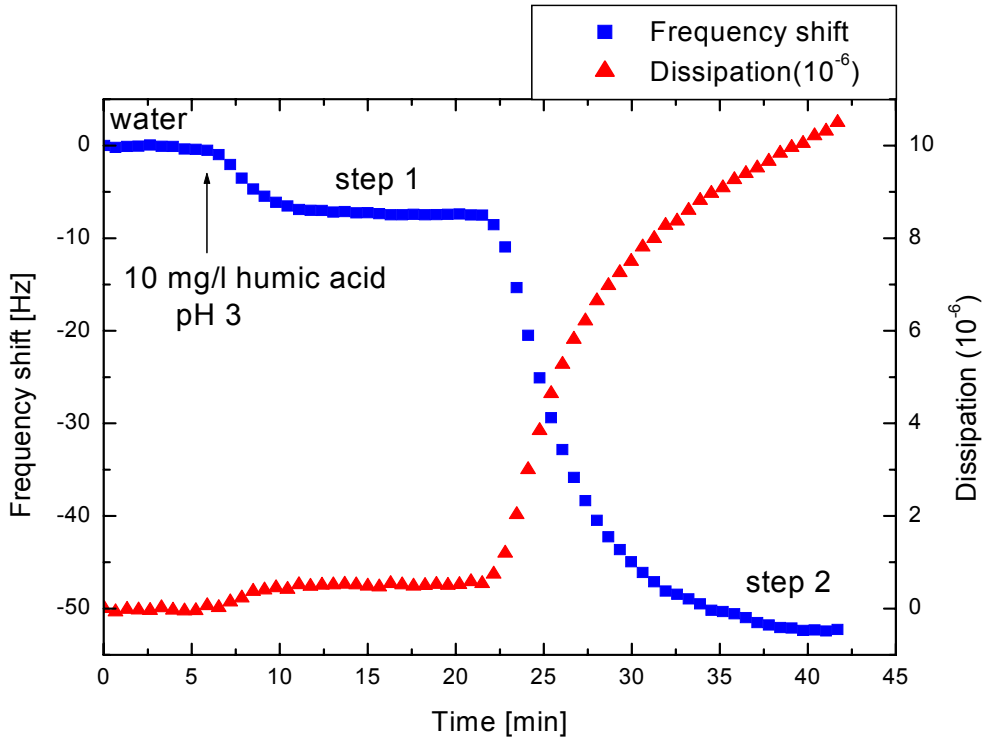

Fig. 4.8: Adsorption of humic acid on an aluminum oxide sensor at a concentration of 10 mg/l and pH 3. Adsorption happens in two steps. The first process stabilizes for a couple of minutes at a relatively low level, and then proceeds to a significantly higher level at a much slower rate.

This is the characteristic adsorption curve for adsorption at pH 3 which has been reproducibly obtained with an error of up to 10% as a maximum. The adsorption is characterised by the existence of two steps, each of which takes place at a different time scale. The first step takes place in less than 5 minutes and, hence, it is the faster one. The second step takes about 20 minutes after beginning, so it is the slower step. At this point, a complete picture about the adsorption at pH 3 cannot be given. One even cannot tell if this is a characteristic behaviour for adsorption of humic acid in general or if it is a special case for this specific pH, until other measurements at other pH values are done.

Dissipation could also yield essential information about the physical nature of the adsorbed film. In addition to the two different time scales in the frequency shift, there are two different scales in the dissipation shift, too. In the first step, dissipation is very small, less than one unit, and, hence, it is consistent with the Sauerbrey conditions for a rigidly attached monolayer, where the frequency shift is proportional to the adsorbed mass. Contrary to that is the dissipation behaviour in the second step, analogue to the frequency behaviour. The dissipation shift is very large, about 10 times higher than for the first step. Such an increase in dissipation can be interpreted on the basis of increasing viscosity. An overall expression for adsorption at pH 3 could then be that a rigidly attached monolayer consisting merely of solid material is adsorbed in the first step followed by multilayer or physically aggregated molecules exhibiting viscous properties due to a substantial amount of entrapped liquid.

Evidently, further experimental approaches are needed so that on one hand the adsorption phenomenon could be proven, and on the other hand these approaches can serve as a test of the reliability of the QCM results. In that sense, XPS was selected as a spectroscopic technique differing in its working principle since it is based on electron emission not on acoustic waves as QCM. At the same time XPS yields absolute amounts and stoichiometries of atoms present on a surface, which is the base of its high importance in either qualitative or quantitative surface analysis. Fig. 4.9 shows the carbon 1s peak of two sensors with humic acid adsorbed on top. One was incubated until the first adsorption step and the other until the second step was finished. Afterwards, both were rinsed with Millipore water and dried with nitrogen. A third bare sensor was used as a reference which contains already some

carbon from air and the manufacturing process. The carbon peak of the reference (bare aluminum) was subtracted from the carbon peak of the three samples (reference, step 1 and step 2), hence that of the reference appears as a zero line. The integrated areas of the carbon 1 s peaks clearly indicate that after step 2 significantly more humic acid is adsorbed on the sensor surface than after step 1.

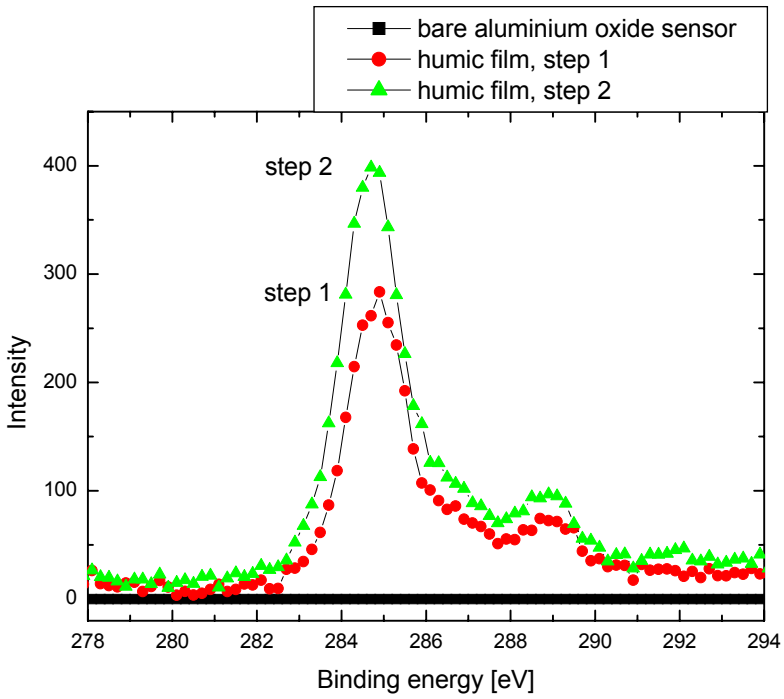

Fig. 4.9: XPS spectra showing the C1s peak for adsorbed humic films at pH 3 from two different QCM measurements, where the experiment was stopped at steps 1 and 2, respectively. Peak areas are 1020 and 1483.

To exactly quantify the amount of carbon, the area under the peak was calculated by integration using origin software. Integration yielded 1483 and 1020 for step 2 and step 1 respectively, i.e. 40% more carbon for step 2. This ratio is not consistent with the frequency shift in QCM. However, according to the explanation of the second step, these physically aggregated molecules are easily washed off from the surface upon rinsing with Millipore water. Additionally, the adsorbate in the second step probably contains a lot of water. Therefore, part of the frequency shift could be correlated to the loading of water into the film. That is the reason why the amount of adsorbate detected in dry state measurements, e.g. in XPS, are not consistent with

the frequency shifts in QCM measurements, especially in the case of the second adsorption step.

It has been a real challenge to show the desorption of the film adsorbed in the second step by QCM since an aluminium oxide coating could hardly persist until the end of a measurement and tended to dissolve during the second step. Further investigations of adsorption at pH 3 were done by means of ellipsometry. An experiment was designed in which silicon wafers with a 150 nm thick aluminium oxide coating were cut in pieces of about 2 x 1 cm each and used as substrates. These substrates were first irradiated by UV light for 10 min to get rid of contamination which could block the adsorption sites and deactivate the surface or, in other words, prohibit adsorption. Humic solutions were prepared at pH 3 and different concentrations starting from 5 to 50 mg/l. Immersion time intervals were selected according to QCM time scales as 15 min for the first step and 150 min for the second step. After the immersion time was over, humic solutions were decanted or poured off from the adsorption glass. Next, Millipore water was poured gently in and the whole glass was then sonicated for 2 minutes. To this point, molecules that are not adsorbed should have been washed off from the surface. The substrate was then withdrawn from water, dried gently with nitrogen gas and kept in a Petri dish for ellipsometry measurement. Figure 4.10 shows the thicknesses of the adsorbed humic film from step 1 and 2 as a function of the concentration of humic solution.

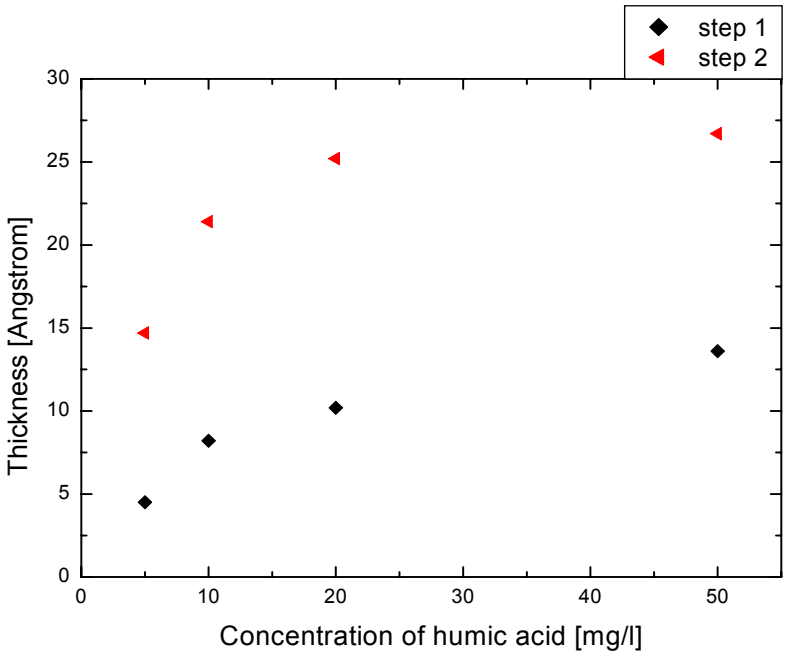

Fig. 4.10: Thicknesses of the adsorbed humic film measured by ellipsometry at different humic concentrations, and at pH 3 (step 1: 15 min. immersion time, step 2: 150 min. immersion time) both were sonicated for 2 min in Millipore water.

Fig. 4.10 describes on one hand the development of thickness as a function of concentration, in that saturation is being reached at a concentration of 20 mg/l. On the other hand there is additional evidence that adsorption at pH 3 takes place at two time scales, 15 and 150 minutes, with two different thickness sequences. Although it agrees with the characteristic adsorption curve of QCM, an exact coincidence cannot be achieved. This is due to the fact that the second adsorption step is formed mainly from physically adsorbed aggregates that can be removed, especially if there is a rinsing step in Millipore water for two minutes following withdrawal from humic solution. This emphasizes the useful character of QCM as an in situ measuring technique which detects everything adsorbed onto the top electrode providing useful information about its viscoelastic character driven by the dissipation expression. The situation looks different, however, in case of an ex situ optical method which is only concerned with the solid adsorbate on the surface after being dried.

4.3.1.2. Adsorption at higher pH values

To study the effect of pH on adsorption, more experiments were needed at different pH values above pH 3 as already discussed in chapter 4.3.1. In figure 4.11, three different adsorption curves for pH 5, 6.8 and 9 are presented, all of them displaying frequency (blue triangles) and dissipation (red circles) as a function of time. After the baseline for salt (0.1 M sodium perchlorate) had been maintained, humic acid at reasonably high concentrations of about 20 or 50 mg/l was added.

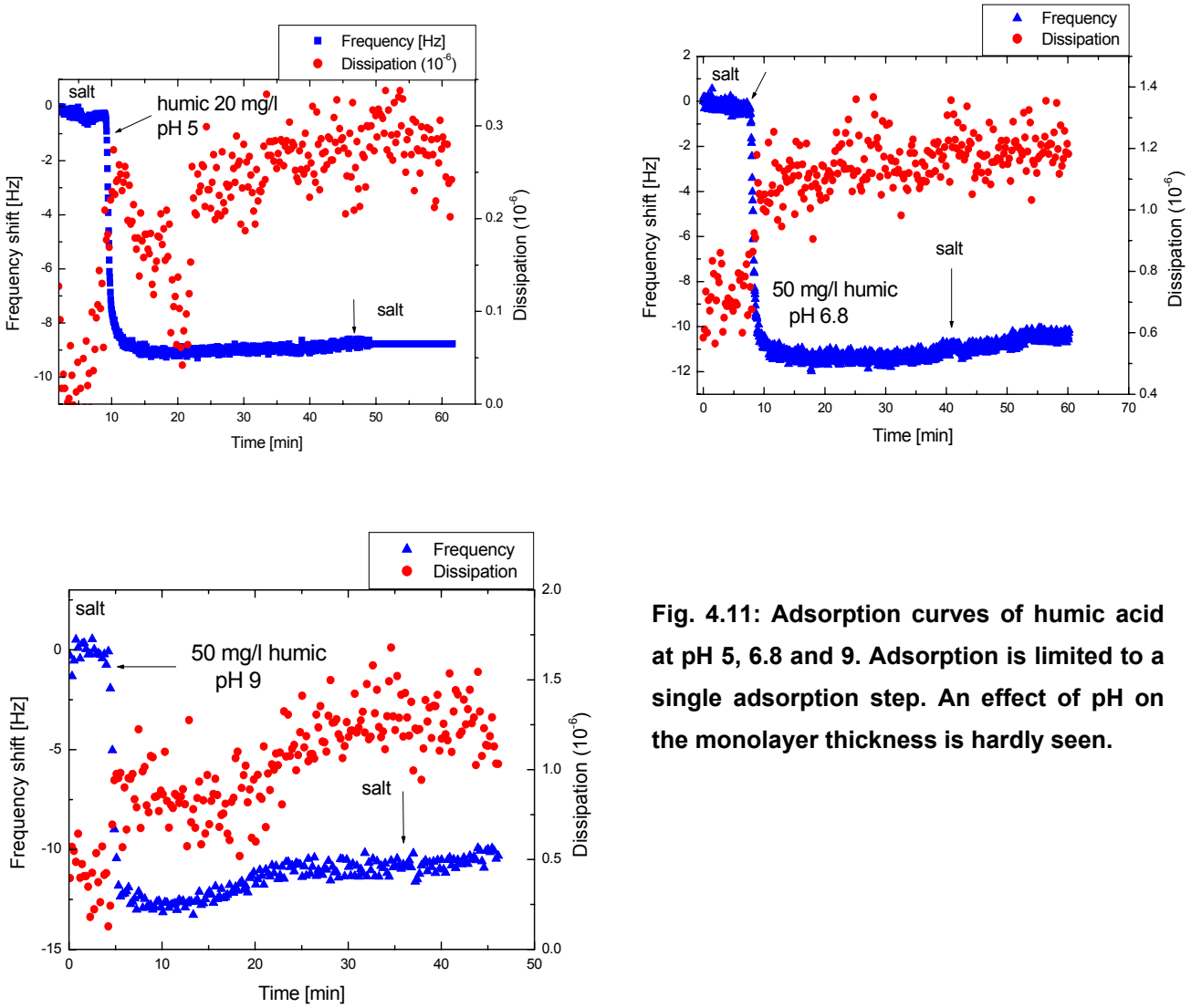

Fig. 4.11: Adsorption curves of humic acid at pH 5, 6.8 and 9. Adsorption is limited to a single adsorption step. An effect of pH on the monolayer thickness is hardly seen.

Adsorption takes place immediately as soon as humic acid reaches the sensor surface. The rapid drop of the curve gives a first feeling of fast reaction rate. After adsorption is completely done and the curve levels off, the salt was added again, which is an important step. The aim of exposing the sensor to salt solution after completing adsorption is twofold: first to find out if the observed sensor response is due to adsorption or only a bulk effect. Second it is used to rinse off the weakly attached molecules to assure that the frequency shift is only due to the molecules adsorbed to the surface. In case of adsorption, frequency does not go back to the original level under any circumstances, while for bulk effects it goes back reversibly. As seen in figure 4.11, frequency is not or only slightly affected by rinsing with salt for all curves. Since humic solutions have different pH values, it was necessary to use

the salt at its neutral pH, about 6.5, which cancels out any pH effect when determining the neat frequency response needed to calculate the thickness. The most interesting observation is that there is no second step. Adsorption takes place in only one step and stops. Note that the experiments were run for a time interval similar to that needed in case of pH 3 for the first and second steps to happen.

This leads to the following interpretation: the first step occurring at pH 3 is actually the formation of a monolayer until complete coverage. Then, enhanced by the acidic conditions, attractive electrostatic interactions take place between the different functional groups which stimulates the formation of aggregates that assemble on top of the monolayer. The latter process does not happen at higher pH values because the partial negative charge is dominating and, hence, the functional groups distributed over the carbon skeleton of humic acid are screened. In this case, a repulsive electrostatic interaction takes place forcing the reaction to stop at the monolayer level.

Regarding the amount adsorbed in the three cases, the neat frequency response is in the range of about 10 ±1 Hz, or in other words, an effect of pH on film thickness cannot be stated. In literature [38-42] a typical result of batch experiments is that adsorption shows a maximum at pH 3 and decreases with increasing pH. This is based on the fact that while humic acid is negatively charged over the whole pH range from 3 to 9, aluminium oxide is positively charged from pH 3 until its point of zero charge at about pH 9. Then it will be negatively charged. Therefore the electrostatic interaction, and also adsorption, will be of maximum value at lower pH values and decreases upwards. However, according to our QCM measurements we can not see an effect of pH on the thickness of the humic monolayer except for that at pH 3. What happens at pH 3, in the second step i.e. after the monolayer has been formed, is an intrinsic event in the bulk of the solution: aggregation of molecules far away from the alumina surface. This aggregation process happens also for a humic solution at pH 3 in a flask if it is left for about three days outside the fridge.

Another method of analysis is plotting dissipation versus frequency, which provides information about kinetics of adsorption as well as the rigidity of the adsorbed film. Dissipation is a comprehensive term for energy losses due to viscoelastic interaction (1) between the adsorbed molecule and the bulk of the liquid, (2) caused by

molecular conformation and intermolecular interactions and (3) due to water and salt molecules penetrating into the adsorbed film. Thus, the lower the D/f factor the less important are all of these contributing factors, and the more rigidly adsorbed are the molecules. Since both dissipation and frequency are equally spaced in time, less data points per interval in the D versus f plot is an indication of a faster adsorption process.

Figure 4.12 shows the plot of dissipation versus frequency for pH 3 and pH 5, taken from the curves in figures 4.8 and 4.11 respectively. For pH 5 clearly seen are the two agglomerations of points referring to the two steady states before and after adsorption. The two steady states are separated by a line of points describing the adsorption step. The fact that dissipation is constant over the range in which frequency drops is a strong indication of the rigidity of the monolayer formed at pH 5. The whole value of dissipation shift is about 0.3 units for the whole frequency shift which is a second indication that the formed monolayer is mainly a solid material and contribution from the bulk of the solution is negligible. Actually the argument holds for pH 6.8 and 9, too, except that the whole dissipation shift is higher than that at pH 5.

On the contrary, adsorption at pH 3 presents a different, however, interesting behaviour. Here, dissipation seems to vary in two phases: first, for the monolayer at the early beginning of adsorption it has a value of less than unity. For the second adsorption step, it tends to increase linearly with increasing frequency over the whole range of adsorption until it reaches more than 10 times the value of the monolayer. This is an indication of a soft layer with high solution content, In other words, this layer affects the resonating frequency through its own shearing and viscosity contribution. On the kinetics one can also learn that, although the time factor is absent in the plots, the dense distribution of points at pH 3 indicates a rather slow process. Looking at the two curves one realizes immediately that they describe two distinctly different phenomena.

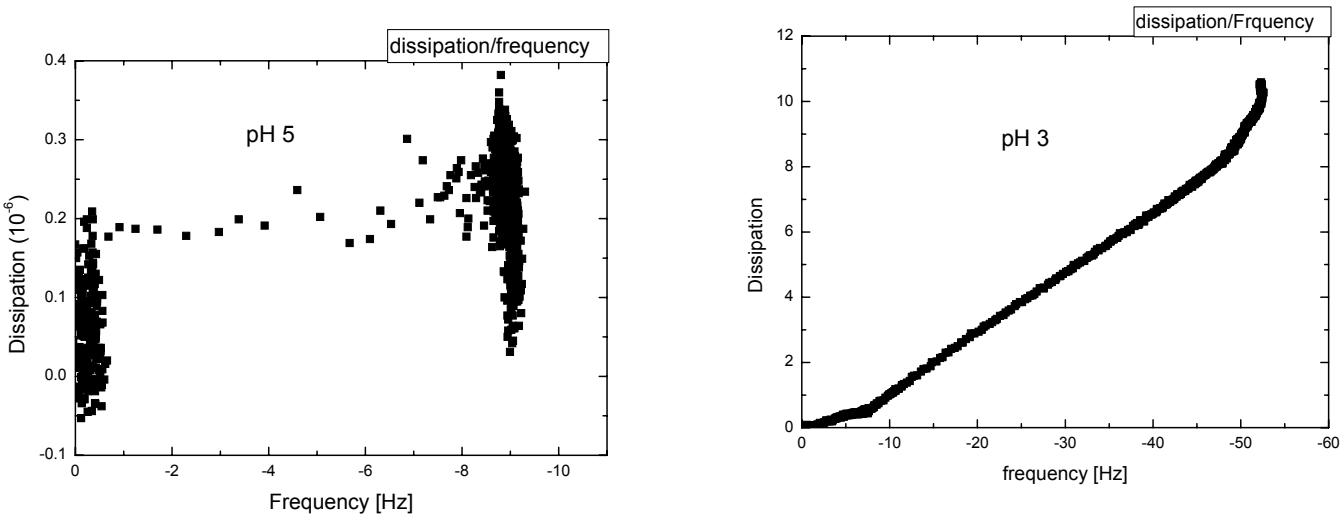

Fig. 4.12: Dissipation versus frequency plots of humic adsorption at pH 5 (left) and pH 3 (right). The curves reveal interesting information on the kinetics as well as the characteristics of the adsorbed layer.

4.3.1.3. Stability at different pH values

Since humic adsorption is a pH dependent process, an interesting question arises: What is the effect of pH on an already existing humic layer. The answer to this question is shown in figure 4.13.

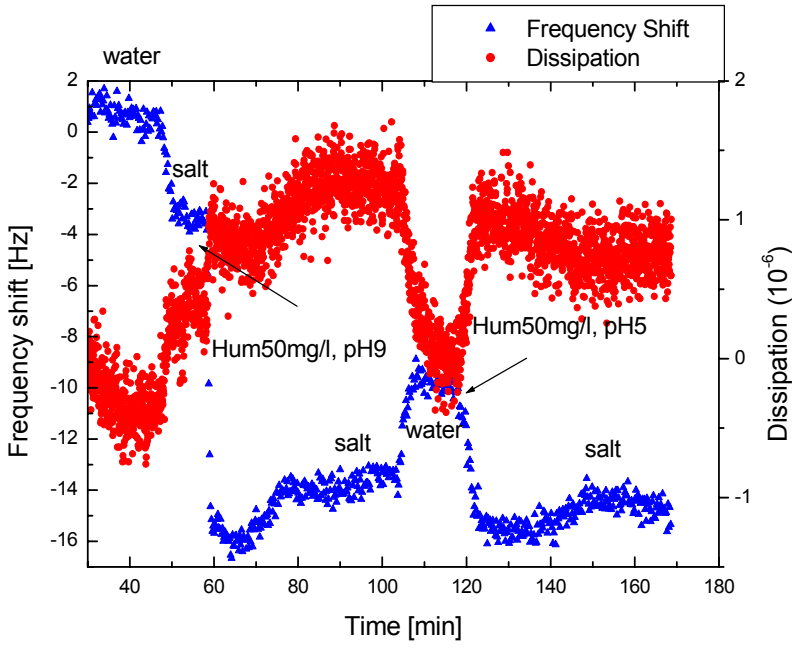

(a)

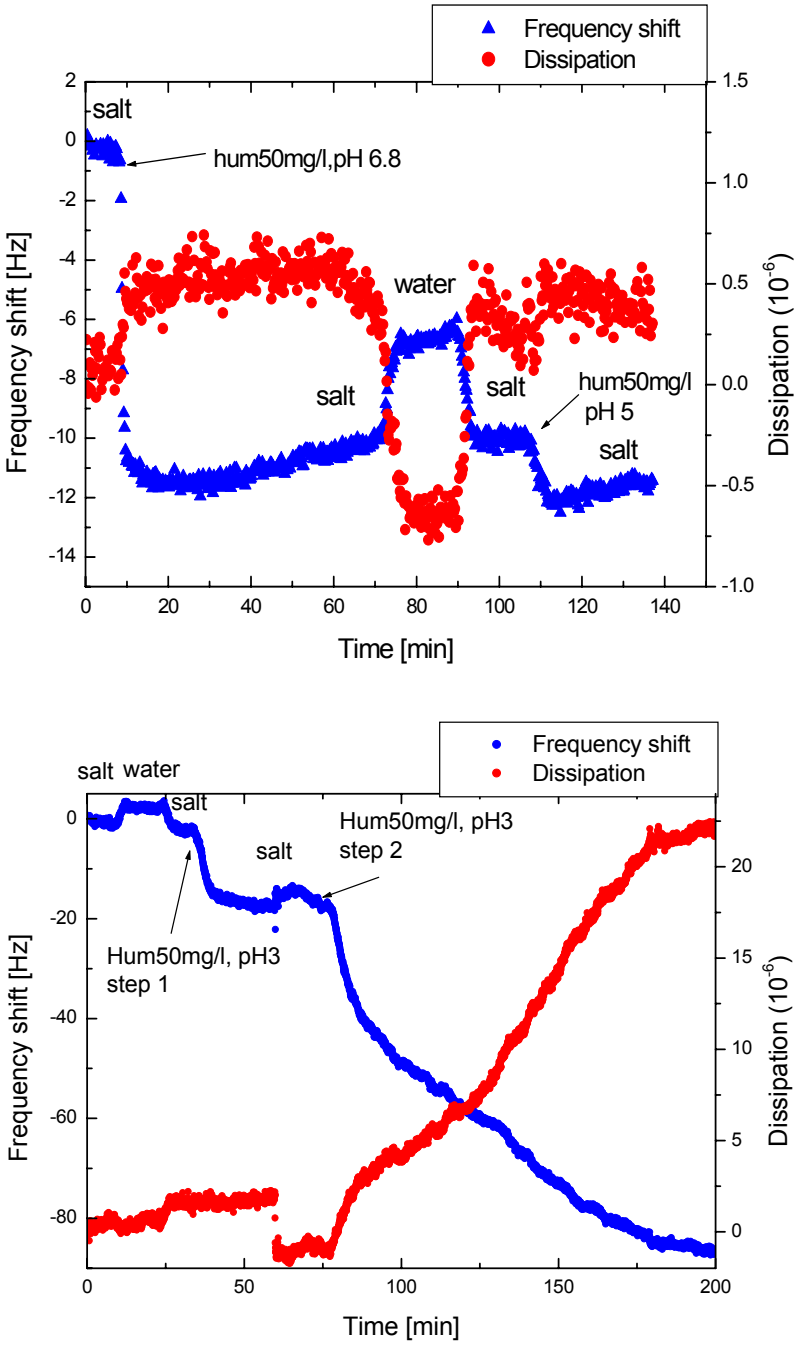

Fig. 4.13: Stability of humic films at different pH: from neutral to acidic (a), from alkaline to acidic (b), and then a typical adsorption at pH 3 curve onto a monolayer adsorbed at pH 5 (c).

In figure 4.13a, the experiment started with the salt baseline. Then humic acid was incubated at a reasonably high concentration of 50 mg/l to ensure maximum adsorption, and at a neutral pH of 6.8. Adsorption occurs to its expected level. A further incubation of humic at the same concentration and pH 5 makes the frequency shift to its previous level at pH 6.8, with a slight difference of about 1 Hz, which cannot be regarded as adsorption.

In figure 4.13b, adsorption starts in alkaline medium at pH 9. A further shift to acidic medium at pH 5 does not affect the adsorbed film. On the same sensor without cleaning, i.e. the adsorbed humic in figure 4.13b still on the surface, humic at pH 3 was incubated (fig. 4.13c). The first step of adsorption at pH 3 occurred which is then followed by rinsing with salt to obtain the salt baseline and to check if it is a real adsorption. Upon further exposure to humic at pH 3, the second step of adsorption happened, too.

Summarizing the three curves, shifting from neutral to slightly acidic as well as shifting from alkaline to acidic medium does not affect the existing adsorbed layer. However, the special case of pH 3 could stimulate adsorption not only on the surface of aluminum oxide but also, amazingly, on the surface of a humic layer. This effect explains explicitly the mechanism beyond humic adsorption in which the pH effect on the alumina surface is mostly absent. The role of aluminum oxide seems to be limited to its hydroxyl groups, i.e. the oxide in its hydrated form, as a receptor of the attacking humic molecule. The power of the attack is pH dependent. Thus the reaction could include the carboxyl groups of humic and the hydroxyl groups of aluminum oxide in a redox reaction leading to a condensation reaction. Adsorption of a humic molecule on a humic layer in the same way and the same amount as on aluminum oxide surface gives a strong preliminary feeling of a chemical reaction acting as the driving force. Under the acidic conditions at pH 3, a protonation of the surface of the adsorbed humic monolayer takes place. Therefore it is possible for a hydroxyl group from the adsorbed humic monolayer to act in the same way as that of the aluminum oxide surface resulting in the same condensation reaction, i.e. the adsorption of a further humic monolayer. Further spectroscopic investigations to determine the binding mechanism are shown in chapter 4.8.

Unfortunately, because of the problem of aluminum oxide dissolution we could not perform experiments under strongly acidic or alkaline conditions, e.g. pH 2 or 10. These experiments could be easier performed on alumina particles in batch experiments.

4.3.2. Determination of thickness using QCM

Two different methods are applicable to determine the thickness of the adsorbed layer by QCM: either using Sauerbrey equation [73] or applying the model introduced by Vionova et al [86]. The simpler version of the model is the case of adsorbed monolayer without bulk effects (see equations 2.20` and 2.22` and chapter 3.5.3). Practically, fitting using the model gives values very close to Sauerbrey and fits well in case of monolayer formation with negligible error. The same is true in case of huge dissipation adsorption and the extended viscoelastic model (see equations 2.20`` and 2.22`` and chapter 3.5.3), in which the adsorbed film is soft enough to cause a viscoelasticity induced frequency shift which can interfere with the original resonating frequency of the sensor. Thus, at pH 3 we can apply both models for the first step but only the extended model applies for the second step. The thickness of the first step obtained is 1.5 nm by fitting to the viscoelastic model and 1.48 nm by Sauerbrey, for the second step 17.2 nm by fitting to the extended viscoelastic model and 9 nm by Sauerbrey.

A comparison of the two different methods is shown in figure 4.14. Evidently, the viscoelastic model and the Sauerbrey equation yield similar values for the monolayer. However, for pH 3, where there are physisorbed aggregates, the calculated thicknesses vary widely.

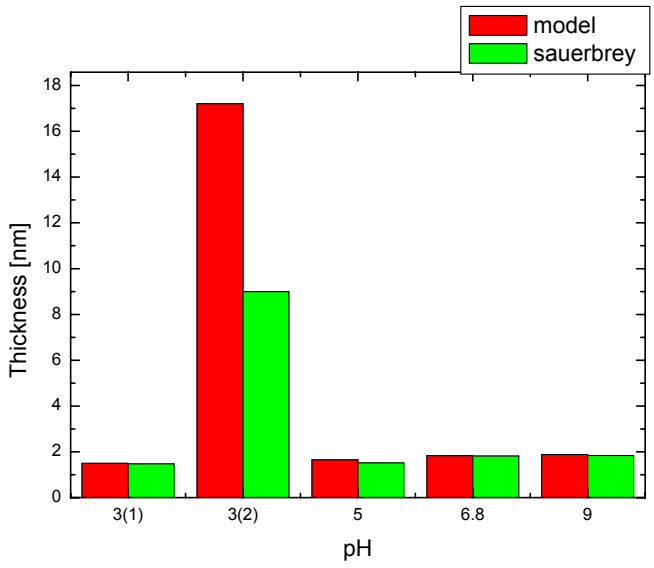

Fig. 4.14: Comparison of the thicknesses of adsorbed humic films obtained by the viscoelastic model and calculated by the Sauerbrey equation.

4.3.3. Effect of concentration

The concentration dependence of humic adsorption for pH 5 and 6.8 is presented in figure 4.15 (a) and (b) respectively. Adsorption was found to already happen at a dilute concentration of 1 mg/l forming a significant portion of the monolayer. Further increase of concentration is only accompanied by a pronounced shift in frequency up to a concentration of 5 mg/l. Saturation happens at a concentration of 10 mg/l. This rapid saturation indicates the high adsorption tendency of the molecule. On the other hand, the reduced coverage in the concentration regime before saturation could be due to the little chance of a molecule to reach the surface at this low concentration.

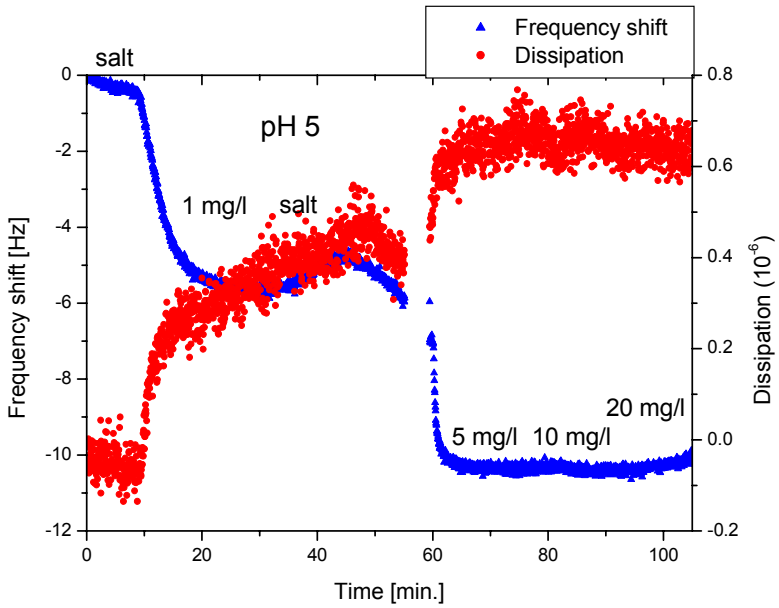

(a)

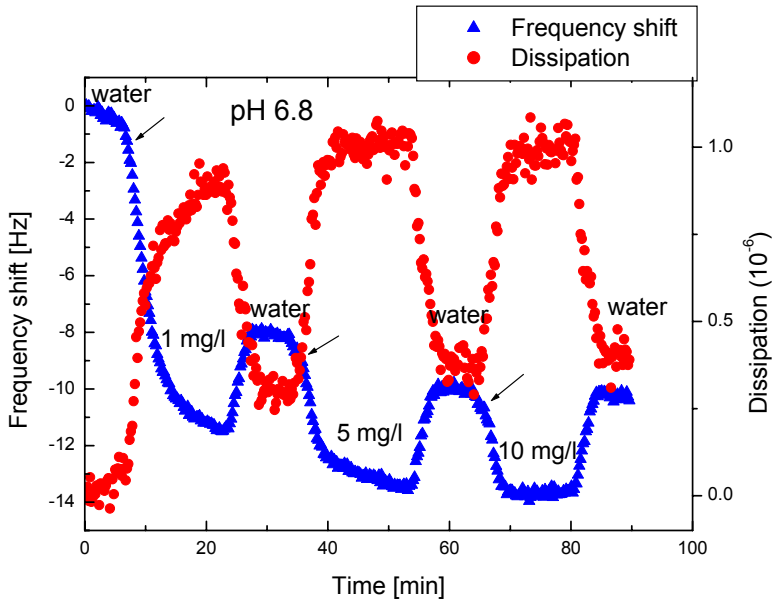

(b)

Fig. 4.15: Concentration dependence of humic adsorption at pH 5 (a) and pH 6.8 (b).

Worth to mention is the small dissipation shift in case of pH 5 which is slightly more in case of pH 6.8. Also, humic to water exchange shows quite high shifts. This all indicates a softer layer at pH 6.8 rather than pH 5.

Due to the problem of aluminium oxide dissolution in QCM experiments, which makes the sensor usable for only one experiment, we cannot vary concentration in discrete steps and recover the surface in between. Thus, concentration had to be continuously increased without recovery step. For this reason, adsorption experiments were also done by ellipsometry (figure 4.16). Each experiment was performed three times with a fresh aluminum oxide coated substrate, and the data were plotted as average values with error bars. A rapid growth of thickness is noticed at dilute concentrations, followed by saturation at concentrations of about 10-20 mg/l. This coincides with QCM results and, therefore, indicates that adsorption onto a neat aluminium oxide surface for discrete values of concentration leads to the same effect as continuous variation of concentration in case of QCM measurements.

Another coincidence is the average thickness at saturation which more or less corresponds to the thickness of a humic monolayer obtained from QCM (about 15 - 20 Å). In contrast to the QCM measurements, higher thicknesses are observed at pH 5 compared to pH 6.8 in ellipsometry. That could be interpreted on the basis of the layer softness that appears as higher dissipation (fig 4.15 b), which at the same time is noticed as an excess load in QCM measurements resulting in higher frequency shifts. Although the above statements hold in case of pH 5 and 6.8, the curve did not stabilize at pH 9 and continued rising up. Presently, this behaviour could only be explained by dissolution of aluminum which on one hand increases the surface roughness, and on the other hand complexes humic which in turn increases the thickness due to formation of agglomerates. A detailed analysis is presented in chapter 4.5.

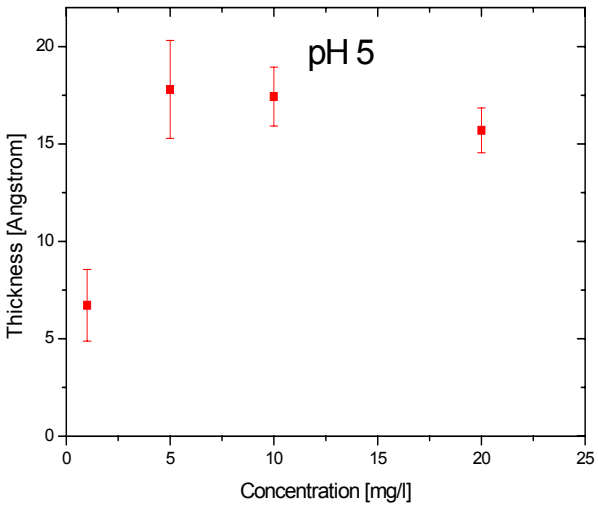

(a)

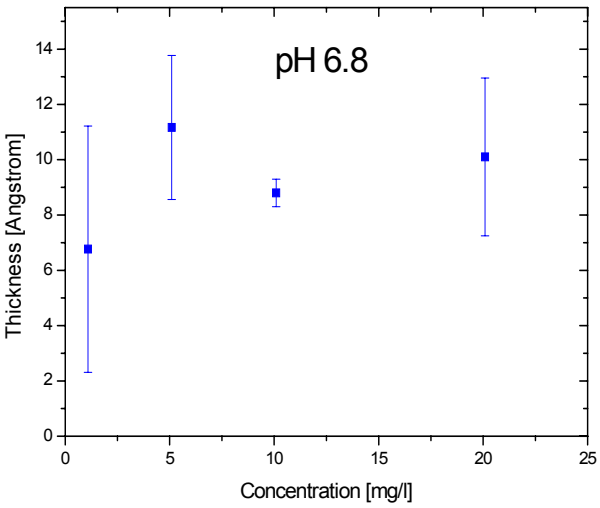

(b)

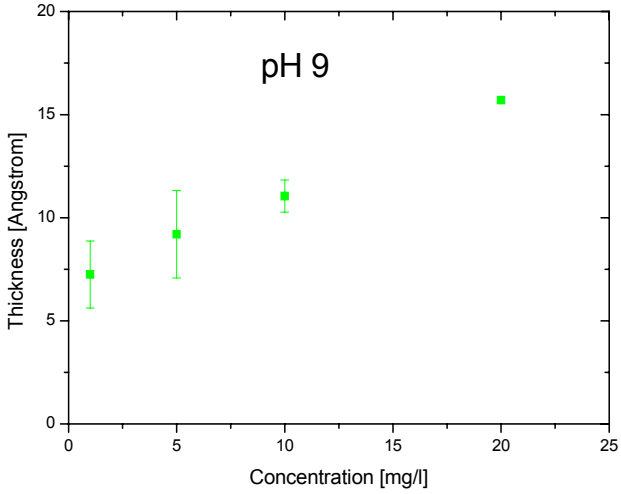

(c)

Fig. 4.16: Development of thickness upon concentration variation, measured by ellipsometry at (a) pH 5, (b) pH 6.8 and (c) pH 9.

4.3.4. Thickness determination by different methods

Figure 4.17 summarizes the result of thickness measurements performed by three different techniques: QCM, ellipsometry and XPS. The concentration was kept constant at 20 mg/l. Values from QCM studies were determined by the Sauerbrey equation, XPS values were calculated using equation 2.25`, and ellipsometry values were taken from figures 4.10 and 4.16.

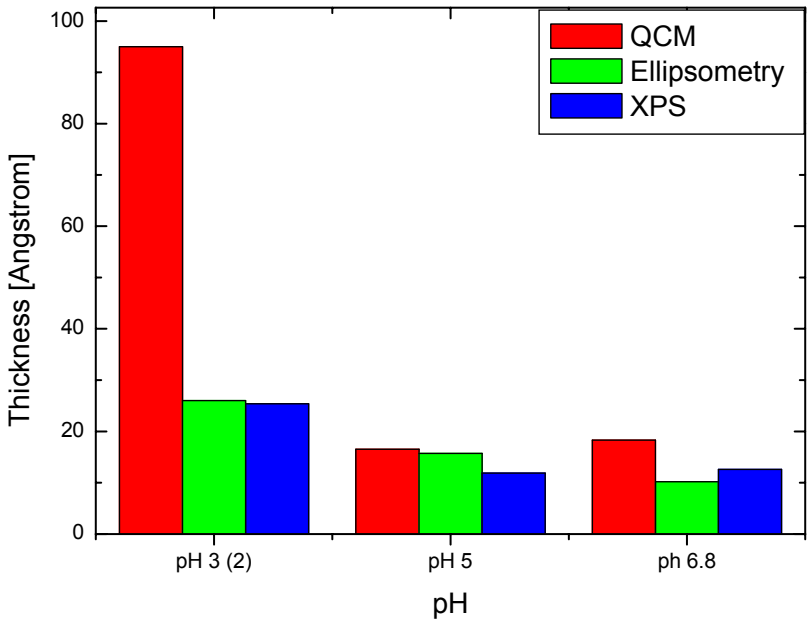

Fig. 4.17: Thickness of adsorbed humic film at a concentration of 20 mg/l determined by three different techniques: QCM, ellipsometry and XPS.

The diagram roughly shows a decreasing thickness by increasing pH. Except for pH 3, the three techniques agree well in that the error is only about ± 2.4 Å for pH 5 and ± 4.1 Å for pH 6.8. Considering the special case of pH 3, XPS and ellipsometry data mostly agree with each other. Both were obtained for a dry surface after ultrasonic treatment and, hence, most of the weakly bound molecules are washed off. In QCM measurements, these molecules are still on the surface.

4.4. Desorption

4.1. Desorption of the adsorbed humic film

Over the last subchapters, many aspects about humic adsorption have been discussed. In the current section, we are now going to discuss the opposite process, which is desorption. On a short time scale, a backshift of the response in QCM experiments was only observed due to bulk effects such as rinsing with water or salt. In addition, ultrasonic treatment for a couple of minutes of wafers prepared for XPS and ellipsometry measurements did not show any desorption of the monolayer. Thus, on short time scales, there is no evidence of desorption either on wafers or sensors. Taking into account the data shown in table 4.1, plasma, UV light and organic solvent treatment were used for up to 20 minutes to regenerate the surface but did not show any effect. Thus, desorption experiments should be performed on a long time scale using only the solvent in which humic acid is dissolved, i.e. water. Because of the instability of the aluminum oxide coated sensor we were not able to do experiments on long time scales using QCM. Not only the layer instability but also drifting is a problem of long-term experiments.

An aluminum oxide coated silicon wafer was used for long time immersions in humic and in water to be measured by ellipsometry. A wafer that was only immersed in water for three days and dried afterwards did not have the same optical constants as prior to water treatment. Thus, it cannot serve as a reference for long-term experiments. Due to this reference problem, ellipsometry is also no suitable technique for studying the adsorption behaviour on long timescales.

Therefore, XPS was selected for this purpose as it is less dependent on alterations of the aluminium oxide layer than QCM-D and ellipsometry. It can be used to both quantify the amount of specific atoms adsorbed onto a surface and the thickness of surface-bound films. Wafers were immersed in humic at a concentration of 10 mg/l and pH 5 for 60 minutes and sonicated afterwards in water for 5 minutes. Next, every wafer was cut into two halves: one half was immersed in water for desorption, the other half was kept under nitrogen to be measured directly. Figure 4.18 presents the carbon 1 s peak of three wafers after humic film formation in comparison to a non-

coated reference wafer (a), and the averaged peak with error bars (b). Figure 4.19 shows the spectra of these wafers after exposure to water.

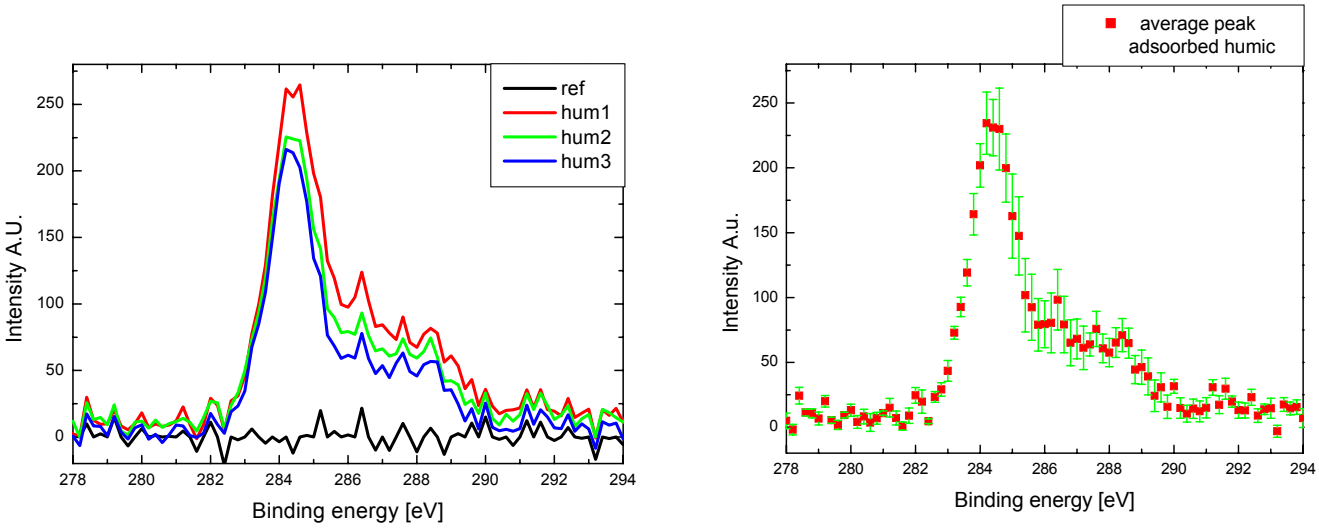

(a) **(b)**

Fig. 4.18: Carbon 1s peak of the adsorbed humic film for three different wafers exposed to the same humic concentration of 10 mg/l at pH 5 in comparison to a non-coated reference wafer (a), and the average of the three peaks plotted with error bars without the reference line (b).

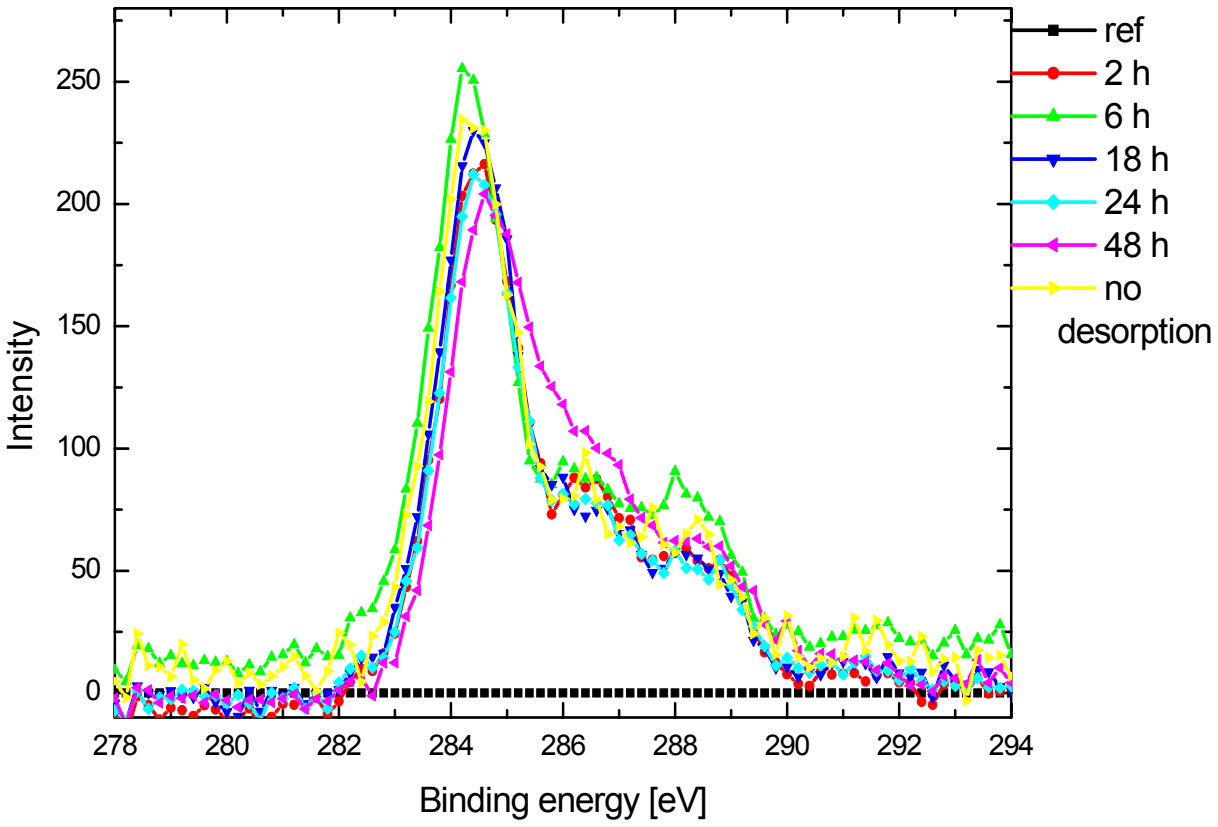

Fig. 4.19: Carbon 1 s peak of the humic film after immersion in water for periods starting from 2 to 48 hours, the black zero line is the reference wafer, the yellow curve indicated as no desorption is the average peak of humic film which was not immersed in water.

The shape and heights of the peaks in fig. 4.19 give a rough feeling that there is no desorption which can be detected after a period of 48 hours immersion in water. However, for exact analysis, the peak areas were calculated, normalised to the area of the averaged peak of the humic film, and plotted versus immersion time in water (fig 4.20). The zero line indicates no humic desorption. Most of the points are occurring at an average value of - 0.2 indicating about 20% desorption. Nevertheless, a time dependence of desorption cannot be observed. Hence, this proportion that has been removed from the surface could also be interpreted as the washing off of some weekly bounded molecules.

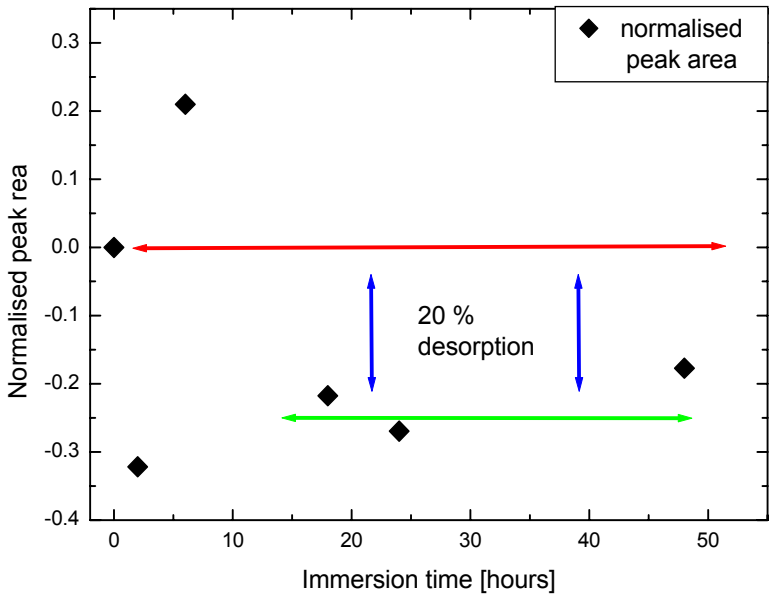

Fig. 4.20: Peak areas for humic-coated wafers after immersion in water (fig. 4.19) are normalised to the average peak area of original humic films and plotted versus immersion time.

4.4.2. Removal of humic film to regenerate the sensor

For adsorption at pH 5, regeneration of the sensor surface was tested in situ by sodium dodecyl sulphate (SDS) but seemed to have no effect at all. Therefore, several regenerating methods were applied to sensors used in QCM measurements for adsorption of 20 mg/l humic. Ellipsometry was applied to determine the efficiency of these methods. The results are summarized in table 4.1.

Method	UV/SDS/UV	Plasma	Dimethylsulphoxide	H_2SO_4/H_2O_2
Time/min.	10 / 30 / 10	20	20	10
Thickness [Å]	32	29.7	30	*dissolved*

Table 4.1: Ellipsometry as a proof of regeneration efficiency, Applying UV/SDS/UV, plasma and dimethylsulphoxide did not affect the adsorbed film. Application of H_2SO_4/H_2O_2 was too aggressive so that the aluminum oxide coating dissolved immediately.

It seems that the humic film at pH 5 is very rigidly attached and hard to be removed by common methods. Unfortunately, the aluminum oxide layer cannot resist very

acidic solutions. To ensure the reliability of these measurements an unused sensor served as a reference for each measurement, and gave film thicknesses of 1.2 and 1.7 [Å]. Such a slight thickness variation may be due to contamination. Since the wet chemical methods are either not capable of removing the humic layer or too aggressive, UV irradiation was applied for longer periods of time. Figure 4.21 shows XPS spectra of the carbon 1s peak of different samples, including aluminium wafers and sensors, with humic adsorbed on their surface and after irradiation with UV light.

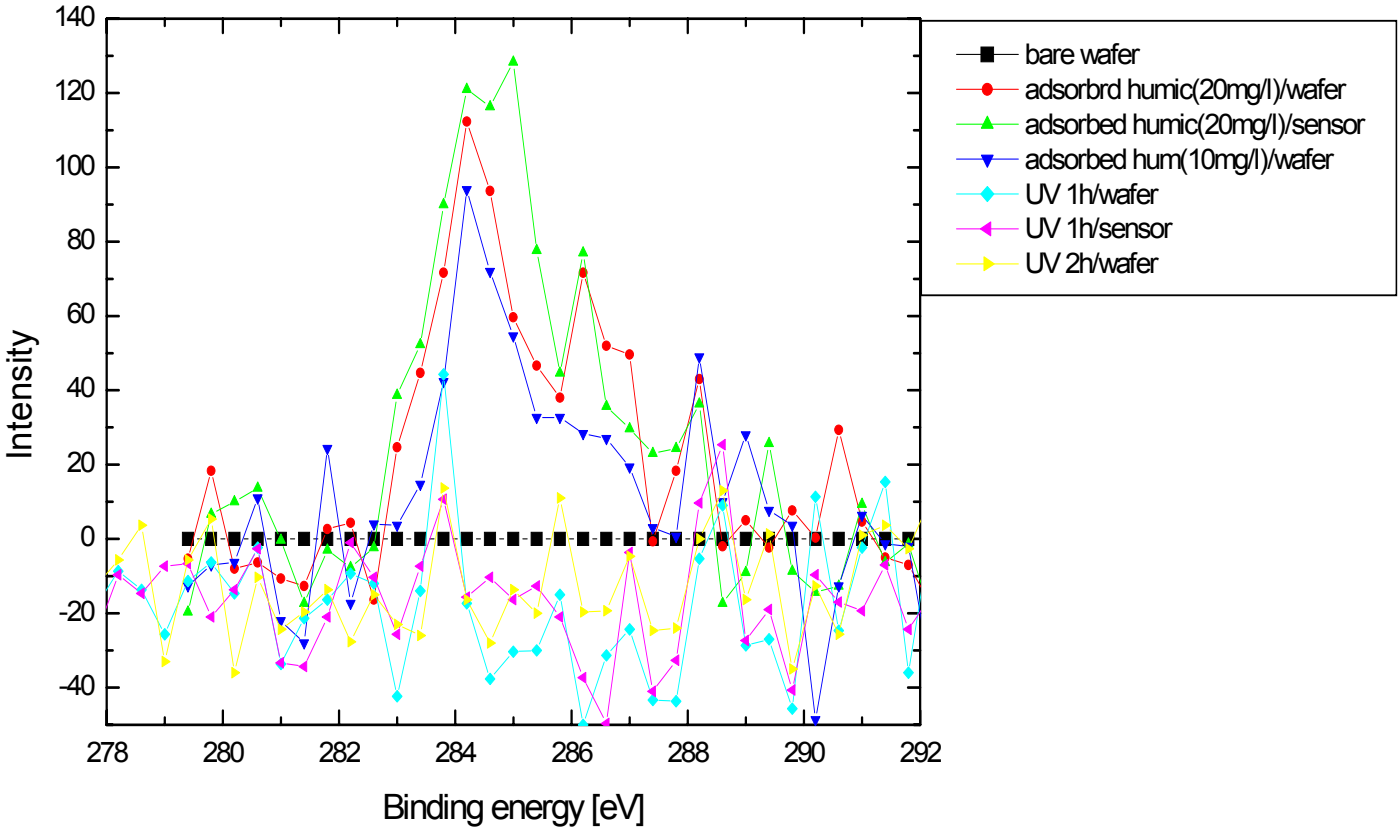

Fig. 4.21: XPS spectra of the carbon 1s peak of different humic-coated samples, including aluminium wafers and sensors, that have been irradiated by UV light to regenerate the surface. Spectra above the zero line (black) are for humic-coated samples prior to irradiation, those under the line are samples which have been irradiated for 1 and 2 hours.

In the experiments, wafers were immersed in humic at pH 6.8 and at concentrations of 10 and 20 mg/l for 45 min. A sensor was used with the same solution in a QCM measurement and humic adsorption was performed on it for 20 min, at a humic concentration of 20 mg/l and pH 6.8. UV treatment was applied for 1 and 2 hours.

After irradiation the amount of carbon left on the surface seems to be less than that already existed on the reference. Hence, negative intensity values are observed.

4.5. Ternary System

4.5.1. Effect of pH

After the binary system has been extensively studied in chapter 4.3, the same systematic study is going to be presented on the ternary system in the current section. Gadolinium chloride was added to the system at a constant concentration of 10^{-6} M keeping the salt concentration constant at 0.1 M just as for the binary system. Gadolinium chloride was selected because gadolinium belongs to trivalent lanthanides which are in the focus of our study. Its chloride salt is soluble in water, and a concentration of 10^{-6} M is consistent with metal trace concentrations in clay environment. Figure 4.22 presents the adsorption curves for the ternary system at concentrations of 5 mg/l of humic, 10^{-6} M of $GdCl_3$, and 0.1 M sodium perchlorate (salt), and pH 5.

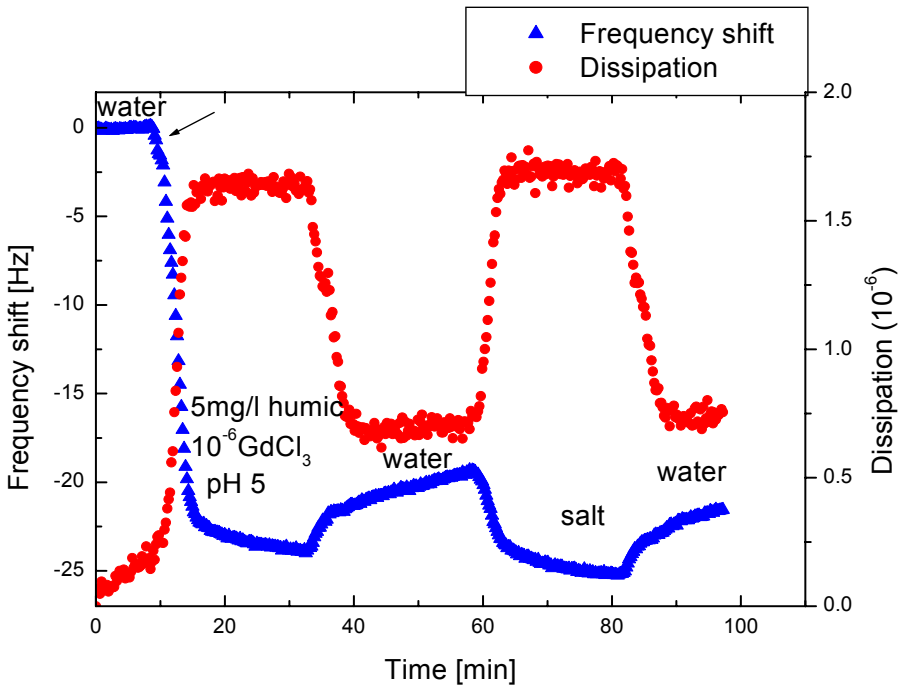

Fig. 4.22: Frequency and dissipation shifts due to adsorption onto aluminium oxide sensors in the ternary system, at a concentration of 5 mg/l humic, 0.1 M sodium perchlorate (salt) and 10^{-6} M gadolinium chloride at pH 5.

Similar to the binary system adsorption happens immediately upon exposing the sensor to humic solutions, with a fast initial rate and a longer time scale for levelling off. The complete process, that takes less than 10 minutes for humic alone, needs for a humic/Gd mixture about 20 minutes. Regarding the quantity of the frequency shift; it is about as double as much as for humic alone. Dissipation shift is about four times as much at the adsorption equilibrium level, and reduces to half of this value upon rinsing by water. This means that introducing gadolinium to the system stimulated the adsorption resulting in duplication of the amount adsorbed, about 35.5 Å calculated by both the viscoelastic model and Sauerbrey, slower kinetics and changing the physical properties of the adsorbed film as indicated by the dissipation term.

Plotting dissipation against frequency (fig. 4.23) reveals additional essential information about the adsorbed film. As seen in fig. 4.23, dissipation increases linearly with increasing frequency over the whole adsorption range until levelling off at a value of about 1.6, which is not the case in the binary system (compare figs. 4.23 and 4.12). Since the time term is absent and only implicitly represented as the density of data points, we can then distinguish between two different kinetic scales: a fast kinetics in the binary system and a slow one in the ternary system.

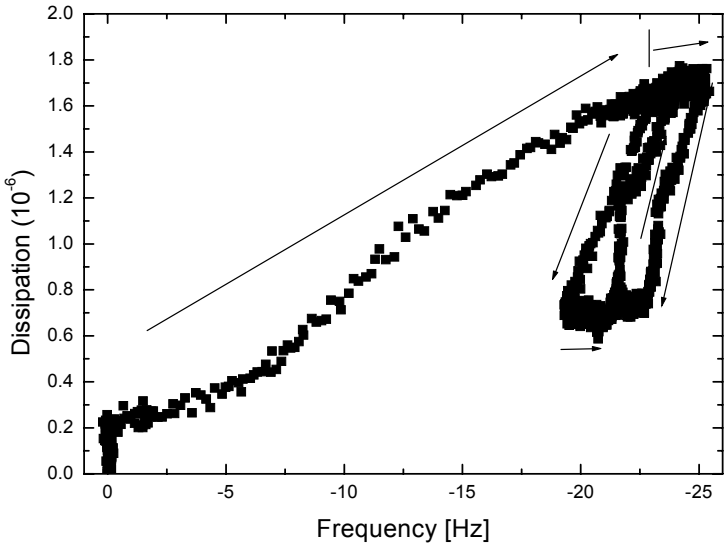

Fig. 4.23: Plot of dissipation versus frequency for the raw data of the ternary system from fig. 4.22. The arrow shows the time course of data acquisition.

The linear increase of dissipation with increasing frequency in addition to the extremely high shift by the time equilibrium has been reached must be compared to a simple plateau accompanied by a slight shift in binary system. These differences may be attributed to internal differences in the structure of the two types of adsorbates. While the monolayer formed in case of the binary system consists of a rigid film of mostly solid material, that of the ternary system seems to be softer and thicker than a simple monolayer. After equilibrium is reached, rinsing with water and salt results in the expected bulk effects on the frequency shift (figure 4.22). Interestingly, rinsing with water reduces the dissipation to more than half its equilibrium value in a salt-containing solution. This effect is seen as a hysteresis in fig. 4.23, showing how dissipation responds massively to ion concentration. These massive changes upon water-to-salt exchange strongly suggest the penetration of salt into the film, causing stretching of the layer, thus, enhancing water uptake.

Based on this discussion the film structure in the ternary system may be considered as a humic monolayer which is attached to the aluminum oxide surface and is bridged by complexed gadolinium molecules to another upper humic layer; hence gadolinium is sandwiched in between. This bridge and the upper layer is the distinctive difference between the two systems and responsible for the formation of a softer and thicker film (fig. 4.24).

Evidently, this structure does not build up on the surface in consequent steps as a lower layer followed by the gadolinium bridge, which is then covered by the upper layer. This picture seems to be wrong, since there is no evidence of three different adsorption steps. Adsorption rather takes place in one step. The right interpretation could be that complexes already formed in solution successively adsorb onto the surface. Another evidence for such type of process is the slower kinetics, compared to the binary system, which would then be due to the increased size of the adsorbing complex resulting in a reduced diffusion and film formation velocity.

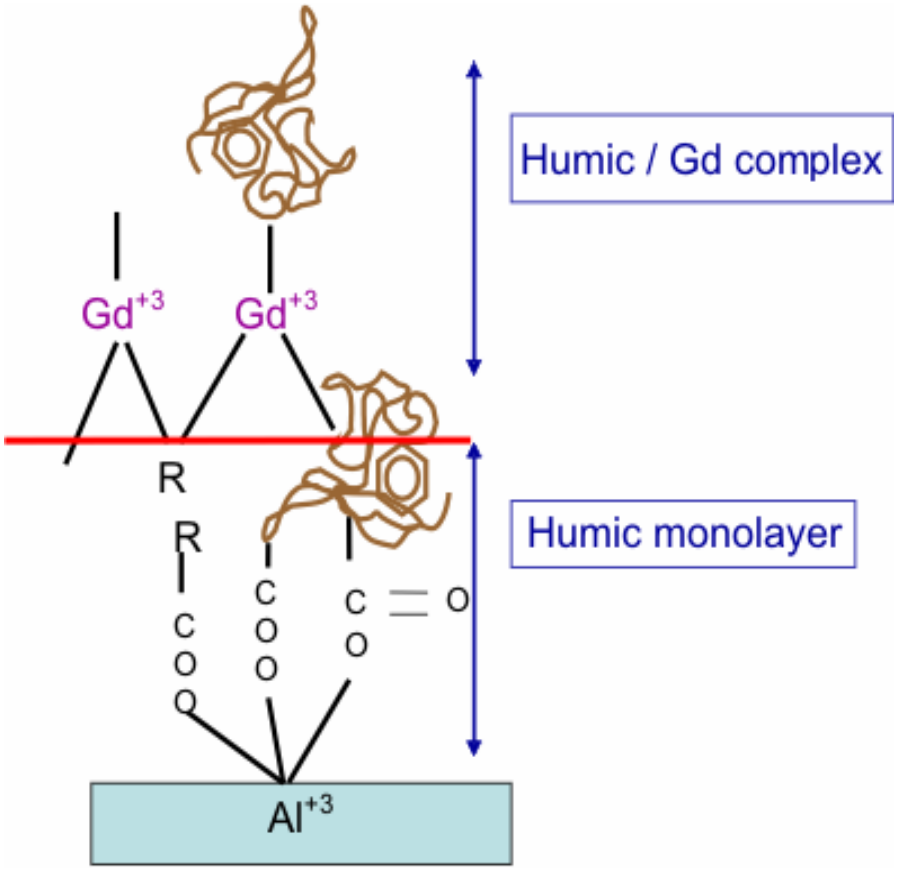

Fig. 4.24: Adsorption of a humic/Gd complex on the surface of aluminum oxide. Adsorption takes place by interaction of humic acid carboxyl groups with the hydrated aluminum oxide. Next to the surface of aluminium a humic monolayer is formed, which is connected to a second humic layer or a humic/Gd complex via a Gd bridge.

Adsorption at pH 3 was also investigated. Figure 4.25 shows the typical adsorption curve of the ternary system at a concentration of 10 mg/l humic, 10^{-6} M Gadolinium chloride and 0.1 M sodium perchlorate. Adsorption takes place in two steps with two time scales and two different frequency shifts. Frequency shifts for both the first and second adsorption step are mostly double as much as in case of humic alone. In addition, the time needed for completing adsorption is as twice as long, too. Applying the extended viscoelastic model yielded thicknesses of 3.1 nm for the first step and 27 nm for the second step. Thus, the hypothesis of a complexation effect by gadolinium is strongly supported. These experiments were performed twice with sensors from the same batch to confirm reproducibility.

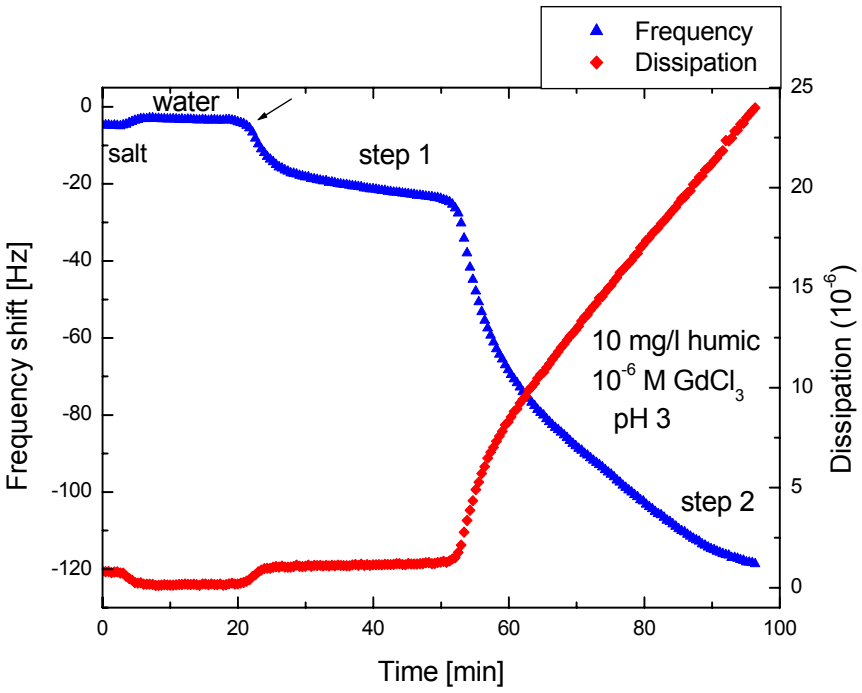

Fig. 4.25: Adsorption in the ternary system at pH 3 for 10 mg/l humic concentration and 10^{-6} M gadolinium. Adsorption takes place in two steps yielding double the amount of adsorbate compared to the binary system as well as a two times slower kinetics for both steps.

The same model for the layer structure that was derived for adsorption at pH 5 applies to the case of pH 3, too. Accordingly, whereas the first adsorption step at pH 3 in the binary system consists of a humic acid monolayer, the first step in the ternary system consists of a layer of humic gadolinium complex as illustrated in figure 4.24. In the same way, the second adsorption step in the binary system refers to physically aggregated humic molecules. In the ternary system, however, it refers to physically aggregated humic/Gd complexed species.

A plot of dissipation versus frequency is shown in figure 4.26. The plot shows the same effect as in case of pH 5: a linear increase of dissipation with increasing frequency. A remarkable difference is that the highest level of dissipation that was ever reached in the whole study, about 25 units, was recorded for the ternary system at pH 3.

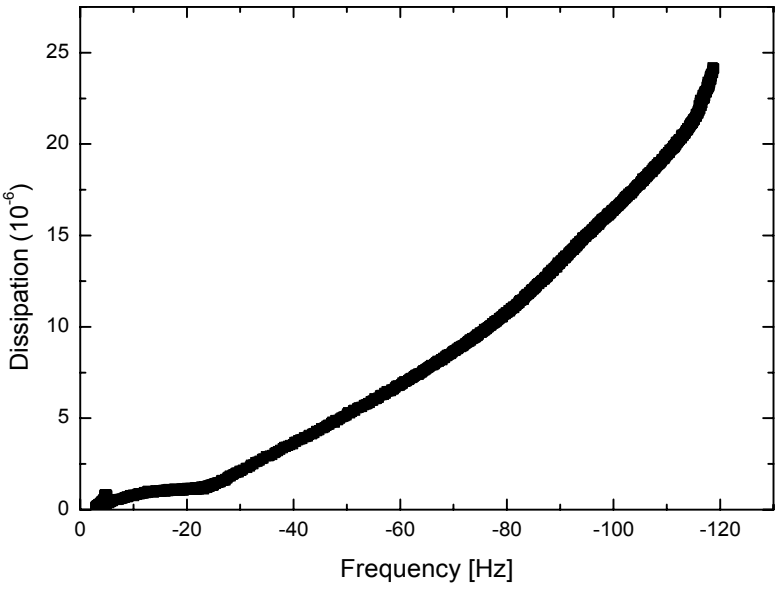

Fig. 4.26: Dissipation plotted versus frequency shift for adsorption at pH 3. Raw data were taken from figure 4.25. The same effect is seen as for pH 5: a linear increase of dissipation with frequency indicating a soft and extended film.

5.2. Concentration effects

In addition to pH, concentration effects were investigated. Figure 4.27 shows the effect of varying the concentration of humic acid at pH 5 and a constant concentration of gadolinium of 10^{-6} M. The baseline was taken for water and neat frequency shifts were then calculated after rinsing by water, i.e. from water to water levels. Variation of humic concentration results in the same effect as in case of the binary system: most of the monolayer already forms at a low concentration of 1 mg/l. Further increase of concentration leads to relatively small frequency shifts indicating the completing of the monolayer until saturation is reached at about 10-20 mg/l. Beside the higher amount adsorbed no other effects due to concentration variation can bee seen. In addition, saturation seems to occur later than in the binary system

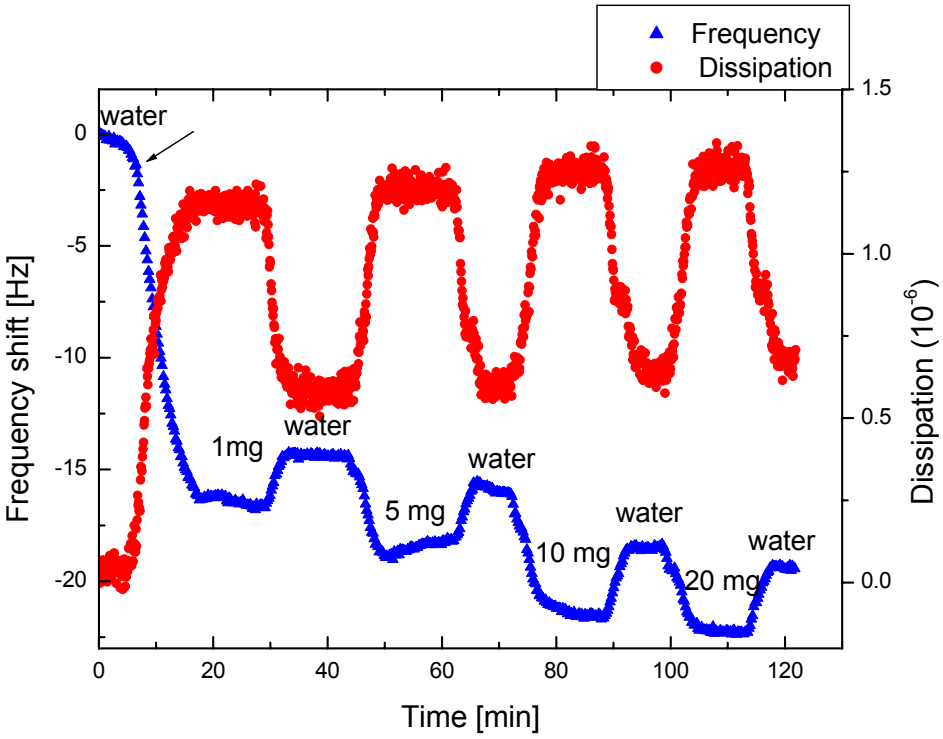

Fig. 4.27: Variation of humic acid concentration in adsorption of the ternary system at pH 5 while keeping the concentration of gadolinium constant. The concentration effect is similar to the binary system.

A plot of dissipation versus frequency (fig. 4.28) shows that an almost linear frequency/dissipation relationship is characteristic of the ternary system. A hysteresis was observed upon rinsing by water, which reduces dissipation to half its value when washing off the humic/Gd layer.

A confirmation of the concentration effect was attained by ellipsometry. For this purpose, solutions with constant gadolinium and different humic concentrations were prepared. The aluminium oxide wafers were irradiated for 10 minutes by UV light, and then were immersed for two hours in the above solutions. The time interval was taken from kinetic experiments (chapter 4.6.2) which suggests saturation after two hours of immersion. Fig. 4.29 shows the ellipsometry results for the development of film thickness upon variation of humic concentration.

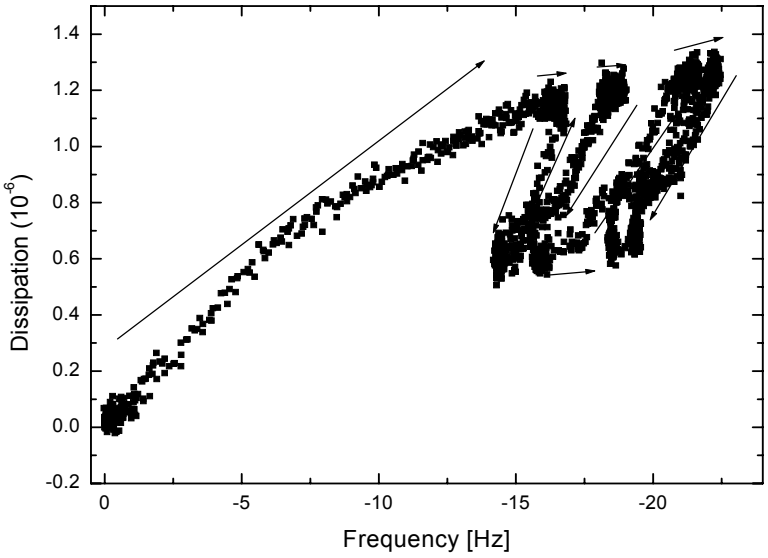

Fig. 4.28: Plot of dissipation versus frequency for varying humic concentrations in the ternary system at pH 5. Raw data were taken from fig. 4.27. The arrow indicates the time course of data acquisition.

The curve shows an almost linear increase of thickness up to a concentration of 10 mg/l followed by saturation, which actually agrees with the QCM results. The average thickness at saturation is, however, quite different in the two experiments: in ellipsometry it is about 23 (± 5) Å, while QCM yields 36 Å by modelling and 32 Å by Sauerbrey.

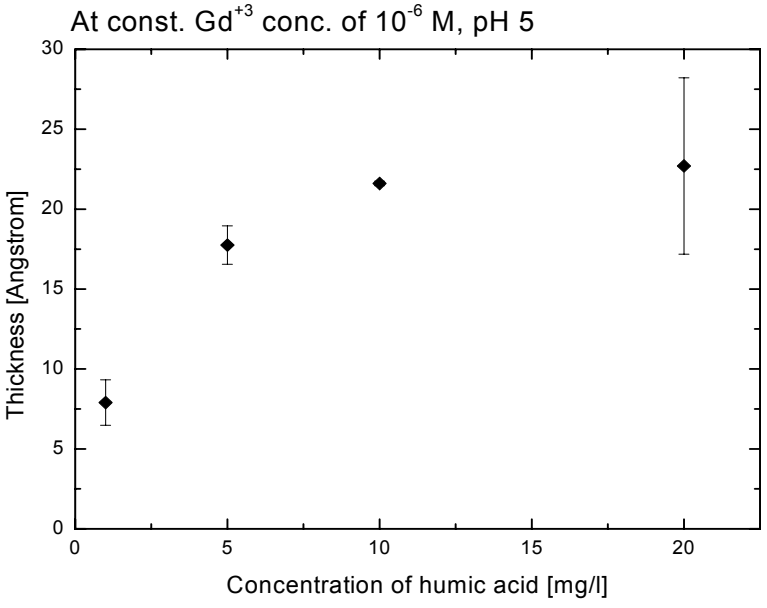

Fig. 4.29: The development of film thickness in the ternary system upon variation of humic concentration while keeping the concentration of gadolinium constant.

4.6. Kinetics of adsorption

In addition to the insight in kinetics gained from QCM experiments, another kinetic study was performed by ellipsometry for both the binary and the ternary system. This study aimed at developing an understanding of the dependence of thickness on adsorption time measured in the dry state, which is preferably to be done by an additional technique to support the results of QCM. Aluminum oxide wafers used to show better stabilities than aluminium oxide sensors. Therefore, they can be used for long immersion time intervals and, thus, provide information that is beyond the capabilities of QCM. For a constant concentration of humic acid (1 mg/l), solutions at different pH values were prepared. Aluminium oxide wafers were then immersed for different time intervals, sonicated and then dried with nitrogen. Figure 4.30 shows the development of film thickness as a function of time for the different pH values.

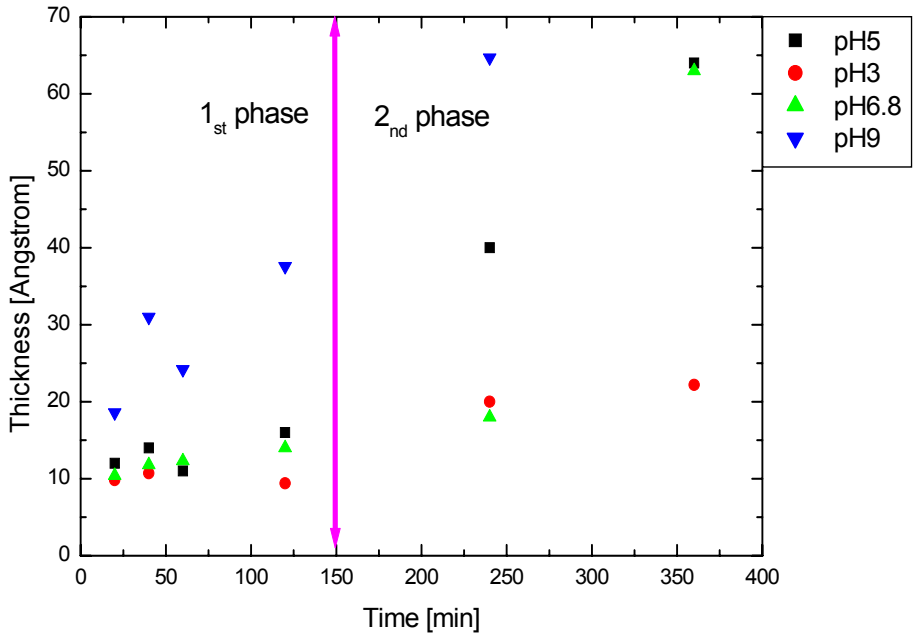

Fig. 4.30: The development of film thickness as a function of time in the binary system for various pH values at constant humic concentration (1 mg/l), measured by ellipsometry. The double arrow at 150 minutes indicates the barrier between the two phases. In the first phase, adsorption of the monolayer takes place, in the second phase, dissolution of aluminum is assumed to happen which complexes humic acid and is the reason of high thicknesses observed.

The shortest immersion time selected was 20 minutes. From this time on we can only see a slight increase of thickness which turns into a plateau during the first 60 minutes. All the different pH values yield almost the same thickness which is lower than 15 Å, except for pH 9 where thicknesses of more than 35 Å are observed. This effect was already noticed in figure 4.16c and attributed to the dissolution of aluminium taking place at this alkaline pH, increasing surface roughness and potentially enhancing adsorption by the formation of Al/humic complexes. After 150 minutes or two hours of immersion, a rapid growth of thickness is seen up to 70 Å. The total time span of the experiment was about 6 hours, and was divided into two regimes indicated by the double arrow at 150 minutes. A first phase is observed in which the adsorbed film is built up, followed by a second phase in which thickness further increases. The reason for the latter behaviour is still not fully understood.

We proceed now to the ternary system (figure 4.31). The same experiment was performed for a constant humic concentration of 5 mg/l, a constant gadolinium concentration of 10^{-6} M and different pH values.

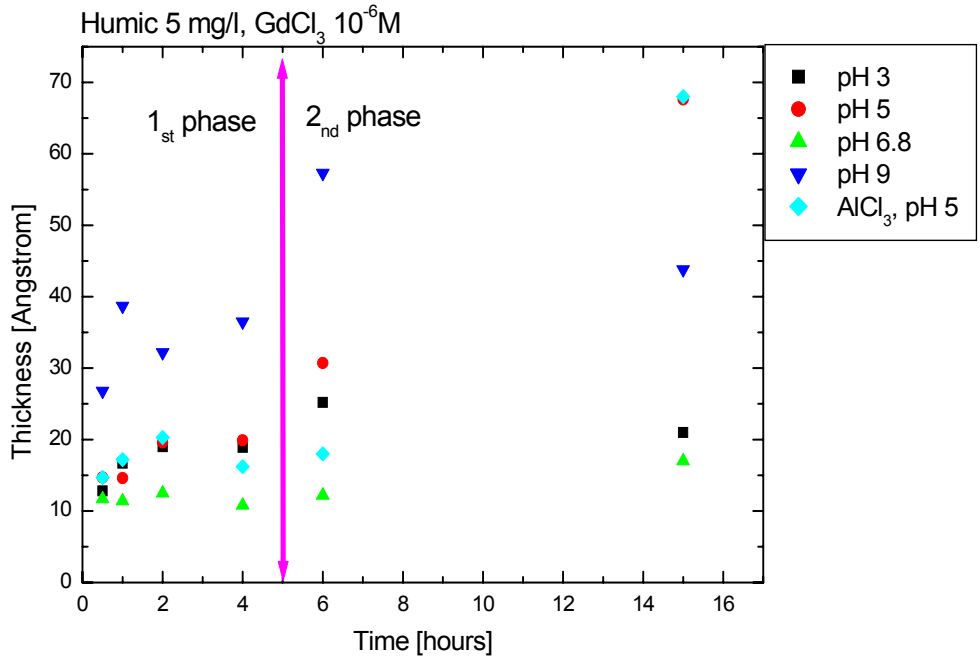

Fig. 4.31: Adsorption kinetics in the ternary system, measured by ellipsometry. Two different regimes are observed with a boundary at about 5 hours. Addition of aluminium ions enhances adsorption and plays the same role as gadolinium.

Interestingly, the same phenomenon was noticed as in the binary system: there are two kinetics regimes separated by a boundary at about 5 hours. The first regime is the build up region of the adsorbed humic/Gd layer, while the second regime is characterized by a rapid increase of film thickness. Also, adsorption at pH 9 yields higher thicknesses than expected. In order to test the effect of dissolved aluminium, aluminium chloride was added to a solution series at pH 5 and at the same concentration as gadolinium. As a result, addition of aluminum yielded the same curve as gadolinium, indicating enhanced complexation.

The overall outcome of kinetics experiments (figure 4.30 and 4.31) is that the adsorbed layer is formed at early immersion times up to one and four hours in the binary and ternary system, respectively. The thickness evolution observed for long immersion is supposed to be due to aluminium oxide dissolution followed by a complexation mechanism.

In order to verify the latter statement, a series of solutions were prepared with a constant humic acid concentration of 10 mg/l and various aluminium chloride concentrations at pH 5. Aluminium oxide wafers were then immersed in these solutions for three hours, the time needed to form the adsorbed layer in the ternary system. First we shall consider the pH changes in this liquid due to increasing the concentration of aluminium chloride. The experiment was performed twice, each time with a different starting pH.

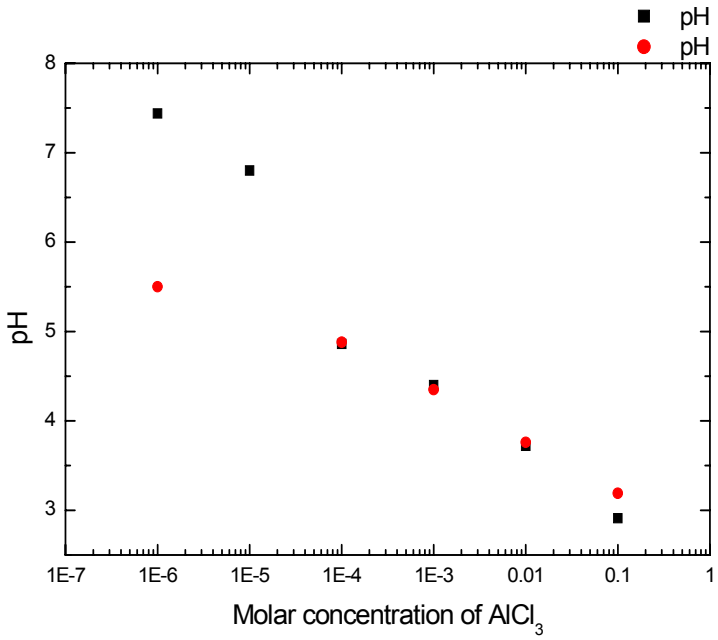

Fig. 4.32: The solution acidity increases drastically when the concentration of $AlCl_3$ is increased. At higher concentrations, corrosion happened sometimes immediately and in other cases during the three hours of immersion time.

As seen in figure 4.32, the pH drops linearly by increasing the concentration of aluminium chloride. This change of pH may affect the dissolution of aluminum resulting in irregular film growth in the presence of humic acid due to complexation effects. To test this hypothesis, various aluminum chloride concentrations were added to 10 mg/l humic solutions, starting at pH 5. After 3 hours of immersion, the thickness of the adsorbed film was measured (figure 4.33). At mild concentrations, where the pH still rather unaffected by the aluminum ion concentration, a humic monolayer is formed with a thickness range similar to that of the ternary system. By increasing the concentration of aluminum chloride, accompanied by pH dropping, the thickness tends to increase by one order of magnitude presumably to enhanced aluminum dissolution and related complexation processes. This effect could explain the second kinetic regime in figures 4.30 and 4.31. Moreover, at concentrations of 0.01 and 0.1 M the surface was corroded to such a high extent that ellipsometry experiments became impossible.

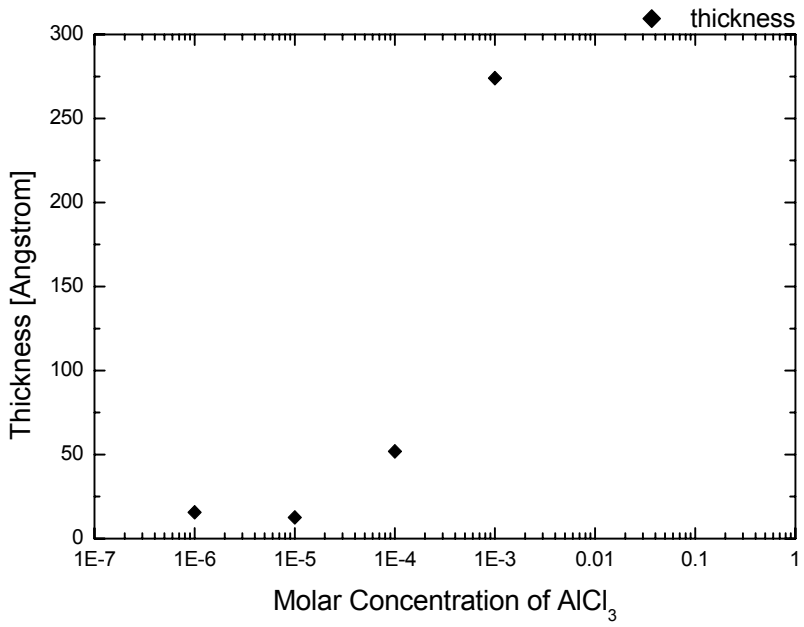

Fig. 4.33: Adsorption of humic (10 mg/l, pH 5) at different aluminum chloride concentrations. Film thickness is increasing with increasing ion concentration. At high aluminum chloride concentrations (0.01 and 0.1 M) the surface was corroded.

Dissolution of aluminium oxide used to be the real obstacle during the whole course of this work. A microscopy image of a corroded aluminium oxide surface is shown in figure 4.34.

Fig. 4.34: Microscopy image of an aluminum oxide sensor used in a QCM measurement. The corroded areas appear as brown spots with respect to the yellow background that represents the aluminum oxide surface, which is actually silver in colour. The image was taken by a digital camera connected to an optical microscope (horizontal scale: 1000 µm).

Consequently, a kinetic study should be limited to the first phase, which is the regime of monolayer build up, and where the process is not disturbed by dissolution effects. Figures 4.35 and 4.36 present a kinetic study done by ellipsometry for the binary and ternary systems, respectively. Solutions were prepared at constant concentrations (5 mg/l of humic acid, 10^{-6} M of gadolinium chloride) and pH 5. Immersion time ranged from 1 to 60 minutes in binary system and 1 to 180 minutes in ternary system. The experiment was repeated three times and the data plotted as average values with error bars. To wash off loosely bound material from the surface after adsorption, sonication for 2 minutes was applied in binary system. In order not to disturb the complex structure in the ternary system, the humic/gadolinium solution was decanted from the adsorption glasses. Next, they were gently flushed with Millipore water until it flows over the rim. Finally, the wafer was taken out gently and dried with nitrogen.

Figures 4.35 and 4.36 clearly show the difference between the two systems in terms of the film formation kinetics as well as the average thickness reached at saturation. Adsorption seems to start at the first minute indicating a fast first attack of the

adsorbing molecules in both systems, which is in good agreement with the results of QCM. The time needed to reach saturation is the main difference in the two systems. While 60 minutes are needed in the binary system, 120 minutes are required in the ternary system, which is double as much and, thus, agrees with QCM measurements, too.

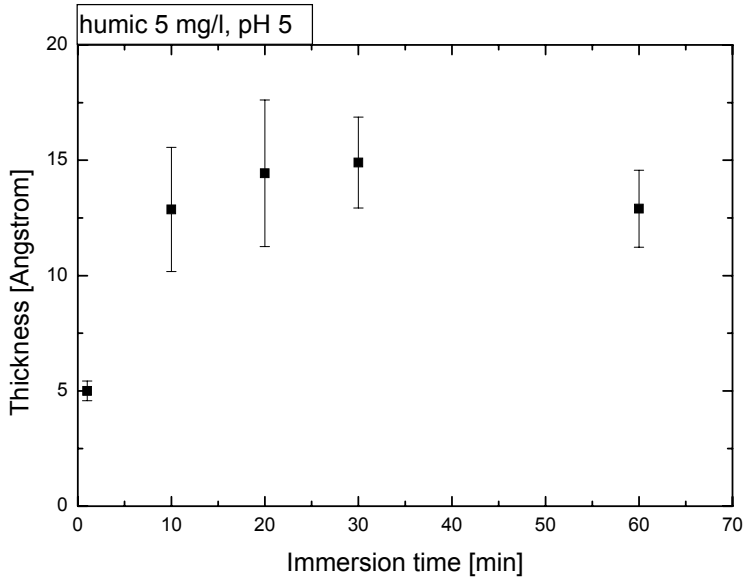

Fig. 4.35: Adsorption kinetics in the binary system.

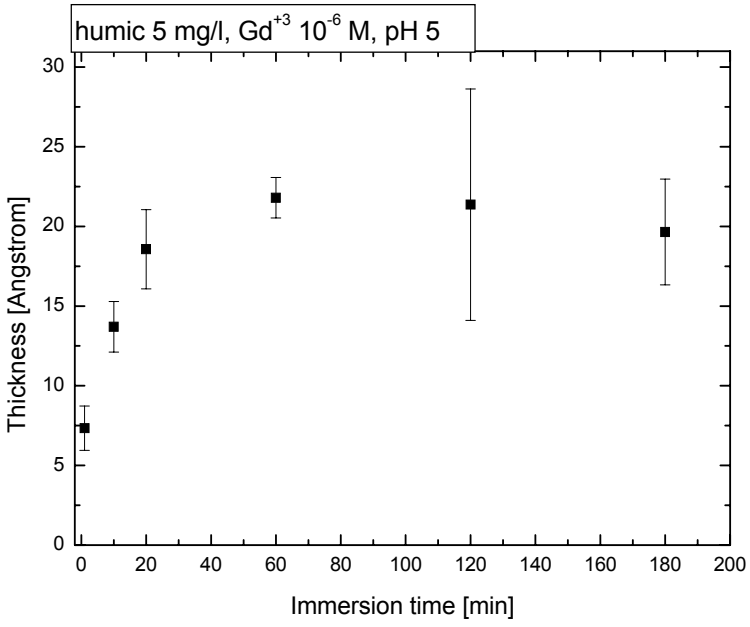

Fig. 4.36: Adsorption kinetics in the ternary system.

To this point the question of kinetics and the main differences between the two systems in focus of our study have been clarified by combining QCM and ellipsometry.

In order to check the reliability of ellipsometry to determine the amount adsorbed in both systems, XPS measurements were done on two wafers which were also used in ellipsometry measurements: one from the binary system after an immersion time of 60 minutes, the other from the ternary system after an immersion time of 120 minutes. A spectrum of carbon 1s of these two wafers in comparison to a reference, which is a bare aluminum oxide wafer, is shown in figure 4.37. The two wafers were measured by ellipsometry yielding thicknesses of 15 ± 2 Å and 22 ± 6 Å for the binary and the ternary system, respectively. By integrating the peak area, the wafer of the ternary system yielded 70% more carbon than that of binary system. The experiment demonstrates that the three surface analytical techniques used, i.e. QCM-D, ellipsometry and XPS, can be applied to the same substrate and successfully complement each other.

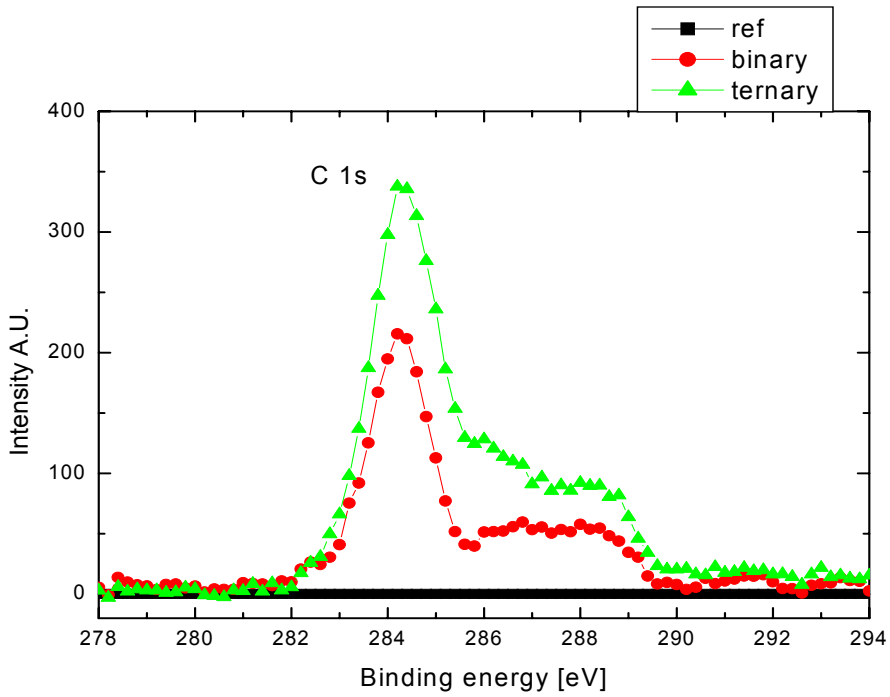

Fig. 4.37: C 1s peak of humic adsorbates on two wafers, one from the binary and the other from the ternary system, which were previously used in ellipsometry measurements (figs. 4.35 and 4.36). The wafer from the ternary system yielded 70% more carbon than that from the binary system.

4.7. Thermodynamics of adsorption

Determination of thermodynamic constants is a basic and interesting approach to characterize adsorption processes. In the current section we are going to use the concentration dependence of humic adsorption as obtained from QCM measurements in both the binary and ternary system and try to fit it with a Langmuir isotherm (equation 2.5). Figure 4.38 shows the frequency shift upon varying the concentration of humic from figures 4.15 (a) and 4.27. The adsorbed mass can then be calculated from the Sauerbrey equation and inserted into equation 2.5 (figure 4.39).

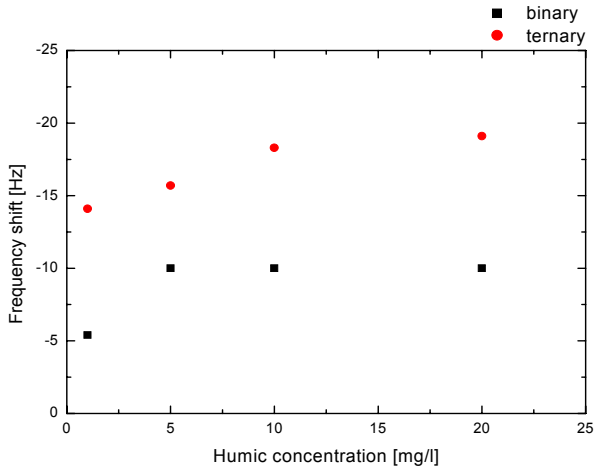

Fig. 4.38: Plot of frequency shifts versus humic concentration for both the binary and ternary system.

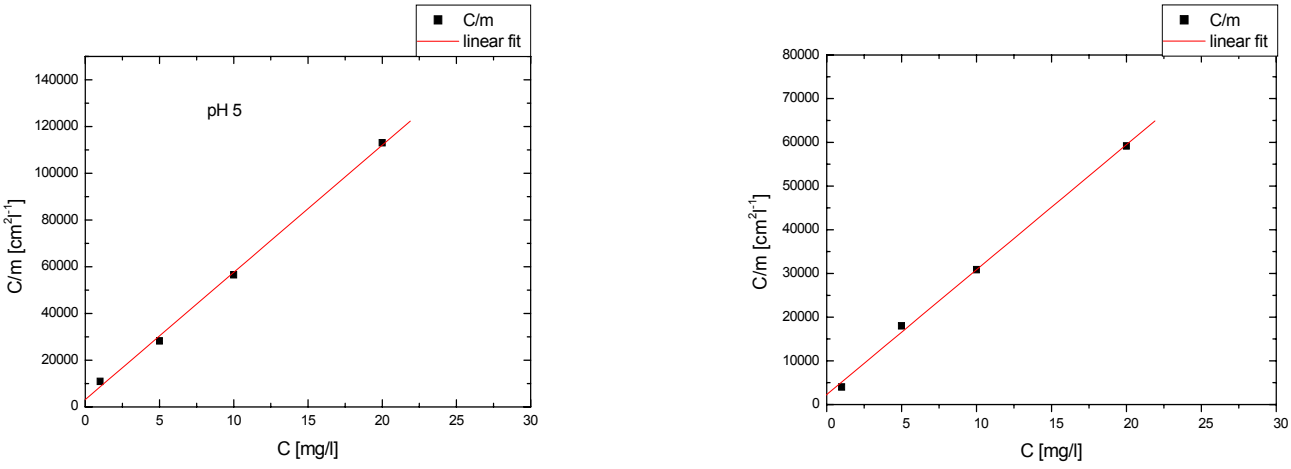

(a) **(b)**

Fig. 4.39: Langmuir isotherm and a linear fit of the binary and ternary systems (a) and (b) respectively. Both systems obey Langmuir isotherm.

At the first sight; we realize that both systems obey the Langmuir isotherm. Thus, we can extract the thermodynamic constants of interest. Constants extracted from the isotherm are: (1) k: equilibrium constant, (2) n^s: number of moles of adsorption sites per gram adsorbent, i.e. it is a measure of the adsorption capacity, and (3) ΔG: free energy of adsorption. The linear fit Y = A + B X was used to calculate the constants of interest. The values are summarized in table 4.2.

parameter / system	A	B	$n^s = 1/B$ [$mg.cm^{-2}$]	$b = 1/A\ n_s$ [$cm^2.mg^{-1}$]	$k = ba$ [$cm^2.mg^{-1}$]	ΔG [$KJmol^{-1}$]
Binary	3162	5443	18.37 x 10^{-5}	1.72	1.699	- 29.737
ternary	2273	2859	34.97 x 10^{-5}	1.26	1.25	- 28.978

a (for water) = 0.988, R = 8.314 $JK^{-1}mol^{-1}$, T = 297° K

Table 4.2: Thermodynamic constants which are extracted by fitting raw adsorption data to Langmuir isotherm (figure 4.39).

The free energy of adsorption is an expression of tendency: a negative value of ΔG is an indication of a spontaneously occurring reaction, which applies to both the binary and the ternary system. Another expression of interest is n^s which is about twice as high for the ternary system. n^s is an expression counting for the maximum amount of adsorption sites in a two dimensional surface, however its higher value in the ternary system is due to the linkage of a humic upper layer by the gadolinium bridge (see fig. 4.24). Since the number of adsorption site is constant in the two systems, so the higher value of n^s in the ternary system is due to the increased thickness upon complexation.

However, in order to get a preliminary feeling of the desorption, we can consider the case of gas adsorption, equation 2.1, to extract the value of equilibrium constant, k, the rate of adsorption, k_a, and the rate of desorption, k_d. In that sense, we can express the surface coverage term, θ, in terms of the frequency shift upon adsorption

as $f/f_{sat.}$, where f_{sat} is the frequency shift at equilibrium, i.e. after levelling off. To calculate the corresponding k_{on}, we can consider the adsorption curve as an exponential growth function as: $\theta = 1 - e^{-k\,`t}$, taking the logarithm function of both sides of the equation, then: $\ln(\theta) = k\,`t$.

Figures 4.40 shows the plots of f_{sat}/f (or $1/\theta$) versus 1/C to calculate the equilibrium constant, and fig. 4.41 shows the plot of ln (f/f_{sat}) or ($\ln(\theta)$) versus time to calculate the rate of adsorption. This set of data corresponds to the adsorption in the ternary system (fig. 4.27).

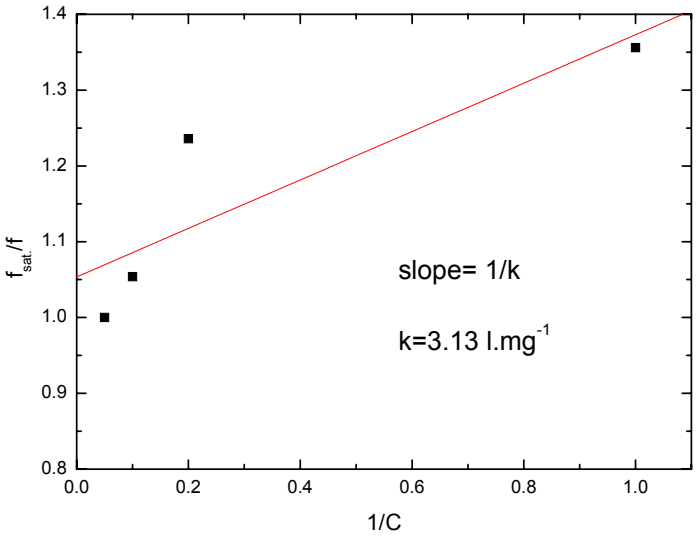

Fig. 4.40: Plot of of ($f_{sat.}$ /f), which corresponds to (1/ θ) in equation 2.1, versus 1/C. The slope of this plot yields the value of the equilibrium constant, k, according to equation 2.1.

The value of k can be obtained from the slope in fig. 4.40, k = 3.13 $l.mg^{-1}$.

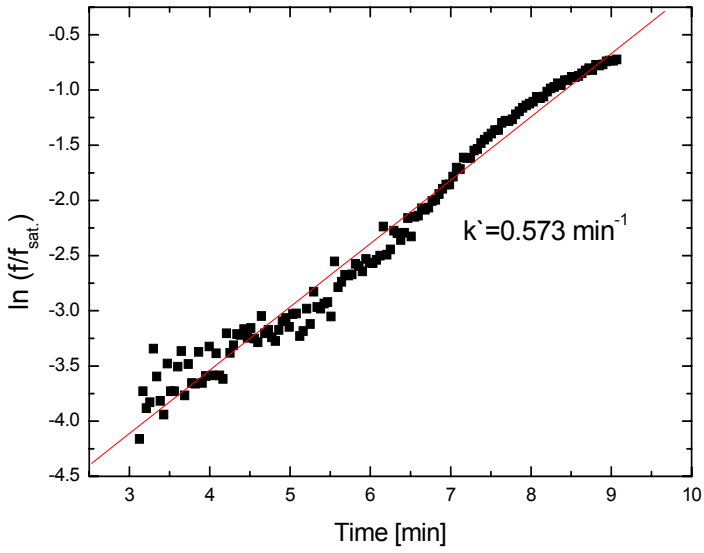

Fig. 4.41: plot pf ln($f/f_{sat.}$) versus time of the raw datao of adsorption in th eternary system (fig. 4.27) which are fitteed to Langmuir isotherm in fig. 4.39 (b). The plot presents data points for the first concentration regime of 1 mg/l and only the linear part of the curve, i.e. before frequency levells off.

The value of k_a can be calculated by dividing the slope (k`) of the curve fig. 4.41 by the concentration of solution which is 1 mg/l: $k_a = k`/C = 0.573\ l.mg^{-1}.min^{-1}$

The value of k_d can be calculated according to equation 2.1 and using the equilibrium constant: $K_d = k_a/k = 0.174\ min^{-1}$. The inverse of k_d gives the time needed for desorption in minutes, t = 5.71 min, which is short enough to be observed in our experiments, and this may be the contradiction to the Langmuir picture in our case.

Although the adsorption data fit well with Langmuir isotherm, there is a contradiction to the adsorption/desorption behaviour observed in our experiments. No significant desorption has been found during 48 hours as seen from XPS measurements, while the derivation of the Langmuir isotherm assumes full reversibility of the adsorption/desorption process. Here an interesting question arises: If the adsorption is irreversible, why does the amount of adsorbed humic increase with increasing concentration? The answer might be due molecular conformation changes or unfolding of the adsorbed molecules directly after adsorption (fig. 4.42). In case of low concentration, the molecules adsorb onto the surface, unfold and occupy a relatively large area due to unfolding. As no multilayers are formed, adsorption stops when the whole surface is covered. By increasing concentration, the adsorption process happens faster, so that the neighbouring adsorption sites are occupied before the adsorbed molecules can unfold. As a result, the average surface area occupied by an adsorbed molecule is smaller than in the dilute case and more molecules will be able to adsorb.

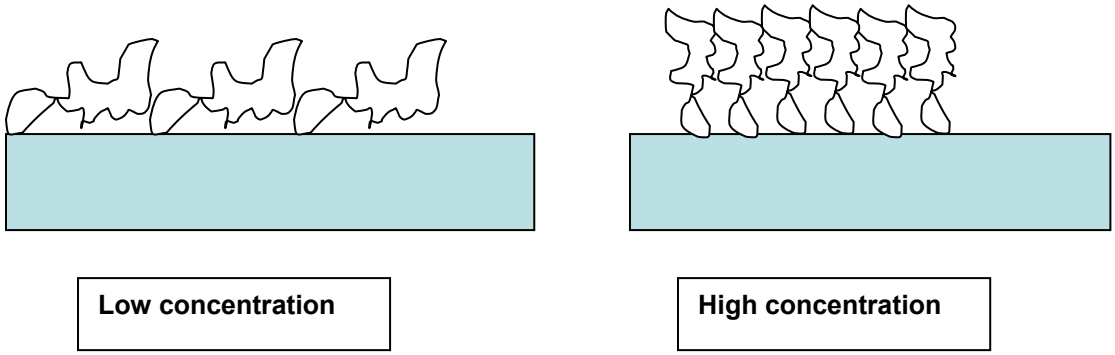

Fig. 4.42: Adsorption accompanied by unfolding. We can differentiate between two cases: at low concentration the adsorbed molecules unfold occupying a larger area than they actually would occupy in their native state. At higher concentration, adsorption happens before the molecules can unfold. Thus, the amount of molecules adsorbed is higher.

The picture of unfolding or molecular conformation is very likely to happen according to the concentration variation studies in figures 4.15 (a, b) and 4.27. In fig. 4.15 (a), frequency is shifted due to increasing concentration from 1 to 5 mg/l, however further increase of concentration does not affect frequency. It may be speculated that a monolayer of unfolded molecules has already been at low concentrations.

In fig. 4.15 (b), most of the frequency shift, i.e. adsorption, is seen at the dilute concentration of 1 mg/l, only slightly more is the shift due to concentration of 5 mg/l, at 10 mg/l there is mostly no effect at all. In fig. 4.27, the ternary system, a similar behaviour is observed.

4.8. Nature of binding

The goal of the current section is to clarify the nature of binding between humic acid and aluminium oxide based on the comparison with a standard molecule which adsorption is well understood. Previous QCM measurements indicated that the adsorption of humic acid on aluminum oxide is irreversible on the time scales accessible, i.e. the time in which the aluminum oxide coating may be considered stable. Therefore, it may be suspected that the binding occurs as chemisorption through an ion exchange mechanism between the carboxyl groups of humic acid and the hydroxyl group of the aluminium oxide in the hydrated form. In the current study we have the opportunity to compare the XPS spectra of adsorbed humic acid, which binding nature is questionable, and that of tridecanoic acid which is known to bind chemically through its carboxyl group.

Tridecanoic acid, $C_{13}H_{26}O_2$ was selected as a carboxylic aliphatic acid and prepared at a concentration of 10^{-2} M in pure ethanol. Aluminum oxide substrates were obtained by evaporating aluminum on silicon wafers to obtain a thickness of 50 nm aluminum with an upper layer of aluminum oxide. To prepare humic thin films, the aluminum substrates were first exposed to UV light at 150 W for 10-15 min. and then immersed in a solution of 20 mg/l humic acid at pH 5. In parallel, other wafers were immersed in tridecanoic acid solution. After 2 hours the substrates were taken out and sonicated for 5-10 min in Millipore water and pure ethanol for humic and tridecanoic acid films, respectively, and then dried with nitrogen gas and stored for XPS measurements.

4.8.1 Carbon spectra

The carbon 1s peak is our first evidence of the existence of organic species on the surface of alumina. Fig. 4.43 shows the C1s peak for tridecanoic acid, humic acid and the reference, which is an aluminum substrate exposed to UV light for 10-15 min but without any contact to any of the two adsorbents. Evidently, the bare aluminum substrate also exhibits some carbon, basically as residue from the fabrication process and carbon contamination from air.

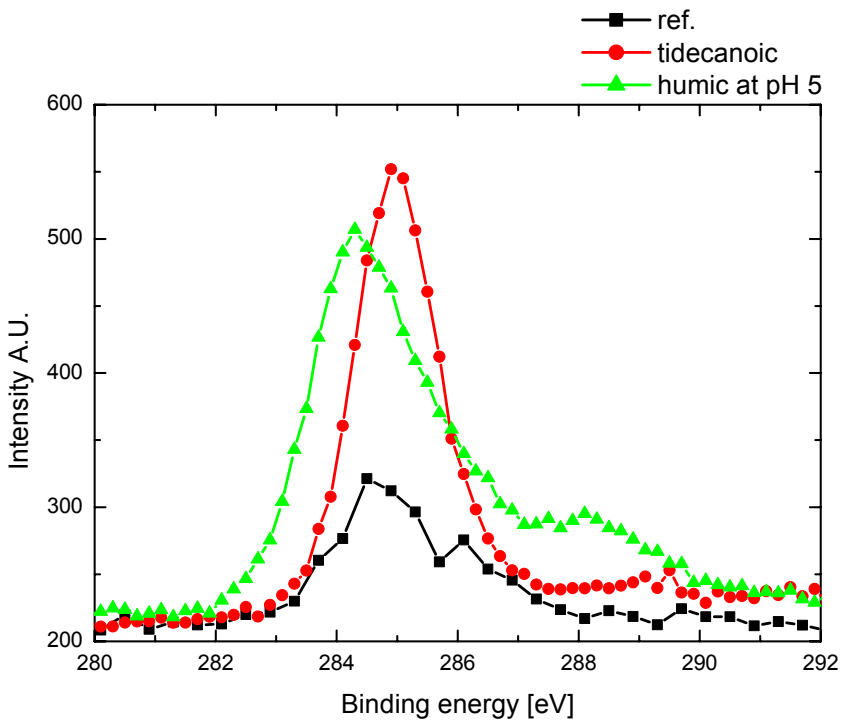

Fig. 4.43: C1s spectra of humic and tridecanoic adsorbed on aluminum oxide in comparison to a non-coated reference.

Peak analysis of humic acid after subtracting the reference peak (fig. 4.44) shows different subpeaks representing different functional groups which exist in humic acid. The main peak represents the C_xH_y, or in general aromatic carbons, other peaks correspond to alcoholic carbons, ester carbons and carboxylic carbon. The plotted C1s peak of tridecanoic acid after subtracting the reference peak (fig. 4.45) shows only two kinds of carbon. The main peak is for aliphatic carbon, distinguished from the aromatic one of humic acid by less than 1 eV. The second and much smaller peak is that of carboxylic acid.

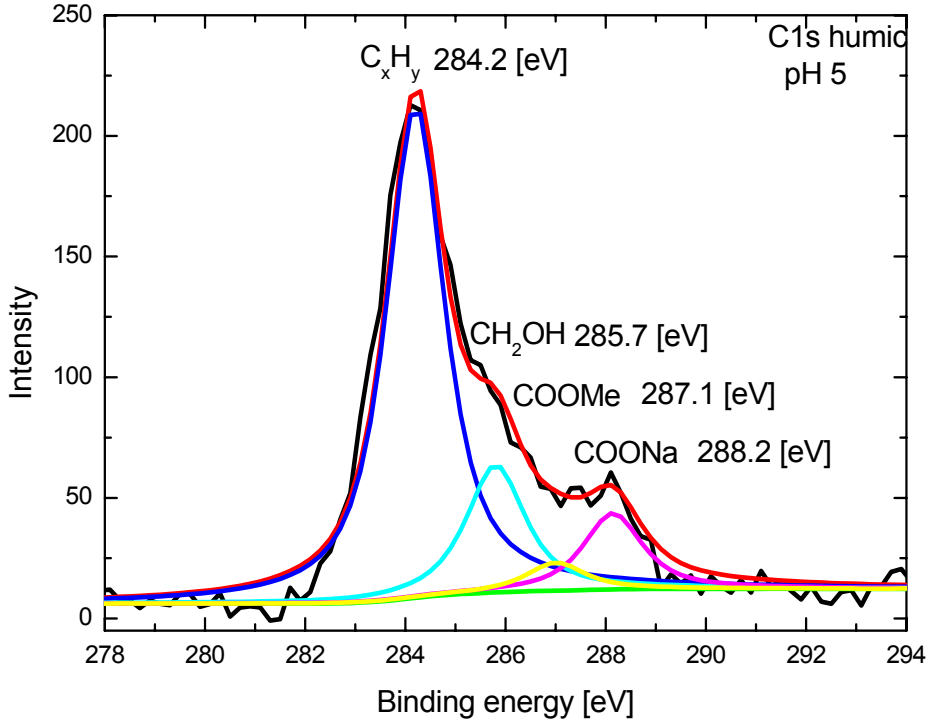

Fig. 4.44: Peak analysis of the carbon peak of humic acid adsorbed onto aluminium oxide at pH 5. Fitting shows different subpeaks characteristic of different functional groups.

.

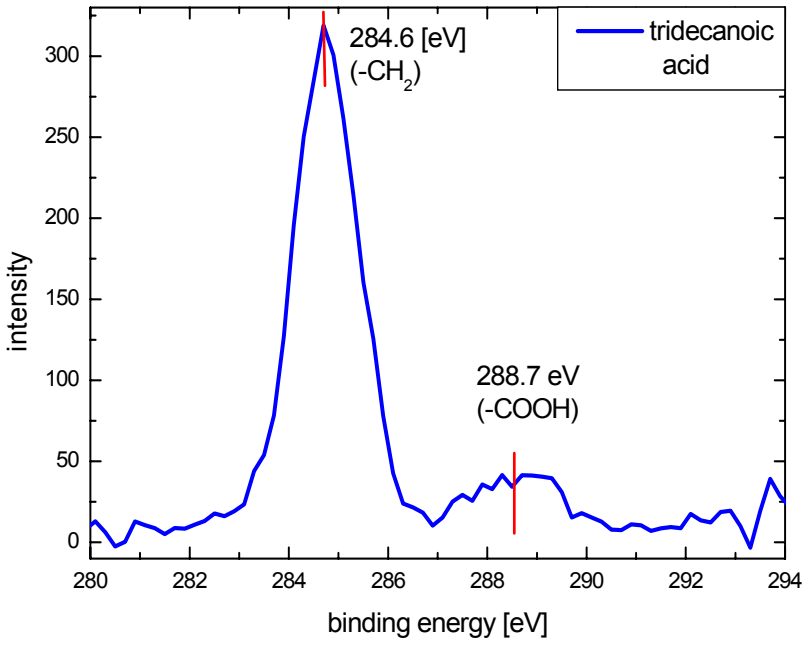

Fig. 4.45: C1s peak of tridecanoic acid after subtracting the reference peak. Shown are two distinctive peaks: one for the carbon chain and the other one for the carboxyl group.

4.8.2. Spectra of aluminum

The idea of recording the spectra of aluminum is to explore the effects of adsorption on the oxidation state of the surface. Moreover, the data can be used to calculate the film thickness of the adsorbate. From a first sight at figure 4.46 a, the adsorption of tridecanoic and humic reduced the intensity of both the aluminum (71.7 eV) and aluminum oxide (74.5 eV) peak. In addition, a little shift of the aluminum oxide peak in case of humic is observed, which is not the case for tridecanoic acid. In contrast, in both cases the position of the aluminum peak remains unaffected. Peak analysis resulted in the same two peaks for aluminum and its oxide, i.e. no other peaks or chemical states can be observed, and a film thickness of 9 Å for humic and 8.7 Å for tridecanoic acid.

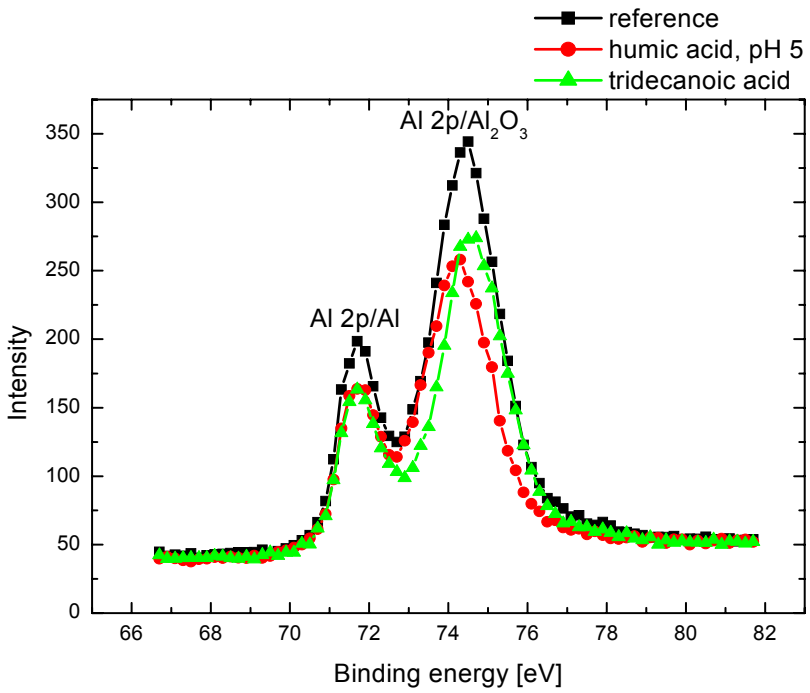

(a)

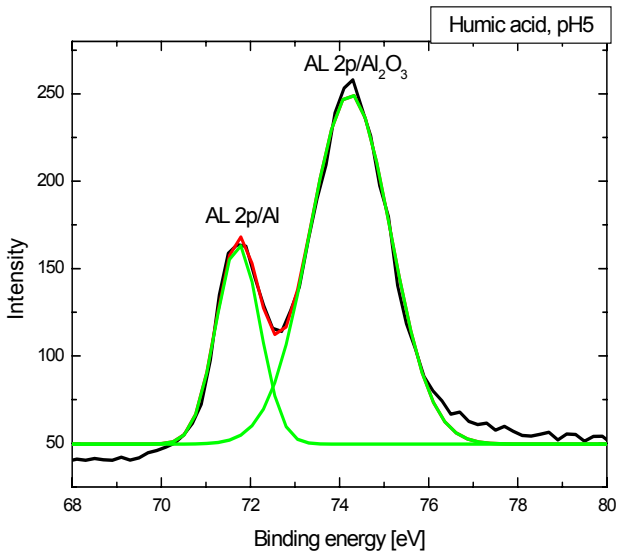

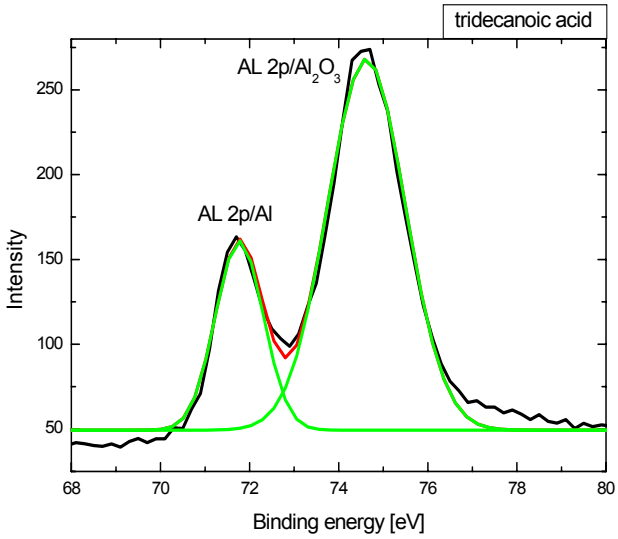

(b) **(c)**

Fig. 4.46: Aluminum 2p spectra of (a) a bare aluminum substrate, and after tridecanoic and humic adsorption at pH 5, (b) peak analysis after humic adsorption at pH 5, (c) peak analysis after tridecanoic acid adsorption. The red line presents the overall peak; the green line presents the subpeaks.

Actually, the difficulty to prove the chemical bonding arises from the nature of aluminum itself, because the aluminum surface is permanently covered with its oxide Al_2O_3, i.e. the trivalent Al^{+3} cation exists already in the spectra. Thus, there is no room to assume a change of the oxidation state to Al^{+3} upon adsorption. On the other hand, aluminium is trivalent and, thus, Al^{+3} will form if aluminum reacts with the carboxylic group of humic acid. In conclusion, we can neither verify nor exclude the existence of such a peak that indicates chemical binding between aluminum and the carboxyl groups of humic acid. Therefore, the comparison with other carboxylic acids could be the key to solution. Figures 4.46 (a, b and c) show that the spectra for humic acid and tridecanoic acid adsorbates are quite identical. To further prove a chemical binding, IR spectra of the carbonyl groups might be helpful.

4.8.3. Spectra of oxygen

We cannot benefit much from the spectra of oxygen except that the reduction of intensity and the little shift upon adsorption is more pronounced for humic than for tridecanoic acid (fig. 4.47). Although other researchers have mentioned the existence of a subpeak indicating the binding of aluminum to the oxygen of a carboxyl group, we cannot find any indication of such a peak here.

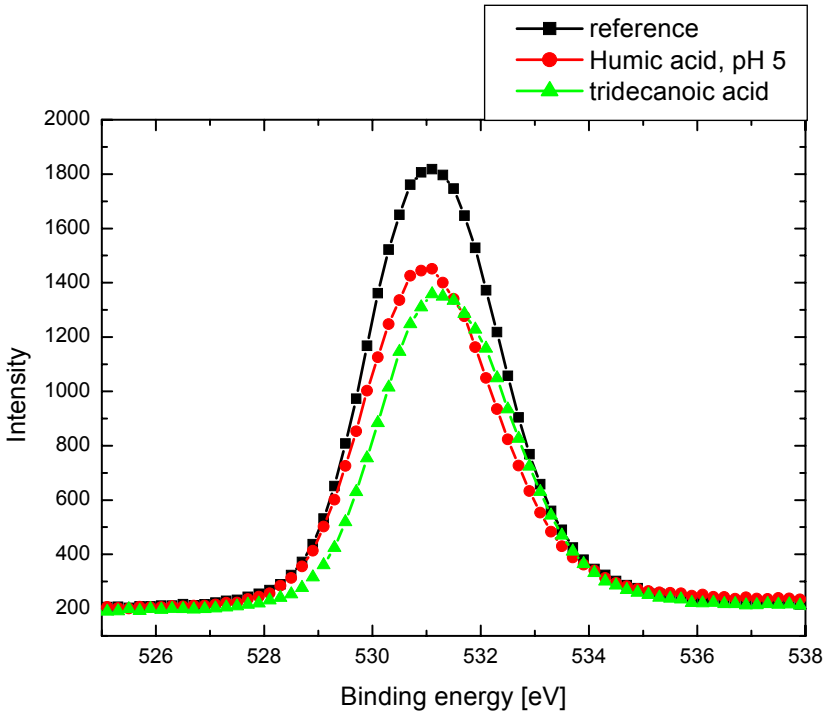

Fig. 4.47: Oxygen 1s spectra of a bare aluminum oxide surface (reference), and after adsorption of humic acid at pH5 and tridecanoic acid.

4.8.4. Effect of pH

The effect of pH on metal oxides cannot be ignored. Therefore, we studied the changes occurring in the aluminum and oxygen peaks of aluminum oxide substrates exposed to Millipore water at pH 5 and pH 3 for about 2 hours. By looking at the spectra of oxygen (fig. 4.48 b), one can realize that under pH 5 conditions there is more oxygen and, thus, more oxide. Also, if we consider the aluminum spectra (fig. 4.48 b), it is again found that there is more oxide at pH 5 than at pH 3. Hydration at low pH could result in a little decrease in the thickness of the oxide film. At pH 5 the ratio of OH^- groups increases. Thus, more aluminum can be reduced due to the need of the vacant p orbital of aluminum to be neutralized by the negative charge and to form the oxide in the hydrated form $Al_x(OH)_y$. Going down to pH 3, the oxide is shown

to be mostly the same, since the surface becomes more protonated, i.e. additional hydroxyl groups are mostly absent.

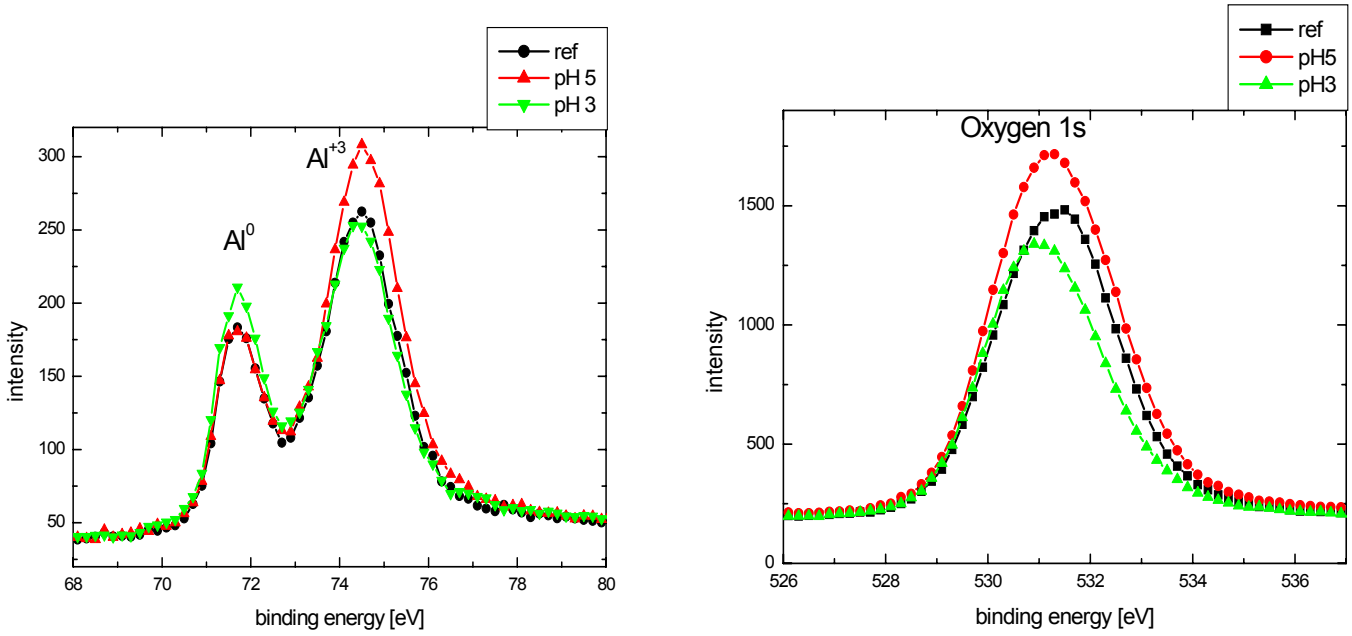

(a) **(b)**

Fig. 4.48: Spectra of a bare aluminum surface (reference) compared to an aluminum surface which was immersed in water at pH 5 and pH 3. Figure (a) presents the Al 2p peak, figure (b) the O 1s peak.

4.8.5. Effect of surface charge

By changing the emission current, the electron flux bombarding the sample surface changes (fig. 4.49). Thus, we can find out if surface charging plays a role in spectra acquisition. The emission current is usually 17 mA and was changed to 5 mA and to 10 mA during the measurement. The experiment was done on an aluminum substrate which was exposed to water at pH 3. It turned out that decreasing the emission current decreases the peak intensity as electron emission from the sample is reduced. However, peak position is not affected as expected for surface charging.

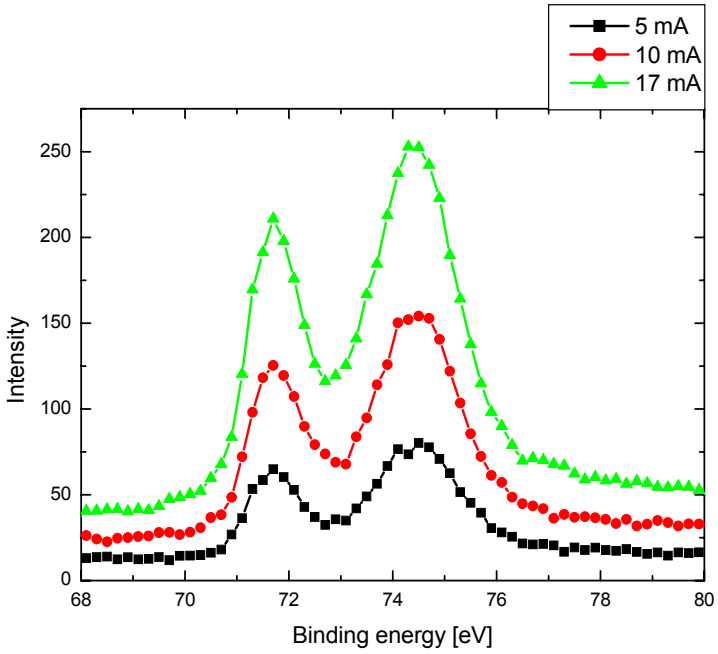

Fig. 4.469: Changing the emission current and its effect on the aluminum peaks.

4.9. Adsorption on silicon oxide

The application of SiO_2 coated sensors was an alternative approach to study the adsorption of humic, since silicates are also a basic constituent of clay and were found to interact with humic acid. Moreover, silicon oxide sensors used to be very stable towards salt and acidic effects. Figure 4.50 shows the adsorption of humic acid on the surface of a silicon oxide surface at a concentration of 50 mg/l and pH3. Interestingly, adsorption happens also in two steps similar to the case of aluminum oxide sensors. The first step is fast and followed by stabilization for few minute, this is followed by the second step which is slow, even slower than the case of aluminum oxide. Adsorption is also accompanied by higher dissipation shift.

Figure 4.51 shows the adsorption of humic acid for different concentrations at pH 3. As seen from fig. 4.51, adsorption increases with increasing concentration. Similar to the case of aluminum oxide, adsorption is very high at pH 3

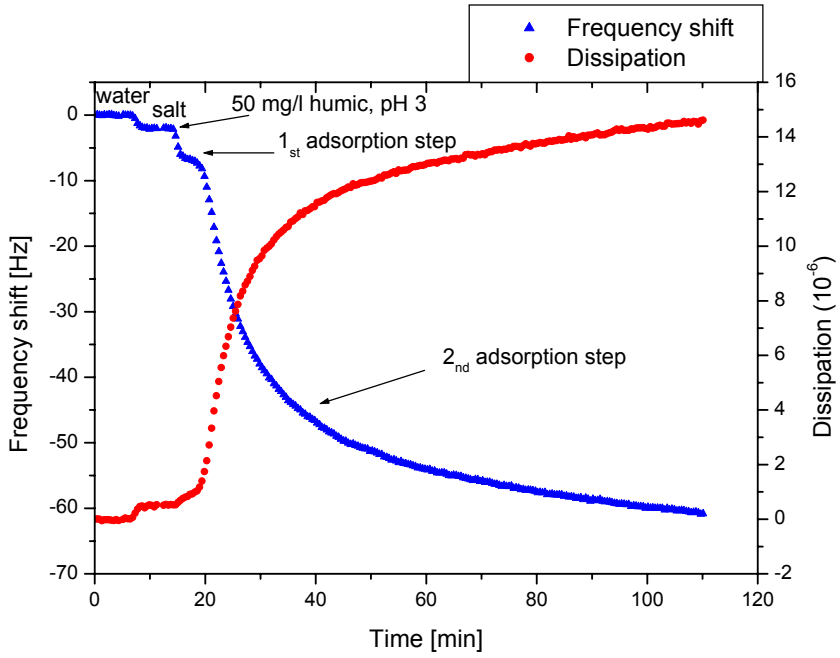

Fig. 4.50: Adsorption of humic acid on silicon oxide sensors at pH 3, the adsorption takes place in two steps similar to the adsorption on aluminum oxid esensors.

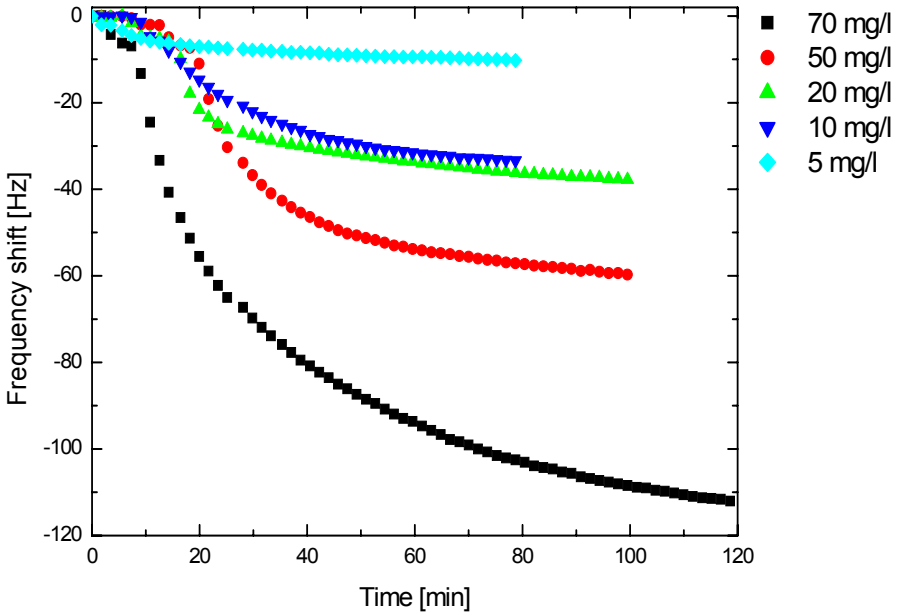

Fig. 4.51: Adsorption of humic acid on SiO_2 coated sensors at pH 3, Massive adsorption is noticed which increases with concentration.

In order to regenerate the surface, a mixture of H_2O_2, NH_4OH and water in a ratio of 1:1:5 was applied at 70 $^{\circ}$C for 5 minutes. This mixture was used to regenerate the surface of the sensor used in measurements of fig. 4.51. However, it was too aggressive so that it dissolved the silicon surface after two cleaning processes. Other regenerating schemes were attempted which are (i) plasma irradiation for 20 min, and (ii) irradiation by UV for 10 min followed by 2% SDS bath for 30 min, and then another 10 min of UV irradiation. A silicon oxide sensor was used for humic adsorption in a QCM measurement and treated by the different schemes after each adsorption. XPS was performed after each cleaning to check the regenerating ability. Figure 4.52 shows the XPS spectra of a humic film adsorbed on a silicon oxide sensor and cleaned by the different schemes. Apparently, the two schemes used to work well and are efficient to remove humic from the surface.

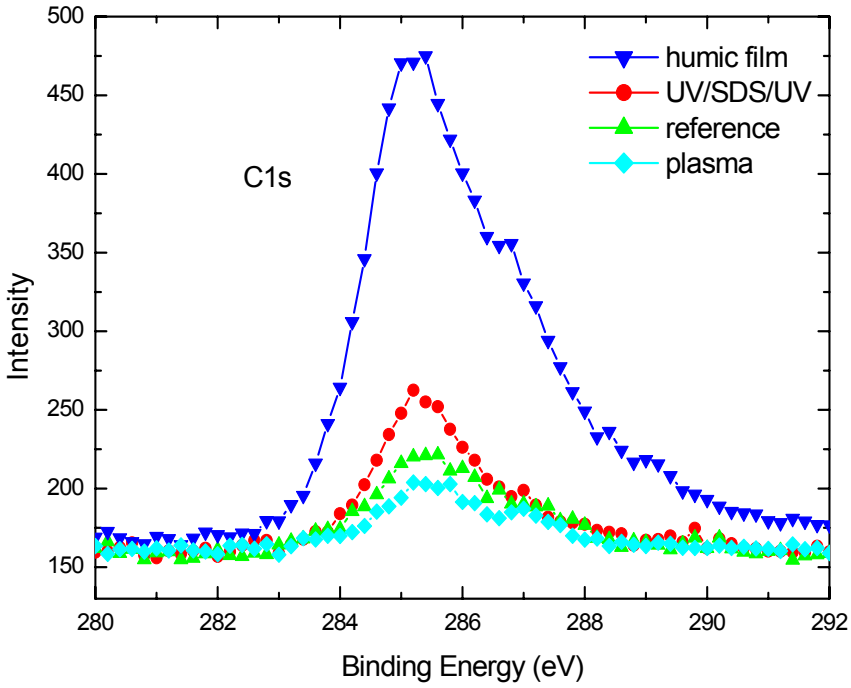

Fig. 4.52: XPS spectra of a silicon oxide coated sensor which was used for humic adsorption and cleaned in separate attempts by plasma and UV/SDS/UV, respectively. The spectra show that both schemes are capable of removing humic from the surface.

Although humic adsorption on silicon oxide coated sensors showed reasonable success, severe problems were encountered to obtain reproducibility for different sensor batches. Moreover, sometimes not only different batches, but also the same

sensor element did not yield the same adsorption curves. At first glance, this problem might be attributed to surface contaminations. However, even on new sensors the measurements were sometimes not successful. We, thus, did not consider this approach as a promising alternative to the use of aluminium oxide coated sensors.

6. Conclusion

To evaluate the environmental risks associated with the long-term operation of repositories for nuclear waste, the migration of radionuclides with long decay times must be analyzed in detail. Therefore, the various interactions between the radionuclides and their environment, i.e. the surrounding rock and soil, have to be studied. Particular attention must be paid to processes involving groundwater, which is usually enriched with products from biological decomposition reactions (so-called "humic materials"). Due to their intrinsic chemical properties, such as complexation- and redox-capabilities, these humic materials may have significant impact on the retention and transport of the radionuclides.

For this purpose, the adsorption of humic material on aluminium oxide model surfaces in the absence (binary system) and presence (ternary system) of lanthanides has been studied. The main experimental technique involved was gravimetric using a quartz crystal microbalance set-up (QCM-D), ellipsometry and X-ray photoelectron spectroscopy (XPS) were also applied as optical and spectroscopic methods. A major obstacle of the project was to prepare aluminium oxide coatings with reasonable stability in aqueous environments of various ionic strength and pH. This problem was solved after testing a variety of coating strategies. The best results were obtained for thermal evaporation of aluminum with a thickness of 50 nm using titanium as an adhesion promoter.

The response of QCM quartz sensor to bulk effects was found to agree well with theoretical calculations of frequency and dissipation response towards viscosity and density variation. On the other hand, the significance of acoustoelectric effects could be excluded.

At pH 3, QCM measurements revealed a two-step adsorption process, which can be explained by monolayer formation and successive adsorption of physical aggregates. For all other pH values studied, only a single adsorption step is observed. The monolayer adsorbed at pH 3, similar to the monolayer adsorbed at higher pH values, consists merely of solid material and is irreversibly adsorbed. The physically aggregated large layer at pH 3 can be easily washed off. By recording the dissipation factor, information about the soft matter character of the adsorbed species was

gained. Mass and thickness of the adsorbed film was calculated according to the Sauerbrey equation and the viscoelastic model.

Adsorption was found to depend on concentration of humic acid, reaching saturation at concentrations of about 10 mg/l. Although the adsorption isotherms are similar to Langmuir-type process, the irreversible adsorption behaviour contradicts this mechanism. The observed behaviour is, thus, better explained by the assumption of humic adsorption in its native state followed by an unfolding process. Adsorption in the ternary system results in similar adsorption curves with slower kinetics and higher adsorbed amounts, about as double as much.

Ellipsometry measurements, in dry state, of humic and humic/Gd^{+3} films on aluminum oxide reveals the same concentration, pH and kinetic effects as shown by QCM in the binary as well as in the ternary system. XPS gave spectroscopic evidence of the adsorption processes. In addition it confirmed the quantitative analysis made by QCM and ellipsometry. Uniquely, XPS offered the opportunity to identify the adsorbed species as shown by the carbon spectra. Moreover, it was applied to study desorption on long time scales which was not possible by QCM or ellipsometry. Here, XPS proved that almost no desorption of humic films is observed after 48 hours of immersion in water.

Considering the results of the three analytical techniques involved it may be concluded that humic acid adsorbs on aluminum oxide in both the binary system and the ternary system by the attack of its carboxyl groups. An ion exchange mechanism is assumed. In the binary system adsorption results in a humic monolayer, while in ternary system it yields a humic monolayer linked vertically to a humic overlayer through the gadolinium metal bridge. Adsorption at pH 3 presents a special case of large layer formation of physically aggregated molecules due to electrostatic attraction enhanced by the availability of positive charges. Adsorption is to great extent irreversible as suggested by the different techniques, which is in favour of chemisorption. Gadolinium retards the adsorption kinetics and increases the adsorbed amounts of humic due to complexation.

6. References

1. Stevenson, F.J. *Humus Chemistry: Genesis, Composition and Reactions*, john Wiley & Sons, New York, **1994.**
2. Atkins, P.W. *Physical Chemistry*, 4_{th} edition, Oxford University press, **1990.**
3. Adamson, A.W. *Physical chemistry of surfaces*, 4th edition, Willey-Interscience, New York, **1982**.
4. Eischens, R. P.; Jacknow, *Proc. 3_{rd} int. congr. Catal.*, Amsterdam 1964, North Holland publishing co., Amsterdam **1965**
5. Unland, M. L. *Science*, 179, 567, **1973**.
6. Schesters, M. A.; Pritchard, J.; Sims, M. L. *Chem. Commun*., 1454, **1970**
7. Somorjai, G. A. *principals of surface chemistry*, Prentice-Hall, Englewood Cliffs, New Jersey, **1972**.
8. Abdo, S.; Howe, R. F.; Hall, W. K. *J. Phys. Chem*., 82, 969, **1978**.
9. F. Albert Cotton and Geoffrey Wilkinson, *Advanced Inorganic Chemistry*, 2_{nd} edition, Interscience pub. **1967**.
10. Ghabbour, E.; Davies, G. *Understanding humic substances*, Royal Society of Chemistry **1999**.
11. Mulder G. J. *J. prakt. Chem*., **1840**, 21, 203, 321.
12. Davies, G.; Ghabbour, E.A. *Humic substances: structures, properties and uses*, Royal Society of Chemistry, Cambridge, **1998**, p. 203.
13. Sein, L. T.; varnum, J. M.; Jansen, S.A. *Environ. Sci. Techol*. 1999, 33, 546.
14. Wershaw, R. L. *Environ. Sci, Technol*., **1993**, 27, 814.
15. Avena, M. J.;Koopal, L. K. *Environ. Sci. Technol*. **1999**,33, 2739-2744.
16. Kinniburgh, D.G.; Milne C.J.; Benedetti, M.F.; Pinheiro, J. P. ; Filius, J. ; Koopal, L. K. ; van Riemsdijk, W. H. *Environ. Sci. Technol*. **1996**, 30, 1687-1689.
17. Jones, M.N.; Bryan, N. Adv. *Colloid interface Sci*. 1998, 78. 1-48.
18. McCarthy, J.F.; Zachara, J.M. *Envron. Sci. Technol*. **1989**, 23, 496-502.
19. Murphy, E.M.; Zachara, J.M.; Smith,S.C. *Environ. Sci. Technol*. **1990**, 24, 1507-1516.
20. Gu, B.; Schmitt, J.; Chen, Z.; Llang, L.; McCarthy, J.F. *Environ. Sci. Technol*. **1994**, 28, 38-46.
21. Davis, J.A. In Contaminants and sediments; Baker R. A., Ed.; Ann Arbor Sci.; Ann Arbor, 1981; Vol. 2, Chapter 15.

22. Vermeer, A. W. P.; Van Riemsdijk, W. H.; Koopal, L. K. *Langmuir* **1998**, 14, 2810-2819.
23. Vermeer, A.W. P.; Koopal, L. K. *Langmuir* **1998**, 14, 4210-4216.
24. Davis, J. A. *Geochem. Cosmochim. Acta* **1982**, 46, 23281-2393.
25. Varadachari, C.; Chattopadhyay, T.; Ghosh, K. *Soil. Sci*. **1997**, 162, 28-34.
26. Gu. B.; Schmitt, J.; Chen, Z.; Llang, L.; McCarthy, J. F. *Geochim. Cosmochim*. *Acta* **1995**, 59, 219-229.
27. Zhou, J. L.; Rowland, S. J.; Fauzi, R. ; Mantoura, R. F. C.; Braven, J. *Water Re*. **1994**, 28, 571-579.
28. Sakuragi, T.; Sato, S.; Kozaki, T.; Mitsugashira, T.; Hara, M.; Suzuki, Y. *Radiochim. Acta* **2004**, 92, 697-702.
29. Choppin, G. R.: The role of natural organics in radionuclides migration in natural aquifer Systems. *Radiochim. Acta* **1992**, 58/59, 113.
30. Rabung, Th.; Stumpf, Th.; Geckeis, H.; Klenze, R.; Kim, J. I. *Radiochim. Acta* **2000**, 88, 711-716.
31. Kosmulski, M.: Standard enthalpies of adsorption of Di- and trivalent cations on alumina. *J. Colloid Interface Sci.* **1997**, 192, 215.
32. Nordén, M.; Ephraim, J. H.; allard, B.: The influence of a fulvic acid on the adsorption of Europium and Strontium by Alumina and quartz: effect of pH and ionic strength. *Radiochim. Acta* **1994**, 65, 265.
33. Vermeer, A. W. P.; Van Riemsdijk, W. H.; Koopal, L. K. *Langmiur* **1998,** 14, 2810-2819.
34. Fein, J. B.; Boily, J. F.; Gueclue, K.; Kaulbach, E. *Cemical Geology* **1999**, 162, 33-45.
35. Alvarez-Puebla, R. A.; Valenzuela-calahorro, C.; Garrido, J. *Langmuir* **2004**, 20, 3675-3664.
36. Alcacio, T.E.; Hesterberg, D.; Chou, J. W.; Martin, J. D.; Beauchmin, S.; Sayers, D. E. *Geochim Cosmochim Acta* **2001**, 65, 1355-1366.
37. Pefferkorn, E.; Rengenbach, E.; Elfarissy, F. *Colloid Polym Sci* **2001**, 279, 498-505.
38. Saito, T.; Nagasaki, S.; Tanaka, S.; Koopal, L. K. *Colloids and Surfaces A: Physicochem. Eng. Aspects* **2005**, 265, 104-113.
39. Baker, H.; Khalili, F. *Analytica Chemica Acta* **2004**, 516, 179-186.

40. Saito, T.; Koopal, L. K.; Van Riemsdjik, W. H.; Nagazaki, S.; Tanaka, S. *Langmuir* **2004**, 20, 689-700.

41. Vermeer, A. W. P.; Koopal, L. K. *Langmuir* **1998**, 14, 4210-4216.

42. Wershaw, R. L.; Leenheer, J. A.; Sperline, R. P.; Song, Y.; Noll, L. A. Melvin, R. L.; Rigatti, G. P. *colloids and Surfaces A: physicochem. Eng. Aspects* **1995**, 96, 93-104.

43. Baalousha, M.; motelica-Heino, Mikael.; Le Coustumer, P. *Colloids and Surfaces A: Physicochem Eng. Aspects* **2006**, 272, 48-55.

44. Elfarissi, F.; Nabzar, L.; Ringenbach, E.; Pefferkorn, E. *Colloids and surfaces A: Physicochem Eng. Aspects* **1998**, 131, 281-294.

45. Filius, J. D.; Lumsdon, D. G.; Meeussen, J. C. L. ; Hiemstra, T. ; Van Riemsdjik, W. H. *Geochim Cosmochim Acta* **2000**, 64, 51-60.

46. Parifitt, R. L.; Fraser, A. R.; Famer, V. C. *J Soil Sci*, **1997**, 28, 289.

47. Gu, B.; Schmitt, J.; Chem, Z.; Liang, L.; McCarthy, J. F. *Geochim Cosmochim Acta* **1995**, 59, 219-229.

48. Kaiser, K.; Guggenberger, G.; Haumaier, L.; Zech, W. *Eurp. J: Soil Sci*. **1997**, 48, 301-310.

49. Evanko, C. R.; Dzombak, D. A. *Environ. Sci Technol*. **1998**, 32, 2846-2855.

50. Kummert, R.; Stumm, W. *J. Colloid Interface Sci.***1980**, 75, 373-385.

51. Zhang, X.; Bai, R. *Langmuir* **2002**, 18, 3459-3465.

52. Zhang, X.; Bai, R. *J. Colloid Interface sci*. **2003**, 264, 30-38.

53. Deng, S.; Bai, R. *J. Colloid Interface Sci.* **2004**, 280, 36-43.

54. Bai, R.; Zhang, X. *J. Colloid Interface Sci.* **2001**, 243, 52-60.

55. Ho, C. H.; Miller, N. H.; *J. Colloid Interface sci.* **1985**, 106, 281.

56. Righetto, L.; Bidoglio, J.; Azimonti, G.; Bellobono, I. R. *Environ. Sci. Technol.* **1991**, 25, 1913.

57. Fairhurst, A. J.; Warwick, P.; Richardson, S. Radiochim. Acta 1995, 69, 103.

58. Murphy, A. M.; Zachara,J. M. *Geoderma*, **1995**, 67, 103.

59. Samadfam, M.; Jintoku, T.; Sato, S.; Oashi, H.; Mitsugashira, T.; Hara, M.; Suzuki, Y. *Radiochim. Acta* **2000**, 88, 717.

60. Tombácz, E.; Dobos, Á.; Szekres, M.; Narres, H. D. ; Klumpp, E. ; Dékány, I. *Colloid Polym. Sci.* **2000**, 278, 337-345.

61. Davis, J. A.; *Geochim. Cosmochim. Acta* **1984**, 48, 679.

62. Zachara, J. M.; Resch, C. T.; Smith, S. C. *Geochim. Radiochim. Acta* **1994**, 58, 553.

63. Allard, B.; Moulin, V.; Basso, L.; Tran, M. T. Stammose, D. *Geoderma*, **1989**, 44, 181.

64. Moulin, V.; Stammose, D.; *Mat. Res. Soc. Symp. Proc.* **1989**, 127, 723.

65. Rabung, Th. ; Geckeis, H. ; Kim, J. I. Beck, H. P. *J. Colloid Interface Sci*. **1998**, 208, 153.

66. Takahashi, Y.; Kimura, T.; Kato, Y.; Minai, Y.; Tominaga, T. *Radiochim. Acta* **1998**, 82, 227.

67. Stumph, Th.; Bauer, A.; Coppin, F.; Fanghänel, Th.; Kim, J. I. *Radiochim. Acta* **2002**, 90, 3445-349.

68. Plaschke,M.; Römer, J.; Klenze, R.; Kim, J.I. *Surf. Interface anal.* **2000**, 30, 297-300.

69. Kumar, S.; Tomar, B.S.; Ramanathan, S.; Manchanda, V. K. *Radiochim. Acta* **2006**, 94, 369-373.

70. Samafdam, M.; Jintoku, T., Sato, S.; Ohashi, H.; Mitsugashira, T.; Hara, M.; Suzuki, Y. *Radiochim. Acta* **2002**, 88, 717.

71. Ballantine, D. S.; White, R. M.; Martin, S. I.; Ricco, A. J.; Zellers, E. T.; Frey, G. C.; Wohltjen, H. *Acoustic Wave sensors: Theory, Design and Physico-chemical Applications.* Academic Press Inc. **1997**.

72. Dahint, R.; *Label-Free In Situ Detection of Proteins and Cells using Acoustic Plate Mode Sensors and Optical at chemically Microstructured Surfaces,* Habilitation Thesis, Department of Chemistry, University of Heidelberg, **1999**.

73. Sauerbrey, G. *Zeitschrift für Physik* **1959**, 155, 206-222.

74. Rodahl, M.; Hök, F.; Krozer, A.; Brezinski, P.; Kasemo, B. *Rev. Sci. Instrum*. **1995**, 66, 3924.

75. Rodahl, M.; Höök, F.; Kasemo, B. *Anal, Chem*. **1996**, 68, 2219.

76. Rodahl, M.; Kasemo, B. *Rev. Sci. Instrum*. **1996**, 67, 3238.

77. Richter, R. P.; Maury, N.; Brisson, A. R. *Langmuir* **2005**, 21, 299-304.

78. Richter, R. P.; Brisson, A. *Biophysical journal* **2005**, 88, 3422-3433.

79. Höök, F.; Rodahl, M.; Brezezinski, P.; Kasemo, B. *Langmuir*, **1998**, 14(4), 729.

80. Höök, F. *Development of a novel QCM technique for protein adsorption studies*, PhD Thesis, Chalmers University of Technolog, **2001**.

81. Kanazawa, K. K.; Gordon, J. G.; *Anal. Chem*. **1985**, 57, 1770.

82. Stockbridge, C. D. *Vacuum Microbalance Techniques*, Plenu Press, **1966**, 5, 147.
83. Rodhal, M.Kasemo, B.; *Sensors & Actuators,* **1996**, A54, 448.
84. Yang, M.; Thomson, M.; *Anal.Chem.* **1993**, 65, 3591-3597.
85. David R. Lide, Handbook of Chemistry and physics, 83_{rd} edition, CRC press, **2002-2003.**
86. Voinova, M. V.; Rodahl, M.; Jonson, M.; Kasemso, B. *Physica Scripta* **1999**, 59(5), 391-396.
87. Brundle, C. R. *Encyclopedia of materials characterization*. Library of Congress, **1992**.
88. Wolsky, S. P.; Czanderna, A. W. Methods and Phenomena; Methods of Surface Analysis, Elsevier Scientific Publishing, **1975**.
89. Grunze, M.; *Lectures* at the Department of chemistry, University of Heidelberg, June **2006**.
90. Herrweth, S. *PhD thesis*, Department of Chemistry, University of Heidelberg, **2002**.
91. Laibinis, P. E.; Bain, C. D.; Whitesides, G. M. *J. Phys. Chem.* **1991**, 95, 7017-7021.
92. Tompkins, H. G.; Irene, E. A. *Handbook of ellipsometry*, William Andrew Publishing, **2005**.
93. Albert, G.; *Diploma thesis*, Department of Physics, University of Heidelberg, **1996**.
94. q-sense user manual D300, **2000**.
95. q-sense, *Educational lecture*, Cambridge, **2005**

Eidesstattliche Erklärung

Ich erkläre hiermit an Eides statt, dass Ich meine Dissertation selbstständig angefertigt und mich dabei keiner anderen als der von mir ausdrücklich bezeichneten Quellen und Hilfen bedient habe. Ich habe an keiner anderen Stelle ein Prüfungsverfahren beantragt bzw. die Dissertation in dieser oder anderer Form bereits anderweitig als Prüfungsarbeit verwendet oder einer anderen Fakultät als Dissertation vorgelegt.

Heidelberg, den 07.02.2008

Mohamed Eita